Reconstruction of environmental change and sedimentation processes during the Pleniglacial using fluvio-lacustrine sediments from volcanically-dammed Paleolake Alf, West Eifel Volcanic Field, Germany

Dissertation

zur Erlangung des akademischen Grades

Dr. rer. nat. (doctor rerum naturalium)

vorgelegt dem Rat der Chemisch-Geowissenschaftlichen Fakultät der Friedrich-Schiller-Universität Jena

von **Luise Eichhorn** (**Dipl. Geogr.)** geboren am 10.10.1986 in Schkeuditz

Gutachter:

1. Prof. Dr. Georg Büchel, Universität Jena
2. Prof. Dr. Reinhard Gaupp, Universität Jena

Datum der Verteidigung: 30.11.2016

Contents

List of Tables

List of Figures

List of Abbreviations

AGC	Automatic Gain Control (seismic)
AMS	Accelerated mass spectrometry
a.s.l.	Above sea level
b2k	Before 2000
BP	Before Present, i.e. 1950 A. D.
cal.	Calibrated
cf	Lat. conferre = compare
CGS	Centimeter Gram Second unit system (meanwhile replaced by SI-units)
Chl	Chlorite
CMP	Common Mid Point (seismic)
coh	Coherent radiation (Rayleigh scattering)
DEM	Digital elevation model
ELSA	Eifel Laminated Sediment Archive
ESR	Electron Spin Resonance
FD	Finite Difference (seismic)
GI	Greenland Interstadial
GS	Greenland Stadial
HA	Humic acid
INFLUINS	Integrierte Fluiddynamik in Sedimentbecken
Ka	Kilo years
κ	Volume-specific magnetic susceptibility
LGM	Last Glacial Maximum
LST	Laacher See Tephra
MFM	Meerfelder Maar
ML	Marker layer
MS	Muscovite
NGRIP	North Greenland Ice Core Project
NMO	Normal Move Out (seismic)
nT	Nano Tesla
LR	Leaching residue
ONB	Olivine-nephelinite and basanite (suite)
OSL	Optically stimulated luminescence
PAAS	Post-Archean Australian Shale
Px	Pyroxene
Qtz	Quartz
REE	Rare earth elements

RTL	Red thermoluminescence
SEM	Scanning electron microscopy
SI	International System of units
SISSY	Seismic Impulse Source System (seismic)
SMOW	Standard Mean Ocean Water
θ	Theta, diffraction angle (XRD)
TC	Total carbon
TD	Total digestion
TFM	Polymer (Total digestion)
TIC	Total inorganic carbon
TIN	Triangulated irregular network
TL	Thermoluminescence
TOC	Total organic carbon
XRD	X-ray diffraction
XRF	X-ray fluorescence
WEVF	West Eifel Volcanic Field

Abstract

Direct measurements of global climate parameters rarely exceed more than 200 years. In order to make reliable future climate predictions and to determine how fast ecosystems adapt to climate change, datasets have to be extended. Therefore, proxies, e.g., grainsize, grain shape or mirco fossil species from climate archives, e.g., sediment archives, are used to indirectly reconstruct changes in sediment transport processes or environmental conditions. These archives are distributed globally across all climatic zones on continents and in marine environments with different temporal coverage and resolutions.

This study focuses on a fluvio-lacustrine sediment archive (33-13.8 cal. ka BP) from the West Eifel Volcanic Field (WEVF) in Germany covering the hitherto less investigated period of the Middle to Late Pleniglacial. In contrast to other investigated archives like maar lakes, fluvial units or eolian deposits, the sediments from Paleolake Alf formed due to volcanic eruptions of the Wartgesberg Volcano Complex that blocked the Alf River valley with scoria and lava and created a dammed lake. In the Alf Valley, this volcanic dam trapped the Middle to Late Pleniglacial sediments which recorded climatically-triggered transport processes. This kind of archive has never been analyzed before in detail from Central Europe.

The main objective of this study was to improve the understanding of the paleoenvironmental change during the Middle and Late Pleniglacial in the West Eifel Volcanic Field including transport media, deposition structure and denudation rate. Specifically, prevailing environmental conditions and sediment transport/ deposition processes in the Alf catchment and lake should be reconstructed in combination with a design of the lake basin architecture. Further, the morphology of the landscape should be reconstructed after the end of the Wartgesberg eruptions which was the initial point of the river impoundment. The trapped sediment volume in the lake was calculated by applying a multidisciplinary approach combining field surveys, sedimentological, geophysical and GIS-based investigations.

According to reconstructions of this study, Paleolake Alf had an elongated shape with a maximum lake level of 410 m a.s.l. and a catchment area of ~ 55 km². Sediment core investigations from the bottomset area of the lake basin revealed (sub)millimeter (*Unit I*) to millimeter (*Unit II*) thick light and dark laminae. Light, clayey silt laminae formed during winter when Paleolake Alf was ice-covered, indicated by dropstones. Seasonal lake ice cover prevented sediment input, wave-induced currents and shore abrasion, and resulted in still-water conditions enabling suspension fallout. Dark, silt-sized laminae were subdivided into *Type I*: Laminae with normal grading, and *Type II*: Laminae with graded sublayers. Normal grading formed during early-season discharge after ice cover break-up when the lake was still

stratified and over- or interflows delivered sediments that fell out of suspension. In contrast, the predominantly occurring graded sublayers formed from repeatedly occurring melting events. The clastic lamination is interpreted to be of seasonal character. After an abrupt grainsize change indicating a hiatus and water level reduction, the lacustrine sequence was covered by gravelly-sand sized sediments. The formation of this hiatus is assumed to be a result from either strong discharge event, backward erosion or a combination of both. This resulted in a dam collapse at ~ 15 cal. ka BP and subsequent erosion of parts of the lacustrine sediments sequence down to an elevation of 385 m a.s.l.. The sand-sized fluvial sediments were transported by the prograding Alf River and deposited over the remaining basin area regulated by a low gradient in front of the dam on one side and underlying lacustrine sediment compaction on the other side.

Landscape reconstructions show the Alf Valley with a pre-eruptive morphology at the area of the younger Pulvermaar-Römerberg Complex, the Strohn lava flow and the Alf Valley before the onset of sediment infill. The positive landforms “Lange Klopp” and Körperichberg consisting of scoria are interpreted as relicts of two eruption centers of the Wartgesberg Volcano Complex. The calculated lacustrine sediment volume amounts to 25 Mio. m³ equalling a Pleniglacial denudation rate of 37.5 mm · ka^{-1} between 33 and 21 cal. ka BP. This value is in the same order of magnitude as the calculated denudation rate from the Allier River basin in French Massif Central between 29 and 16 ka BP.

The high-resolution study of the sedimentary sequence of Paleolake Alf showed that the basin architecture resembles that of modern reservoirs and that several sedimentation structures are similar to maar lake records in the vicinity. The predominantly graded sublayers in Paleolake Alf laminae indicate repeated melting events or precipitation during Late Pleniglacial spring/summer. By correlating the Paleolake Alf record with the NGRIP ice core, the slight grainsize coarsening and the calcium increase in the lacustrine sediments (*Unit II*) could be explained with a change from Interstadial to Stadial ~ 26.3 ka BP. ^{14}C dating on the deepest lacustrine sediments are in the same order of magnitude as the dated Wartgesberg eruption ages by other scientists. However, in future, the sediments should be analyzed with another dating technique – paleomagnetic.

Zusammenfassung

Globale, direkt gemessene Klimaparameter reichen selten weiter als 200 Jahre in die Vergangenheit zurück. Um jedoch zuverlässige Klimaprognosen machen und Aussagen darüber treffen zu können, wie schnell sich Ökosysteme an Klimaveränderungen anpassen können, müssen Datenreihen erweitert werden. Dazu können Proxies wie Korngröße, Kornform oder Mikrofossilarten, z.B. aus Sedimentarchiven verwendet werden, die Veränderungen in Transportprozessen oder Lebensbedingungen widerspiegeln, welche indirekt klimatisch gesteuert werden. Diese Archive existieren weltweit in allen Klimazonen auf Kontinenten und im Meer in unterschiedlichen Zeitspannen und mit verschiedener Auflösung.

Diese Arbeit befasst sich mit einem fluviolakustrinen Sedimentarchiv (33-13.8 cal. ka BP) aus dem Westeifel Vulkanfeld in Deutschland welches den bisher wenig untersuchten Zeitabschnitt des Mittel- bis Spätpleniglazil umfasst. Im Unterschied zu anderen untersuchten Archiven dieser Zeit wie Maarseen, Fluss- oder Lössablagerungen, sind die Sedimente des Paläosee Alf durch Eruptionen des Wartgesberg- Vulkankomplex entstanden, dessen Lava und Schlacke das Alftal abgedämmt haben und sich folglich ein Stausee bildete. Im Alfbachtal wurden die mittel- bis spätpleniglazialen Sedimente welche klimatisch gesteuerte Transportprozesse aufgezeichnet haben, durch einen vulkanischen Damm erhalten. Eine solche Art von Archiv wurde nie zuvor in Mitteleuropa im Detail untersucht.

Das Hauptziel dieser Arbeit war es, die Paläoumwelt während des Mittel- und Spätpleniglazials in der Westeifel besser zu verstehen, insbesondere im Hinblick auf Transportmedien, Ablagerungsstrukturen und Denudationsraten. Im Speziellen sollten die vorherrschenden Umweltbedingungen, sowie Transport- und Ablagerungsprozesse im Alf Einzugsgebiet und See rekonstruiert und mit einem Modell der Beckenarchitektur kombiniert werden. Außerdem sollte die Landschaftsmorphologie kurz nach Ende der Wartgesberg Vulkanausbrüche – dem Startpunkt des Anstaus rekonstruiert werden. Das abgelagerte Sedimentvolumen im See wurde durch einen multidisziplinären Ansatz ermittelt, der Feldstudien, sedimentologische, geophysikalische und computergestützte GIS-basierte Untersuchungsmethoden vereint.

Basierend auf den Rekonstruktionen dieser Arbeit hatte Paläosee Alf eine längliche Form mit einem max. Seespiegel von 410 m ü. NN sowie eine Einzugsgebietsgröße von ~ 55 km². Sedimentuntersuchungen an Bohrkernen aus dem beckentiefsten Bereich zeigten (sub)millimeter- (*Unit I*) bis millimeterdicke (*Unit II*) helle und dunkle Laminen. Die hellen, tonig, siltigen Laminen bildeten sich während des Winters, als der Paläosee Alf eisbedeckt

war. Die Eisbedeckung verhinderte den Sedimenteintrag, welleninduzierte Strömungen und Küstenabrasion, wodurch Stillwasserbedingungen eine Sedimentation aus der Wassersäule hervorriefen. Die dunklen, siltigen Laminen wurden mikroskopisch in zwei Typen unterteilt: *Typ I*: Laminen mit normaler Gradierung, und *Typ II*: Laminen mit gradierten Sublagen. Die normale Gradierung bildete sich während frühsaisonaler Abflüsse nach dem Eisaufbruch, als der See noch geschichtet war und Ober- und Zwischenabfluss Sedimente transportierten, welche dann in der Wassersäule abregneten. Die gradierten Sublagen hingegen bildeten sich durch wiederholte Schmelzwasserabflüsse. Die klastische Lamination wird als saisonal interpretiert. Diese lakustrinen Sedimente wurden von fluviatilen, kiesigen Sanden überdeckt, sichtbar durch einen abrupten Korngrößenwechsel, welcher auf einen Hiatus und Seespiegelabsenkung hindeutet. Dieser entstand vermutlich entweder durch ein Starkniederschlagsereignis, rückschreitende Erosion oder einer Kombination aus beidem. Dadurch brach der Damm ~ 15 cal. ka BP und Teile der lakustrinen Sedimente wurden bis auf 385 m ü. NN erodiert. Die darüber liegenden Sande wurden durch das progradierende Delta des Alfbachs in das Becken transportiert und durch das geringe Gefälle und Kompaktion der lakustrinen Ablagerungen sedimentiert.

Das Ergebnis der Landschaftsrekonstruktion zeigt das Alftal mit der prä-eruptiven Morphologie des heutigen Pulvermaar-Römerberg-Komplexes, den Strohner Lavastrom sowie das Alftal vor der Sedimentauffüllung. Die Vollformen “Lange Klopp” und Körperichberg bestehen aus Schlacke und wurden als Relikte zweier Eruptionszentren des Wartgesberg Vulkankomplexes interpretiert. Das berechnete Seesedimentvolumen beläuft sich auf 25 Mio. m³, was einer pleniglazialen Denudationsrate von 37.5 mm · ka^{-1} zwischen 33 und 21 cal. ka BP entspricht. Dieser Wert liegt in der Größenordnung der berechneten Denudationsrate zwischen 29 und 16 ka BP vom Allier Flussbecken aus dem französischen Zentralmassiv.

Die hochauflösende Studie anhand von Sedimenten des Paläosee Alf ergab zum einen, dass die Beckenarchitektur des pleniglazialen Alfstausees der eines modernen Stausees gleicht und einige Sedimentationsstrukturen denen benachbarter Maarseen ähneln. Die hauptsächlich gradierten Sublagen in den Paläosee Alf Laminen deuten auf mehrmalige Tauphasen oder Niederschläge während des spätpleniglazialen Frühjahrs/Sommers hin. Durch Korrelation des Paläosee Alf Archivs mit dem NGRIP Eisbohrkern konnte festgestellt werden, dass der Korngrößen- und Calciumanstieg in den lakustrinen Sedimenten (*Unit II*) mit einem Wechsel von Interstadial zu Stadial um ~ 26.3 ka BP erklärt werden kann. Die ^{14}C Datierungen der tiefsten Seesedimente liegen im Bereich datierter Wartgesberg-Ausbruchsalter anderer

Wissenschaftler. Dennoch sollen die Sedimente zukünftig durch ein weiteres Datierungsverfahren – der Paläomagnetik – untersucht werden.

Chapter 1

1. Introduction

Surface temperature has been globally recorded by humans since 1850 in the HadCRUT data set (Brohan et al. 2006). Compared to geological times, this period is not sufficient for making statistically reliable future climate predictions. To improve these climate predictions, there is a need for archives, e.g., sediment records, ice cores, tree-ring records or speleothems where climatic information is indirectly preserved as proxy data, e.g., as stable oxygen isotope variations or elemental ratios.

Such paleoclimatic archives are globally distributed across all climate zones on all continents, including high mountain areas and in marine environments, however differing in temporal resolution and coverage. Of particular interest for paleoclimate research is the Quaternary period spanning the past ~ 2.4 Ma (Hewitt 2000). Some of the oldest terrestrial climate records covering the Quaternary in Central Europe were derived from limnic sediments of e.g., the Heidelberg basin, Germany (Gabriel et al. 2013): Pleistocene and Pliocene; Lac du Bouchet, Massif Central, France, (Reille et al. 1998): Pleistocene since 325 ka BP; the "Füramoos" basin, Germany (Müller et al. 2003): the past 140 ka; and the Eifel Laminated Sediment Archive (ELSA) stack, West Eifel Volcanic Field, Germany (Seelos et al. 2009, Sirocko et al. 2005, Sirocko et al. 2016): the past 132 ka. Other terrestrial climate archives are e.g., the loess profile "Dolní Věstonice", Czech Republic (Fuchs et al. 2013): the past 110 ka; speleothems in the "Villars cave", France (Genty et al. 2003): the past 85 ka; and tree-ring records from Central Europe (Friedrich et al. 2004): the past 12.46 ka.

A hitherto insufficiently studied period of the Quaternary is the Weichselian Glacial Period (115 – 11.6 ka BP, Litt et al. 2007). Pedosedimentary, eolian, fluvial and lacustrine archives are preserved at certain locations and spread from France and England (Antoine et al. 2003); Scotland (Gemmell and Ralston 1984); the Netherlands and Belgium (Vandenberghe 1985), Denmark (Kolstrup and Mejdahl 1986) over Poland (Kasse et al. 1998) and Germany (Antoine et al. 2001).

For this study, especially the Weichselian Pleniglacial (~ 60 and 14.4 ka BP, Litt et al. 2007) is of main interest which is embedded between the Weichselian Early and Late Glacial. In Germany, there are a few locations documenting the paleoenvironmental and climatic conditions of the Pleniglacial. Here, high-resolution archives, e.g., varved lacustrine sediments from the West Eifel maar lakes in Rhineland-Palatinate (Brauer 1994, Negendank

1989, Zolitschka 1989) and varved glaciolimnic sediments from Brandenburg (Juschus 2012, Neugebauer et al. 2012); eolian deposits from Rodderberg in Rhineland-Palatinate (Zöller et al. 2010) and "Nussloch" in Baden-Württemberg (Antoine et al. 2001); and fluvial units from the brown-coal mine Nochten in Saxony (Bos, et al. 2001) should be mentioned. Since the type of archive influences the spatial and temporal resolution, it is important to investigate new archives of the Pleniglacial as it was done in this thesis.

This study focuses on a special kind of archive – a dammed lake. These lakes form when primary-built dam material, e.g., glacial ice (Liestøl 1956), lava (Mathews 1956) or reworked debris material from e.g., moraines (Vuichard and Zimmermann 1987) or landslides (Trauth and Strecker 1999) block drainage and cause impoundment. These dammed lakes can persist from hours to thousands of years depending, most importantly, on the characteristics of the dam material (Costa and Schuster 1988) and occur preferentially in mountainous, glacial and volcanically active areas.

Of particular interest for this thesis are volcanically-dammed lakes. Ca. 1000 of such lakes exist worldwide (Likens 2010), presently e.g., on the Snaefellsnes peninsula of Iceland where the eruption of the scoria cone Vatnafell impounded a river and formed Lake Baulárvallavatn ~ 400 ka BP (pers. com. Haraldur Sigurdsson, Icelandic volcanologist, 2014). Lake Kivu situated in the Central African Rift Valley formed due to seven major volcano eruptions damming the drainage system (Likens 2010). Block facies of the Mt. St. Helens eruption, USA, formed the Coldwater and Castle lakes in 1980 (Capra 2007). Similar material created the lakes Akimoto, Onogana and Hibara after the eruption of the volcano Bandai, Japan, in 1888 (Capra 2007).

1.1 Study area in the frame of Quaternary climate

The investigated sediment record of this study entirely covers the Weichselian Late Pleniglacial – the temporal classification is shown below (Fig. 1.1). First, a short introduction of the climatic development of Central Europe during the Weichselian is given in order to understand the climatically-driven processes that are postulated for the studied Paleolake Alf archive.

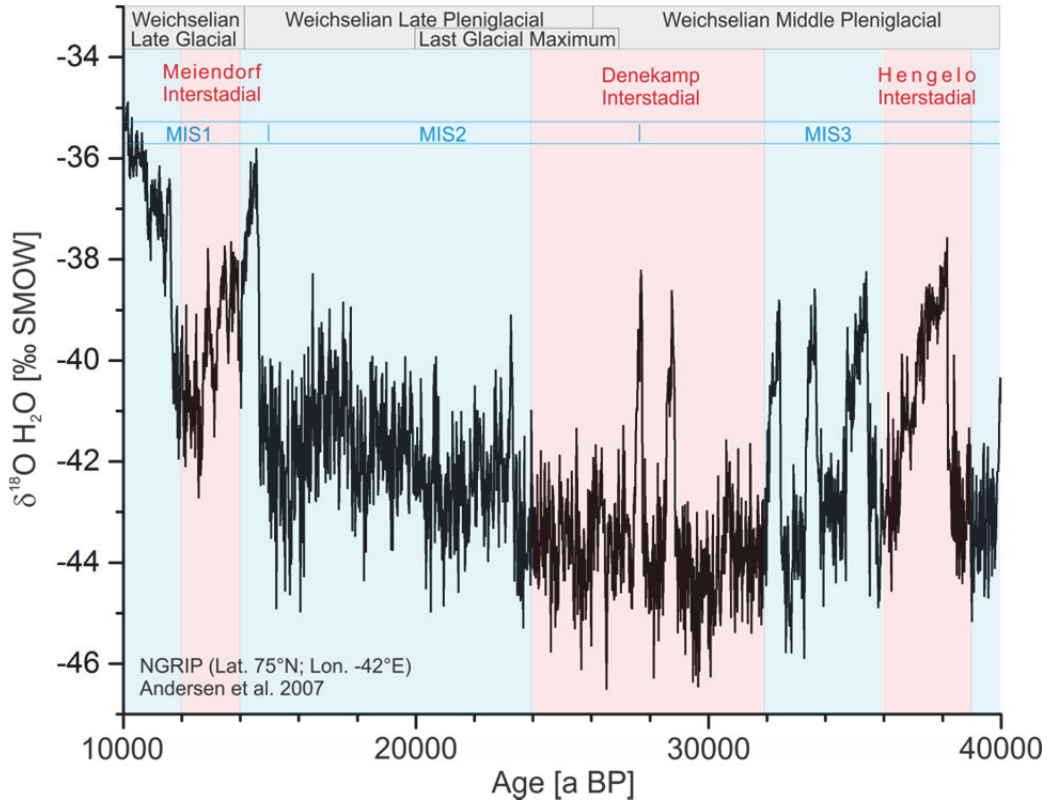

Fig. 1.1: Weichselian Pleniglacial and Late Glacial are presented with Stadials (blue) and Interstadials (red) on the NGRIP $\delta^{18}O$ curve (Andersen et al. 2007). Stratigraphic definitions were compiled from data by Behre et al. (1992), Bos et al. (2001), Huijzer and Vandenberghe (1998) and Schirmer (1999).

1.1.1 General aspects to Quaternary climate development

During the Weichselian, Central European climate has generally been cold and dry. Climate conditions were largely controlled by (a) the Scandinavian Ice Sheet which caused a high albedo and sent katabatic winds that drained off towards the foreland (Staiger et al. 2007) originating from stable highs on the central ice sheet (Gates 1976) and, (b) the vast extent of the North Atlantic sea ice which reduced the force of the Gulf Stream transporting heat to Europe (Huijzer and Vandenberghe 1998, Marks et al. 2015), and (c) anticyclone air masses from the Russian continent causing low temperatures and permafrost (Huijzer and Vandenberghe 1998, Velichko et al. 1997). Further, episodic volcanic eruptions in the German Eifel Volcanic Fields (Förster and Sirocko 2016), the French Massif Central (Nomade et al. 2016) and on Iceland (Grönvold et al. 1995) emitted sulfate aerosols reflecting solar radiation and might have supported cooling.

The Early Middle Pleniglacial (41-39 ka BP) in Central Europe was characterized by cold, arid conditions with sparse vegetation cover, active eolian sand sheets and loess – similar to the present High Arctic (Huijzer and Isarin 1997). In the lowlands, a low-shrub to grass shrub tundra with cottongrass hummocky mires prevailed which was dominated by seasonally-

frozen ground to discontinuous permafrost at mean annual temperatures of -1°C (Bos et al. 2001, Huijzer and Vandenberghe 1998). During the Hengelo and Denekamp interstadials, permafrost degraded forming thaw lakes (Mol et al. 2000) in a shrub-tundra with spread Cyperaceae (Litt et al. 2007). In regions higher than 200 m a.s.l., continuous permafrost occurred at max. mean annual temperatures of -5 °C (Vandenberghe 1993).

From the Middle to Late Pleniglacial, temperature in Central Europe dropped significantly to -8 °C, ice-wedges developed and vegetation changed to dwarf shrubs (e.g. *Betula nana*, *Salix repens*, *Juniperus*), grasses (e.g. *Festuca*, *Poa*), sedges (*Carex*), tall herbs and mosses (Bos et al. 2001, Kasse et al. 1998).

The Late Pleniglacial including the Last Glacial Maximum (27-20 ka BP, Huijzer and Vandenberghe 1998) was characterized by a major ice advance of the Scandinavian Ice Sheet which covered the northern parts of England, Ireland, Northeast Germany and Scandinavia in full extent and a more continental climate (Bos et al. 2001). Dry and harsh winters dominated with snow patches persisting up to 9 months and ice-wedge casts formed. Due to a decreasing snow thickness during winter, reduced isolation triggered continuous permafrost expanding from the present UK, Belgium, The Netherlands and Germany to Poland (Vandenberghe 1993). Sparse vegetation was dominated by sedge-grass-moss tundra equaling the present-day arctic tundra or semi-polar to polar desert, e.g., Bos et al. (2001), Kasse et al. (1998), Mol et al. (2000), Sirocko et al. (2016) and Vandenberghe (1993). The sea level was 120 m below that of present-day (Huijzer and Vandenberghe 1998), and southern parts of the North Sea shelf and the English Channel fell dry and were dissected by river systems draining into the Atlantic Ocean (Fig. 1.2). Due to the sea level drop and increasing arid conditions deflation, coversand and loess deposition was enhanced (Bos et al. 2001), coupled with low precipitation (Huijzer and Vandenberghe 1998, Lauer et al. 2014). Westerly wind systems influenced dust transport (Renssen et al. 2007) with progressive coarsening between 30 and 22 ka BP (Antoine et al. 2009). Loess accumulated on top of fluvial sands and gravels at, e.g., the Weiße Elster (Lauer et al. 2014) and in the East Eifel at Tönchesberg or Remagen-Schwalbenberg (Frechen et al. 2003). Highest loess accumulation was determined along the Rhine River (Middle Rhine), e.g., at Wallertheim with 6930 $g \cdot m^{-2} \cdot a^{-1}$ and "Nussloch" with 1213-6129 $g \cdot m^{-2} \cdot a^{-1}$ (Frechen et al. 2003). The peaks of loess sedimentation were at ~ 25 ka BP (Antoine et al. 2009) and during the LGM (20 ka BP) according to Seelos et al. (2009).

Central European fluvial systems were characterized by incision during interstadials (onset of Middle Pleniglacial) and aggregation during stadials forming ephemeral streams with stable

channels (Kasse et al. 1998, Mol et al. 2000). At the transition to the LGM, the coldest period of the Weichselian, river floodplains were bare of vegetation and most ephemeral streams were replaced by high-energetic braided river systems (Kasse et al. 1998, Vandenberghe and Woo 2002), e.g., Weiße Elster (Lauer et al. 2014). A recent example for a braided river system is given from Iceland, Fig. 1.3.

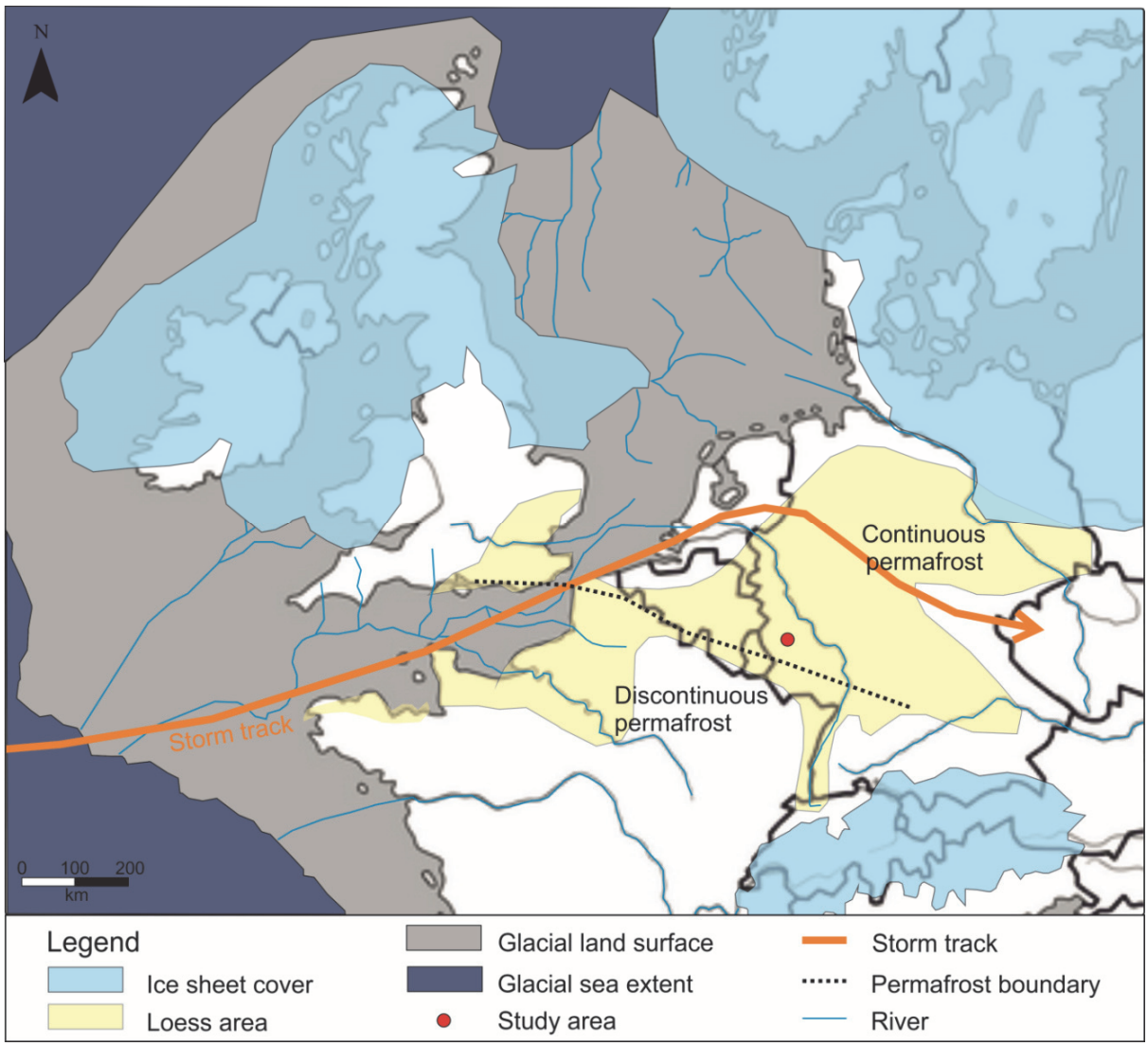

Fig. 1.2: Map shows the distribution of land surface (gray and white), ice sheet (blue) and sea (dark blue) during the LGM in Western and Central Europe compiled from maps by Antoine et al. (2009), Huijzer and Vandenberghe (1998), McNulty and Cookson (2012), Vandenberghe and Pissart (1993). Source: modified after stepmap.de.

Fig. 1.3: Recent braided river system at Skaftafell (left) and a U-shaped valley near Blönduós with grass-shrub vegetation, a braided river and snow patches (right) in Iceland (© L. Eichhorn 2014).

The mountainous West Eifel was influenced by permafrost with intense solifluction. Slopes and plateaus were covered by a mixture of angular frost-weathered regolith and fine-grained loess (Gebhardt 1963). The physical weathering of the Devonian greywackes and schists promoted solifluction movement in the tree-less tundra. In the quarry Merten (WGS84, 32 U, E: 345956; N: 5560932), the deposition structures of the Gemündener Maar tephra indicate strong winds from NW direction, flow structures were associated with solifluction (Frechen 1971). Wienecke (1979), and Büchel and Lorenz (1982) described ice-wedges in the Trautzberger Maar and Sprinker Maar tephra, and Mertes (1983) determined cryoturbation structures and polygonal cracks. During a field campaign in 2013, an ice-wedge pseudomorphosis was observed in the Wartgesberg quarry (Fig. 1.4).

Fig. 1.4: Ice-wedge pseudomorphosis in the Wartgesberg quarry (WGS84, 32 U, E: 352377; N: 5552712), (© G. Büchel 2013).

1.1.2 Study area in the West Eifel Volcanic Field

The study area is situated in the Alf Valley, 5 km southeast of the city Daun in the central part of the Rhenish Massif (Fig. 1.5). The catchment area is characterized by bedrock consisting of weakly metamorphic clay-, silt- and sandstones of the Siegenian (Saxler Formation) and Emsian stage (Eckfeld Formation) of the Lower Devonian (Meyer 2013), and the NE-trending Variscan "Siegen Thrust" (Langenstrassen 1983), Fig. 1.6.

These predominantly clastic sediments originate from the former Old Red continent and were slightly metamorphosed during the Variscan orogeny in the Carboniferous (Felix-Henningsen 1990). Permian to Cretaceous sediments were not preserved due to Tertiary uplift. The Tertiary is characterized by deep weathering forming the Mesozoic-Tertiary weathering mantle and erosion creating peneplains and troughs (Felix-Henningsen 1990, Löhnertz 2003, Meyer 2013). Since the Tertiary, the Rhenish Massif was uplifted by max. 200 m (in the study area ~ 120 m, Demoulin and Hallot 2009) which is caused by several reasons like (a) lithospheric folding due to compressional intraplate stresses related to the Alpine arc (Cloetingh et al. 2005), (b) lithospheric thinning beneath the Rhenish Massif (Prodehl et al. 1995) and (c) rising of the Eifel mantle plume (Ritter et al. 2001). Accelerated uplift occurred

since 800 ka with a rate of 0.16 mm · a^{-1} in differentiated blocks (Meyer and Stets 1998). Main center of uplift was the SE Eifel. The recent uplift amounts to 0.2 mm · a^{-1} (Demoulin and Hallot 2009).

During the Quaternary, the Rhenish Massif was affected by volcanism starting ~ 0.7 Ma BP and formed the East and West Eifel Volcanic Fields (WEVF) (Schmincke et al. 1983).

The study area is part of the WEVF which expands over 600 km² from Ormont to Bad Bertrich and contains ~ 250 eruption centers (66 % scoria cones, 30 % maars and tuff rings, 2 % scoria rings, 2 % pyroclastic vents, Büchel 1993). The eruption centers are clustered mainly along NW-SE and E-W striking linears (Büchel 1994) which are controlled by the present tensional litholospheric stress field (Schminke et al. 1983) (Fig. 1.5).

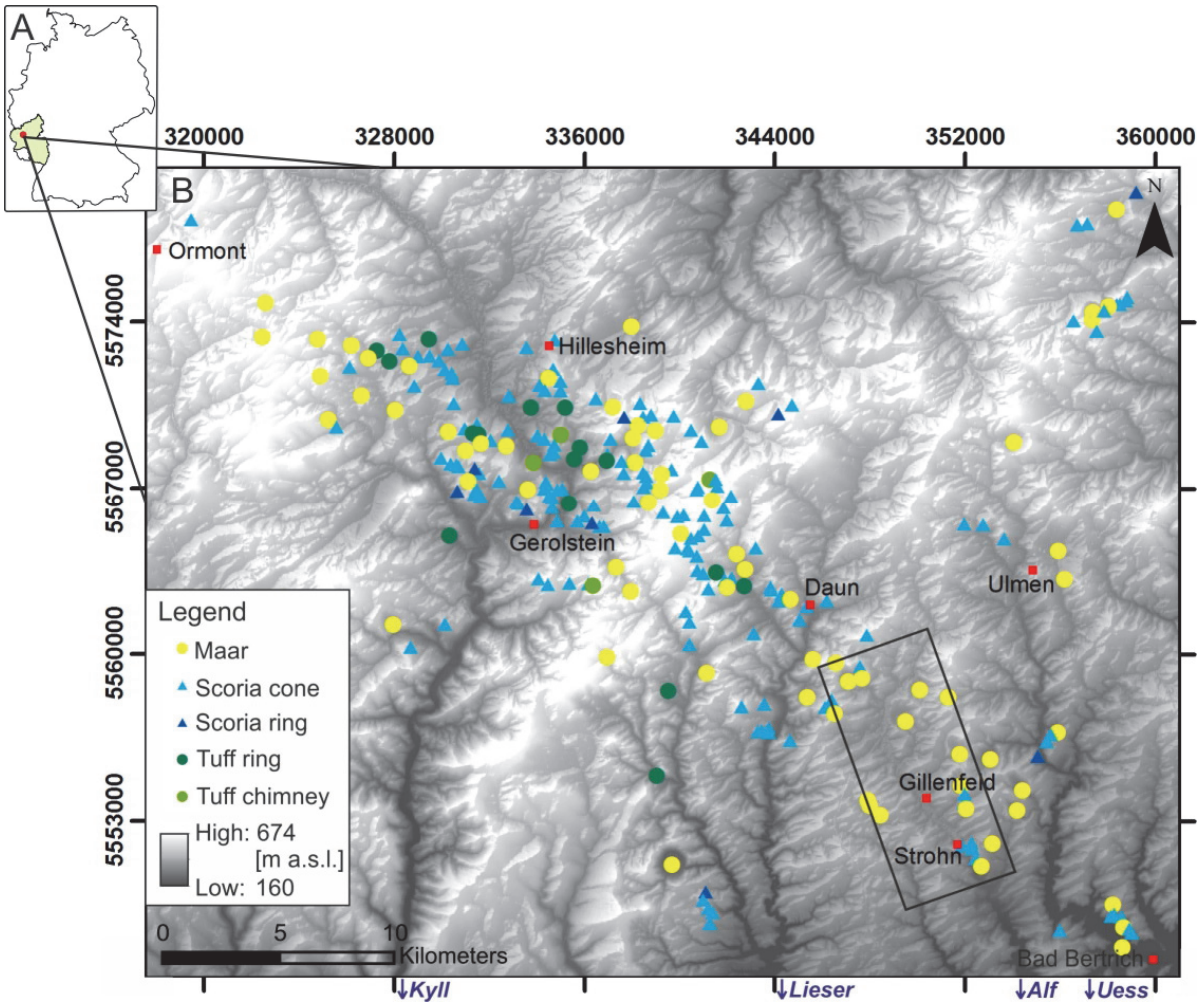

Fig. 1.5: (A) West Eifel Volcanic Field located in Germany (red dot) within the state of Rhineland-Palatinate (in green) showing eruption centers (B) concentrating around Hillesheim, Gerolstein, Daun and Gillenfeld after Büchel (1994) in NW-SE orientation. Main rivers are named and marked with a blue arrow indicating the flow direction. Black rectangle shows study area. Coordinates of this and further maps are given in meters of WGS 1984, UTM Zone 32N. DEM source: ©GeoBasis-DE / LVermGeoRP (2014).

The study area is part of the northern Alf Valley with an elevation between 550 and 390 m a.s.l. which belongs to the West Eifel low mountain range. It extends between the Dauner Maar Complex in the northwest, the Pulvermaar-Römerberg-Complex to the east and the Wartgesberg Volcano Complex to the southeast, see Fig. 1.6.

According to the effective "Köppen-Geiger classification", today this area belongs to maritime oceanic climate zone, type Cfb, (Kottek et al. 2006) with a mean annual air temperature of 8 °C and a precipitation of 774 mm, (Gillenfeld, www.climate-data.org). The oldest human-made tools found in the region originate from the Paleolithic (> 8000 a before Christ), first human settlements were established during the Mesolithic (8000-5000 a before Christ, Nakoinz 2001). Today settlements, extensive pasture farming, agriculture and forestry characterize the landscape consisting of peneplains (Löhnertz 2003) which are dissected by river valleys and volcanoes (Fig. 1.6).

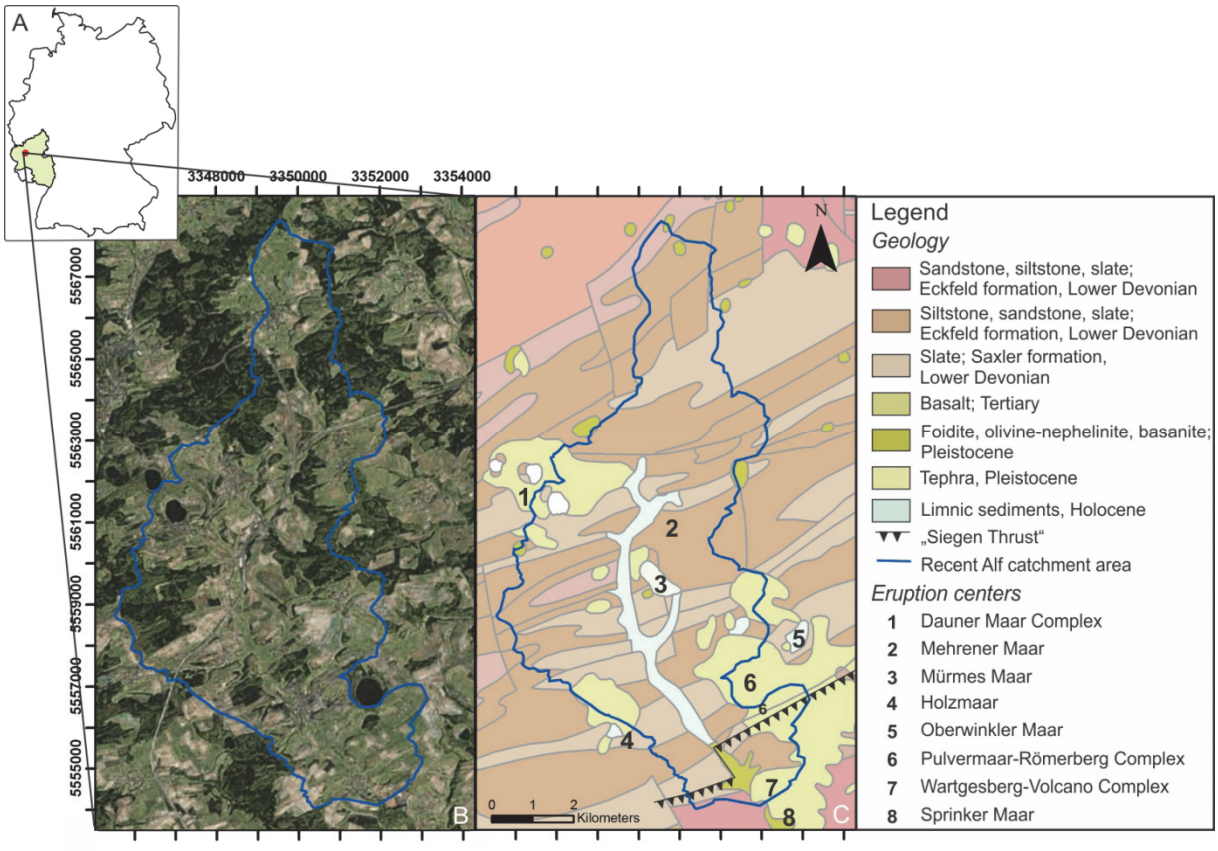

Fig. 1.6: Study area (A) located in the Alf Valley, within the state of Rhineland-Palatinate (in green) and the West Eifel Volcanic Field (red dot), is shown as satellite imagery (B) with the recent Alf catchment (Esri, DigitalGlobe) and with geology and eruption centers (C) (Büchel 1994, Zitzmann et al. 1987).

The oldest maars in the study area are Mehrener Maar (e.g., Wienecke 1979), Mürmes Maar (Büchel, pers. com. 2016), Meerfelder Maar (e.g., Woda 2000) and Oberwinkler Maar, (e.g., Sirocko et al. 2013), for ages see Table 1. Then, the Dauner Maar Complex erupted with the

Eastern and Western Schalkenmehrener Maar, Gemündener Maar and Weinfelder Maar (Hopmann et al. 1960, Schaber and Sirocko 2005, Woda et al. 2001) followed by the Wartgesberg eruptions (Mertz et al. 2015, Pirrung et al. 2007, this study) including Holzmaar (Brauer 1994, Negendank 1989) and Sprinker Maar (Schaber and Sirocko 2005, Table 1). Shortly after, the Pulvermaar-Römerberg Complex (including Strohner Maar) erupted (Büchel 1984, Zöller and Blanchard 2009). As shown in Table 1, volcanic activity was enhanced in the WEVF between ~ 0.4 and 0.01 Ma BP emitting mafic and silica-undersaturated magmas of the Foidite-suite like leucites and nephelinites (42 %), melilite-bearing foidites (32 %), e.g., Pulvermaar, and the olivine- nephelinite and basanite-suite (ONB): Basanites (8 %), e.g., Wartgesberg (Mertes and Schmincke 1985, Schmincke et al. 1983).

Table 1: Assumed order of eruptions in the study area (ESR: Electron Spin Resonance, (R)TL: (Red) Thermoluminescence, OSL: Optically stimulated luminescence, b2k: before 2000).

Name of eruption center	Method	Age [ka] BP	Reference
Mehrener Maar	Morphology	>100	Wienecke (1979)
Mürmes Maar	Morphology	~100	Büchel (pers. com. 2016)
Meerfelder Maar	^{14}C on charcoal	41.2	Schaber and Sirocko (2005)
	ESR on quartz	87±8	Woda (2000)
	^{40}Ar/^{39}Ar on glass	81±23	Leyk and Lippold (1997)
	TL on xenolith	42.3	Zöller (1989)
	Field observations	~Denekamp Interst.	Büchel and Lorenz (1982)
Oberwinkler Maar	^{14}C on bulk	64	Sirocko et al. (2013)
	^{14}C on bulk	23-52.6	Schaber and Sirocko (2005)
Dauner Maar Complex:			
Schalkenmehrener Maar	^{14}C on bulk	>27.8	Schaber and Sirocko (2005)
Gemündener Maar	ESR on quartz	30±4	Woda et al. (2001)
	Uran-Thorium on tuff	40±20	Meyer (1994)
	Field observations	Last Glacial	Büchel and Lorenz (1982)
Wartgesberg-Volcano Complex	^{14}C on humic acid	33 cal.	Eichhorn et al. (this study)
	RTL and OSL	33.6±0.4	Schmidt et al. (in prep.)
	Ice-core tuning + ^{14}C	27.9±2 b2k	Sirocko et al. (2016)
	^{40}Ar/^{39}Ar	31±11 (Plateau age)	Mertz et al. (2015)
	^{14}C on humic acid	31 cal.	Pirrung et al. (2007)
Holzmaar	^{14}C	28	Brauer (1994)
	^{14}C	29.5	Negendank (1989)
Sprinker Maar	^{14}C on bulk	24	Schaber and Sirocko (2005)
Pulvermaar-Römerberg Complex	TL	21±3	Zöller and Blanchard (2009)
	Morphology	15-20	Büchel (1984)

During the Middle Pleniglacial ~ 31±11 ka Plateau age (^{40}Ar/^{39}Ar, Mertz et al. 2015), the Wartgesberg Volcano Complex erupted in the Alf Valley inducing a dam of scoria and lava that impounded the Alf River and formed Paleolake Alf.

Over several thousand years, periglacial clastic material predominantly from the catchment accumulated in the Paleolake Alf basin forming a paleoenvironmental archive. Periglacial means that it is peripheral to the Pleistocene ice sheets or glaciers with seasonal presence of

freezing and thawing of the perennially-frozen ground or permafrost (French 2007). The volcanic dam in the Alf Valley prevented these trapped periglacial deposits from erosion. They are still preserved and visible in the recent valley morphology due to a flat valley bottom compared to the V-shaped neighboring valleys.

The Alf Valley shape anomaly in combination with the prominent Wartgesberg Volcano Complex was in the focus of several research investigations (Hemfler and Büchel 1991, Hopmann et al. 1960, Rahm 1958). Further, the Strohn lava flow originating from the Wartgesberg Volcano Complex was investigated by Cipa (1956), Wienecke (1979) and Lange (2014). The eruption age of the Wartgesberg Volcano Complex was determined by, e.g., Mertz et al. (2015) and Sirocko et al. (2016). Since the Strohn lava flow is an important aquifer for drinking water abstraction, several exploration wells and wells (16) were conducted since 1940. In this context, scientific interest on the fluvio-lacustrine sediment infill increased (Pirrung et al. 2007 and this study).

The particularity of the fluvio-lacustrine sediment archive of Paleolake Alf is its continuous persistence over 12,000 a covering the Middle to Late Pleniglacial (33-13.8 cal. ka BP with a hiatus between 21 and 16 cal. ka BP) due to a volcanic dam. This archive differs from the surrounding maar lake records e.g., Holzmaar (Brauer 1994) or Meerfelder Maar (Zolitschka 1989) due to its larger catchment area recording not only eolian deposition but also enhanced discharge by precipitation and meltwater, thus recording more regional environmental effects than the isolated maar lakes. A limnic paleoarchive caused by a volcanic dam was not studied in detail from Central Europe so far.

1.2 Objectives

This thesis aims to improve the understanding of paleoenvironmental changes during the Middle to Late Pleniglacial in the West Eifel Volcanic Field by sedimentological investigations focusing on transport media, deposition structure, and GIS modelling to reconstruct the paleosurface and to calculate denudation rates.

Therefore, the following overall research questions are addressed:

- Where does the sedimentary material come from, how does the basin architecture look like and how did the basin develop? (**Chapter 3)**
- What conditions and processes prevailed in the Alf catchment area and Paleolake Alf ? Is the clastic lamination (Fig. 1.7C) attributed to clastic varves (Fig. 1.7A, B)? (**Chapter 4)**
- How much material was deposited in the archive and how did the valley look like at the end of the Wartgesberg eruptions? **(Chapter 5)**

In order to define answers, sediment cores of the archive were studied by a combination of sedimentological, mineralogical, microscopic, geochemical and petrophysical methods. Further, samples for ^{14}C dating were taken; literature for comparison with present-day reservoirs and periglacial lake sediment structures was used. Finally, the recent catchment morphology was analyzed by geophysical surveys, remote sensing and GIS-based methods, and geological outcrops.

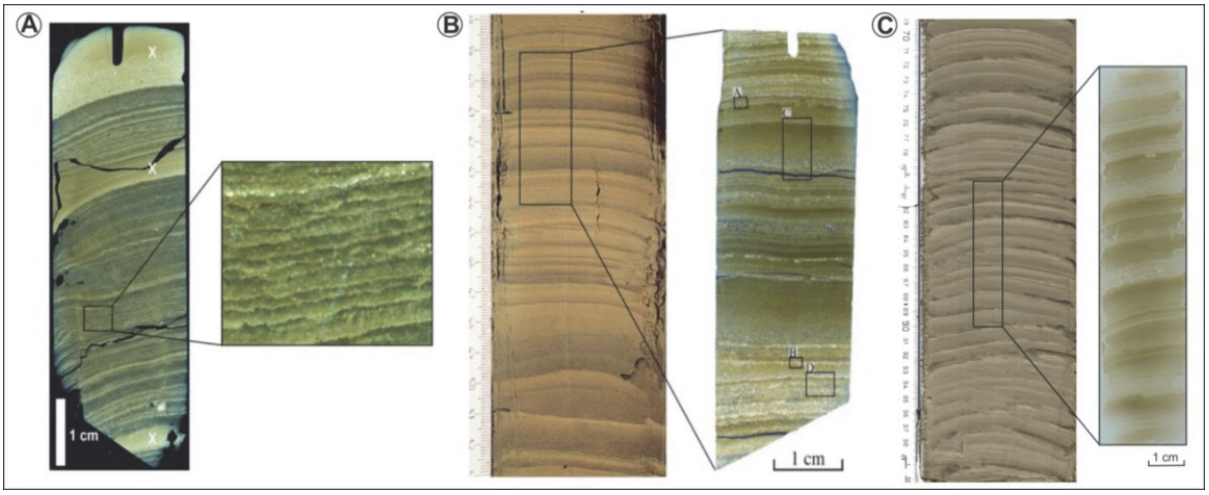

Fig. 1.7: Photos show clastic varves from the continuous permafrost region on Ellesmere Island, Canada: (A) Lower Murray Lake (Cook et al. 2009) and (B) Sawtooth Lake, (Francus 2008). Photo (C) presents lamination from Paleolake Alf (core 5807-91, this study) for comparison.

1.3 Thesis outline

This thesis is composed of five chapters. The introductory **first chapter** includes the site description, the scientific state-of-the-art and the research objectives.

In the **second chapter**, all applied methods are briefly described; further details are given in the context of the following three chapters that are based on manuscripts.

The **third chapter** deals with the basin architecture and the evolution of the Paleolake Alf archive. Several co-authors contributed to this chapter who are mentioned at the beginning as this chapter is a draft for a planned publication. The data were obtained by myself except for shear wave seismic data that were surveyed by U. Polom. XRF data were determined by S. Stahl in the laboratory of B. Zolitschka, clay mineralogy was determined by Andreas Bauer, and the magnetic survey was accomplished by T. Lange. The chapter was written by myself under the supervision of M. Pirrung and G. Büchel. Improvements were given by all co-authors.

The **fourth chapter** covers the question, whether the lamination can be characterized as varves and which sedimentary processes occurred in the lake and the catchment. The data were determined by myself except for the XRF data determined by S. Stahl in the laboratory of B. Zolitschka and XRD measurements obtained by R. Bolanz and M. Wierzbicka-Wieczorek. The chapter was written by myself under supervision of M. Pirrung and G. Büchel. Improvements were given by all co-authors. This chapter is another draft for a publication which will be resubmitted soon.

The **fifth chapter** investigates the paleosurface reconstruction of the Alf Valley and includes the volume calculation of the Strohn lava flow and the sediment infill. The chapter was written by myself and supervised by M. Pirrung and G. Büchel. The GIS model was created by J. Engelhardt and myself. Magnetic survey data were included from T. Lange and refraction data processing was conducted by M. Henschen. Co-authors are mentioned at the beginning as this chapter is a further draft for a planned publication.

The main results of this thesis are summarized in the **sixth chapter** (synthesis) also including an outlook to future research in the Alf Valley.

Chapter 2

2. Material and Methods

In order to tackle the research questions regarding sediment origin, process reconstruction, basin architecture and sediment quantification, a multiproxy approach containing field surveys, sedimentological, microscopic, geochemical, geophysical and GIS–based investigations was applied.

2.1 Sediment analysis

For this study, 28 core lithologies and descriptions from the State Office for Geology and Mining in Rhineland-Palatinate (Mainz), the State Company for Mobility Rhineland-Palatinate (Trier and Gerolstein), the Water Supply Company Cochem-Zell and the Engineering Company "Wasser und Boden GmbH" (Boppard) were available. The cores were drilled in the Alf Valley between 1940 and 2014. Their data are summarized in an MS Excel file containing archive number, x- and y-coordinates (WGS 1984 UTM Zone 32N), elevation, and lithologic units with thickness. Therefore, the material was classified into 10 simplified lithotypes: topsoil, gravel, sand, silt, clay, clay-silt-rhythmic unit, mafic scoria, mafic ash, mafic lava and Lower Devonian siliciclastic rocks. In some cases, layer descriptions consisted of complex notes like "coarse clay mixed with fine sand and silt, less pebbly". Then, the dominating fraction (first component) was used to define the lithotype. Due to the partial lack of precise coring positions provided by drilling companies in the 1940s that used topographic or cadastral maps for localization, the still visible coring locations (5807-24, -25, -26, -27) were re-measured in the field using a Differential Global Positioning System by Dr. K.-H. Köppen, Engineering Company "Wasser und Boden GmbH", (Table 2).

In this study, the following three cores 5807-91, 5807-B8 and 5807-89 were analyzed in detail (Fig. 2.1) and later compared to results of core 5807-70, investigated by Pirrung et al. (2007). They were drilled using wireline drilling (diameter: 110 mm) by H. Anger's Söhne Bohr- und Brunnenbaugesellschaft mbH, Hessisch Lichtenau, commissioned by the Water Supply Company Cochem-Zell.

The upper- and lowermost parts of the cores were stored in wooden boxes covered with a plastic film, whereas most of the fine-grained, clay-silt rhythmit units were kept in plastic liners. After coring, all cores were stored in the water works Strohn. First, lithological descriptions applying engineering geology criteria were performed by Dr. K.-H. Köppen. Therefore, the liners were cut on two sides to remove a ~ 6 cm wide calotte.

Table 2: Core labeling and coordinates. Altitude refers to ground surface at the coring site.

Core	Year	Max. Depth [m]	Altitude [m a.s.l.]	UTM coord.		Geographic coord.	
				E	N	Latitude	Longitude
5807-70	2006	37	392	350223	5554406	50°7.378'N	6°54.280'E
5807-91	2012	40	391.3	350587	5553848	50°7.083'N	6°54.598'E
5807-B8	2014	29	391.7	350721	5553926	50°7.127'N	6°54.709'E
5807-24	1958	50.5	391.0	351325	5553210	50°6.750'N	6°55.232'E
5807-25	1958	57.7	389.9	351353	5553303	50°6.800'N	6°55.253'E
5807-26	1958	52.5	392.1	351251	5553361	50°6.830'N	6°55.166'E
5807-27	1958	31	390.1	351151	5553465	50°6.885'N	6°55.080'E
5807-88	2012	21	404.3	348480	5557822	50°9.194'N	6°52.736'E
5807-89	2012	29	400.7	348573	5556967	50°8.734'N	6°52.835'E
5807-90	2012	17	398.3	349209	5555730	50°8.077'N	6°53.398'E

Several months later, all cores were transported to Jena, the wooden boxes were stored at room temperature and the plastic liners in a climate chamber (York International) at 10 °C at the Institute for Geosciences, Department Mineralogy at the Carl-Zeiss-Promenade 10. In order to get a better overview of the core cross sections, the liners of core 5807-91 were wet-cut using a diamond saw blade and tab-water at the mason Spaete GmbH in Jena. The sediments of core 5807-B8 were fresher and softer and could be split using a snell. After core splitting and lithological description, halves of the cores 5807-91 (10) and 5807-B8 (17), with a total length of 27 m, were digitally photographed using the high resolution DMT Core-Scan® from GFZ Potsdam at the INFLUINS Drilling site in Erfurt (Appendixes A.1, A.2).

2.1.1 Grainsize

Granulometry was determined at the sediment laboratory of the Institute of Geosciences Jena. Grainsizes of up to 300 µm (core 5807-91: 6.75-22.97 m) were determined using the Laser Particle Sizer "analysette 22" (Fritsch GmbH, Germany) on 43 fresh sediment samples. For each measurement, between 30 and 60 g of fine-grained wet sediment was mixed with distilled water and natrium pyrophosphate (20 g per liter) for dispersion. After homogenizing, grains of diameters between 0.31 and 300 µm were measured. Volume-specific grainsize distribution-data were calculated based on the Fraunhofer-/Mie-theory (Fritsch).

36 sediment samples with grains > 300 µm were oven-dried (core 5807-91: 1.7-5.4 m, 24.5-31.3 m; core 5807-89: 0.5-25.5 m). For each measurement ~ 100 g of weighted sample material was dry-sieved for 15 minutes in a vibratory sieve shaker (Fritsch GmbH, Germany) using metal sieves (Retsch GmbH) with mesh sizes of 63, 200, 630 and 2000 µm. From these samples, the mass-specific grainsize distribution was determined.

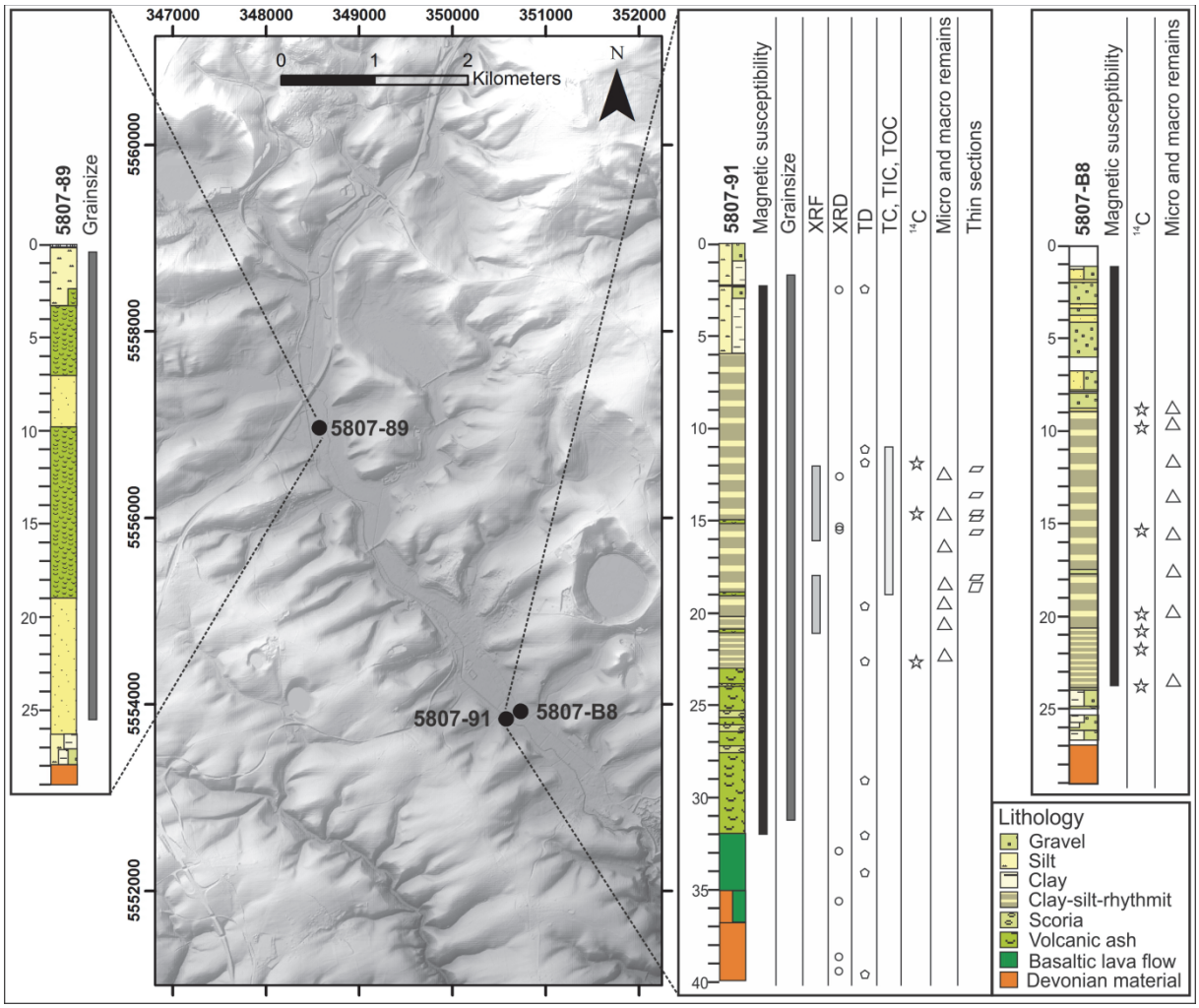

Fig. 2.1: Study area showing the three analyzed core locations with core sections analyzed by several methods (XRF: X-ray fluorescence, XRD: X-ray diffraction, TD: Total digestion, TC: Total carbon, TIC: Total inorganic carbon, TOC: Total organic carbon). DEM source: ©GeoBasis-DE /LVermGeoRP (2014).

2.1.2 Magnetic susceptibility (volume-specific)

The volume-specific magnetic susceptibility κ was detected on cores 5807-91 (2.2-32 m, 2309 data points) and 5807-B8 (1.1-23.89 m, 1785 data points) using the Bartington Instruments "MS2" system, Oxford, England (Dearing 1994) at the Institute of Geosciences Jena. For fine-grained sediments (clay to fine-sand fraction), the split sediment core surface was smoothed with a metal scraper and covered with thin wrapping film (MultiTEC). Then, the measurement was carried out using the Bartington point sensor MS2El (High Resolution Surface Scanning Sensor). Drift correction was done using air as reference level (0) after every five sediment measurements. For coarse-grained material like tephra, the whole core was measured using the Bartington ring sensor MS2C (125 mm internal diameter) if the core recovery was > 90 %. Drift correction was done as mentioned above. All in all, 4094 points

were measured; sensor values given in the Centimeter Gram Second (CGS) system were converted into the International System of Units (SI) using the formulas:

$$\text{Point sensor: } \kappa^{SI} = (\kappa^{CGS}.\ 4\pi)$$

$$\text{Ring sensor: } \kappa^{SI} = \frac{\kappa^{CGS}.\ 4\pi}{1.64^{1}}$$

[1] core diameter correction factor determined using a chart provided by the manufacturer; κ values are displayed in 10^{-6}.

2.1.3 Element contents by means of X-ray fluorescence (XRF)

X-ray fluorescence (XRF) scan data were obtained using an ITRAX XRF core-scanner (Cox Analytical systems, Sweden, Croudace et al. 2006) at the laboratory of B. Zolitschka, GEOPOLAR (University of Bremen) by S. Stahl. The measurement was carried out on a single line scan on a subsampled minicore (U-channel) with the Mo-tube at settings of 20 kV, 10 mA and 10 s exposure time on core 5807-91. Core meters 12-16 m, 18-21 m with 5 mm (1402 data points) and 15-16 m with 200 µm (4936 data points) vertical resolution were chosen due to the presence of regular, horizontal lamination without or with rare event layers. Measured elements (Al, Si, P, S, Cl, Ar, K, Ca, Ti, V, Cr, Mn, Fe, Ni, Cu, Zn, Ga, As, Br, Rb, Sr, Y, Zr, Ba, Ta, W, Pb, Fe^{2+}, Fe^{3+}, CO_1, CO_2) were summarized in an MS Excel file. Element data produced by the scanner are semi-quantitative and are expressed as total counts (cnts), i.e. integrated peak area. Element data were normalized against Mo coh to account for matrix differences and displayed with a 5 point running mean.

2.1.4 Mineralogy by X-ray diffraction (XRD)

X-ray diffraction (XRD) was examined using a diffractometer (Bruker D8 AXS Advance DaVinci) at Cu Kα radiation (λ = 1.54058 Å) at the Institute of Geosciences Jena. Therefore, samples were dried, ground, homogenized and placed on a plastic sample-holder by Bruker with exception of individual laminae. Due to the few amount of a single lamina sample material, the fresh sediment of the light and dark laminae was dispersed with ethanol on a silicon single crystal sample-holder (911) by Bruker. Eight bulk samples were analyzed from core 5807-91 containing gravel (depth: 2.4 m), light and dark laminae of the silt-clay rhythmic sequence (12.7, 15.3, 15.4 m), scoria (32.9 m) and Devonian rocks (35.6, 38.9, 39.5 m), e.g. in Fig. 2.2. Diffraction data were collected between 5 and 130 °2θ with a step size of 0.02 °2θ and a dwell time of 10 s. For noise reduction from Fe-fluorescence, the energy window of the detector was set to 0.18-0.25 V. All samples were

matched by a full-profile fit with the program DifracEVA® version 4.0 using the database PDF-2 released in 2011.

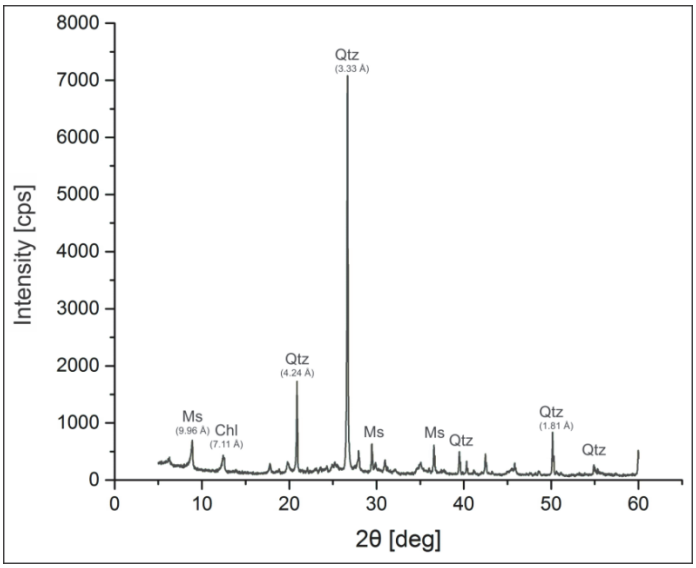

Fig. 2.2: X-ray diffractogram of a dark lamina at 15.375 m depth from core 5807-91 shows diffraction reflexes identified as quartz, muscovite and chlorite.

Clay mineralogy

Clay fraction separation was done by F. Linde on four samples of core 5807-91 (depth: 13.5, 16.5, 15.5, 22.6 m) at the sediment laboratory of the Institute of Geosciences Jena using Atterberg cylinders (Fischer Scientific). The time of settling rate (Stoke's Law) was adjusted to room temperature. Natrium pyrophosphate (20 g per liter) was added for dispersion. Sample preparation including Sr^{2+} saturation and XRD measurement was done by A. Bauer at the Institute for Nuclear Waste Disposal (INE) Karlsruhe Institute of Technology (KIT), Eggenstein-Leopoldshafen, according to Bauer et al. (2006) and Finck et al. (2015).

2.1.5 Total and (in)organic carbon

Total carbon (TC) and total inorganic carbon (TIC) measurements were carried out by I. Hilke using a VarioMaxCN analyzer (Elementar, Germany) at the Max Planck Institute for Biogeochemistry in Jena. Hand-ground (agate mortar and pestle) material of 36 samples was weighted to ~ 250 mg (core 5807-91, 11.1-19.1 m depth) and filled in sample holders, which transferred the samples into a combustion tube filled with tungsten trioxide (WO_3) heated to a temperature of 1100 °C. After quantitative oxidation, the sample passed a second combustion tube heated to 900 °C. Then, the gas mixture was reduced in a tube filled with tungsten and heated to 830 °C. Nitrogen and carbon dioxide were separated by the "purge and trap" principle quantifying first nitrogen, then carbon dioxide in a thermal conductivity detector.

For the TIC measurement, the same procedure was applied on the retained sample, after removing carbonate with non-oxidizing acid for (5 % HCl). For accuracy and reliability of the results, glutamine acid (Merck KGaA Germany) and certified reference soil material 1.1 (HEKAtech GmbH Analysentechnik, Germany) were measured after every 20th sample as a standard. Samples were measured twice. The standard deviation for measured C was between 0.28 and 1 %. Total organic carbon (TOC) was indirectly quantified by subtracting TIC from TC.

2.1.6 Radiocarbon dating

AMS-Radiocarbon measurements were carried out via accelerator mass spectrometry (AMS) using the 3 MV Tandetron 4130 AMS at the Leibniz-Laboratory for Radiometric Dating and Isotope Research in Kiel, Germany, as described by Nadeau et al. (1997). The analysis was applied on extracted humic acids (HA) and leaching residues (LR) for 10 bulk samples of the cores 5807-91 (depth: 11.9 (LR), 14.6 (LR), 22.8 (LR, HA)) and 5807-B8 (8.9 (LR), 9.8 (LR), 15.3 (HS, LR), 19.9 (HS, LR), 20.9 (HA, LR), 21.8 (HA, LR), 23.8 (HA, LR)). The conventional radiocarbon ages were converted into calibrated calendar years (cal. a BP) by applying the online software CALIB 7.1 (Stuiver and Reimer 1993) using the IntCal13 calibration dataset (Reimer et al. 2013).

For establishing a composite age-depth model, a linear interpolation between the calibrated calendar mean values was used. The age-depth model presented in this study is only based on ^{14}C dates of the humic acid fraction extracted from bulk and wood as their ages fit better to the eruption ages of the Wartgesberg Volcano Complex, dated by Sirocko et al. (2016) and Mertz et al. (2015), whereas leaching residue ages seem to be several thousands of years too old. Therefore, the age-depth-model contains one sample of core 5807-91, five samples from core 5807-B8, and another seven samples of core 5807-70 (Pirrung et al. 2007). Core-to-core correlation was conducted using core lithologies, magnetic susceptibility and one marker layer (ML) (Fig. 2.4).

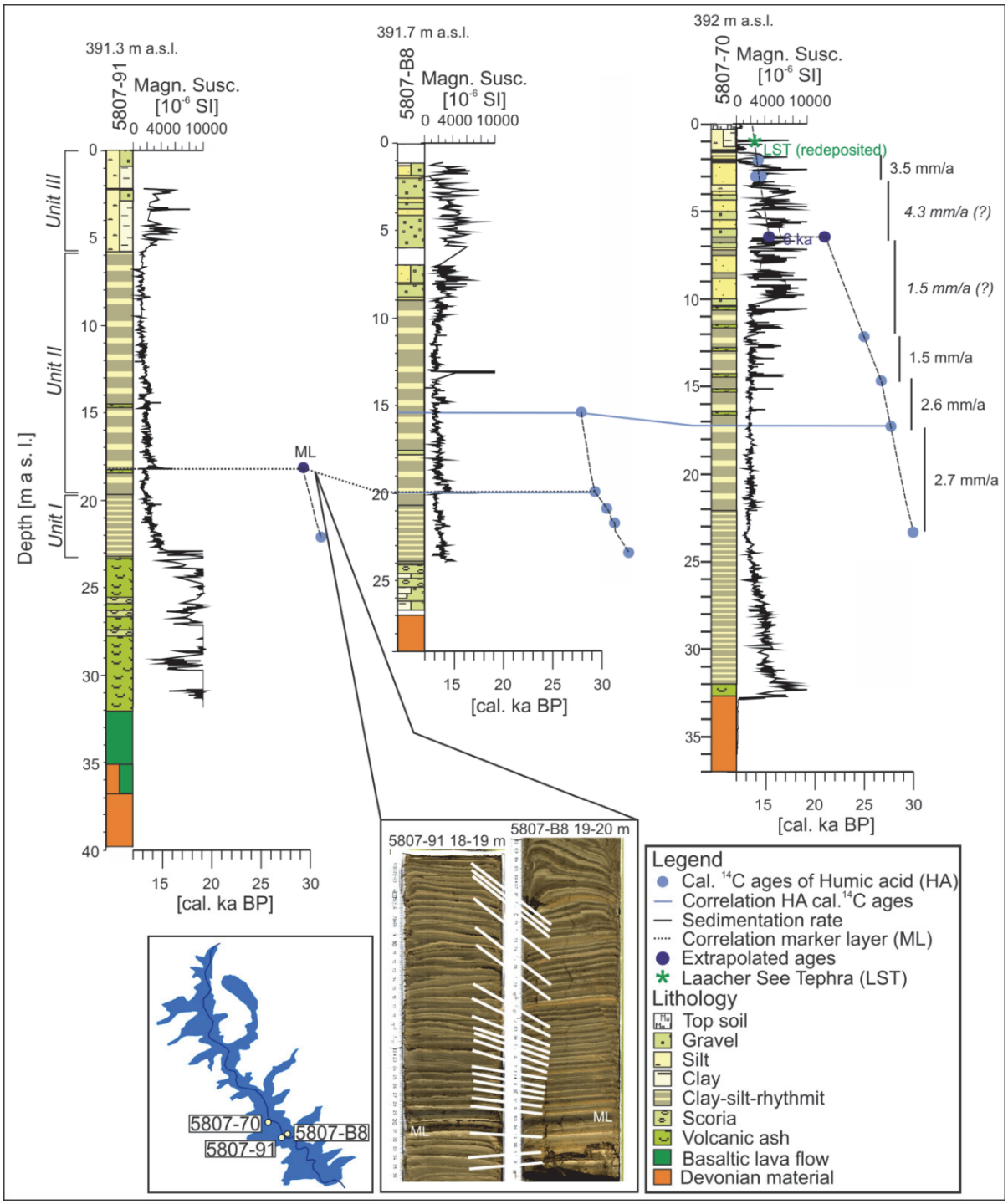

Fig. 2.3: Core-to-core-correlation using humic acid ^{14}C ages and a marker layer is displayed. Sedimentation rates of *Units II* and *III* were extrapolated. *Units I* and *II* cover a period between 33-21 cal. ka BP, *Unit III* between 14.2 and 13.8 cal. ka BP. Core location (bottom left) and marker layer correlation (bottom middle) is inserted.

2.1.7 Micro remains

Micro and macro remains were extracted from 16 samples taken at 1-2 m distance. Therefore, 20 ml of fresh sediment from the cores 5807-91 (depth: 12.5, 14.5, 16.3, 18.3, 19.4, 20.6, 22.2 m) and 5807-B8 (8.8, 9.7, 11.7, 13.5, 15.6, 17.5, 19.8, 21.6, 23.3 m) was wet-sieved using metal sieves (Retsch GmbH) with mesh sizes of 200 and 630 µm. Sieve residues were rinsed in an evaporating dish using deionized water and dried in a drying oven (WTC Binder GmbH) at 40°C for three days. The micro and macro remains were picked in the picking tray S 370 (Krantz) using the Zeiss Stevi DV4 stereomicroscope (Carl Zeiss Microscopy GmbH Jena, Germany), a moist needle and a synthetic brush (daVinci). For documentation, two valves of each ostracod species *Candona neglecta* and *Cytherissa lacustris* were critical point-dried, glued on a sample holder and sputter-coated with gold. Scanning electron microscopy (SEM) was carried out by S. Meschner with a FEI Philips XL30 ESEM at 10 kV (Philips, Amsterdam, Netherlands) using the software *Scandium* with a working distance between 23.4 and 24 mm, probe size 3 and magnification of 76 x at the Institute of Systematic Zoology and Evolutionary Biology with Phyletic Museum Jena, Fig. 2.5.

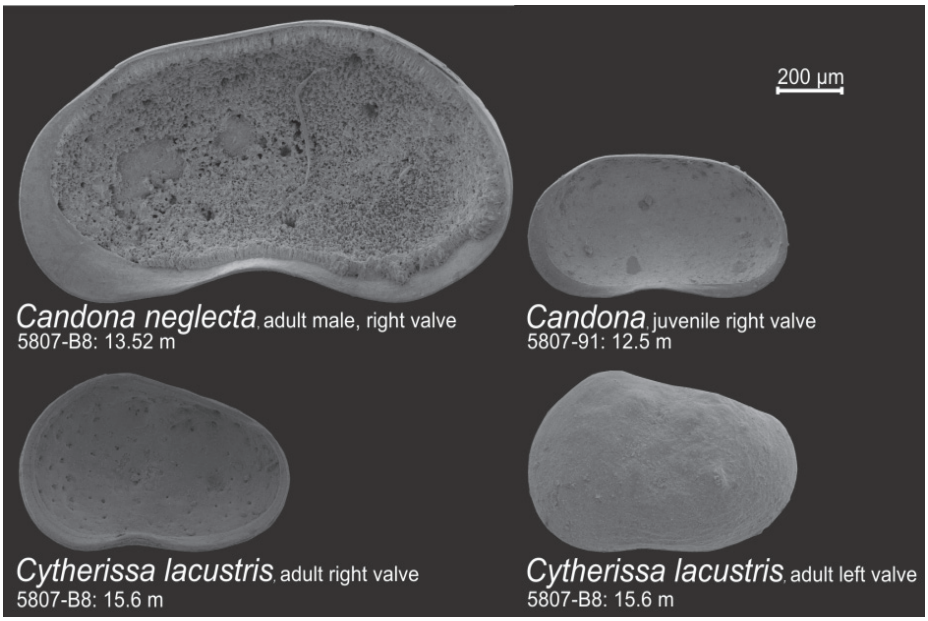

Fig. 2.4: SEM micrograph of ostracod species *Candona neglecta* and *Cytherissa lacustris* found in cores 5807-91 (depth: 12.5 to 18.3 m) and 5807-B8 (8.8 to 17.5 m), identified by P. Frenzel.

2.1.8 Thin sections and microfacies

Six large format sediment slabs (10 x 2 cm) with 2 cm overlap were cut from core 5807-91 between 18.48 and 18.90 m depths due to regular lamination (Figs. 2.6A, B). The samples were shock-frozen using liquid nitrogen for three to five minutes, put in manually-folded

aluminum moulds and freeze-dried for 44 h starting with a temperature of -51 °C. The freeze-dried samples were impregnated with epoxy resin Araldite 2020 using the proportion of 100 g resin to 30 g hardener (Huntsman U.S.A.). A vacuum was applied to extract air bubbles and to allow the resin to penetrate even into the fine pores of the sediment. All further steps concerning cutting, mounting and polishing of the impregnated sediment slabs to a sample thickness of 30 µm were carried out by MKfactory at Potsdam Golm. The final thin sections were sealed with a glass cover (Fig. 2.6C). Microfacies analysis was carried out under plain and crossed light with magnifications between 5 x and 40 x using a petrographic microscope Axioplan 2 (Carl Zeiss Jena GmbH, Germany). Thin section images were taken with a microscope-mounted digital camera (KYF75U, JVC) and the AxioVision (Rel. 4.8) software, Fig. 2.6C.

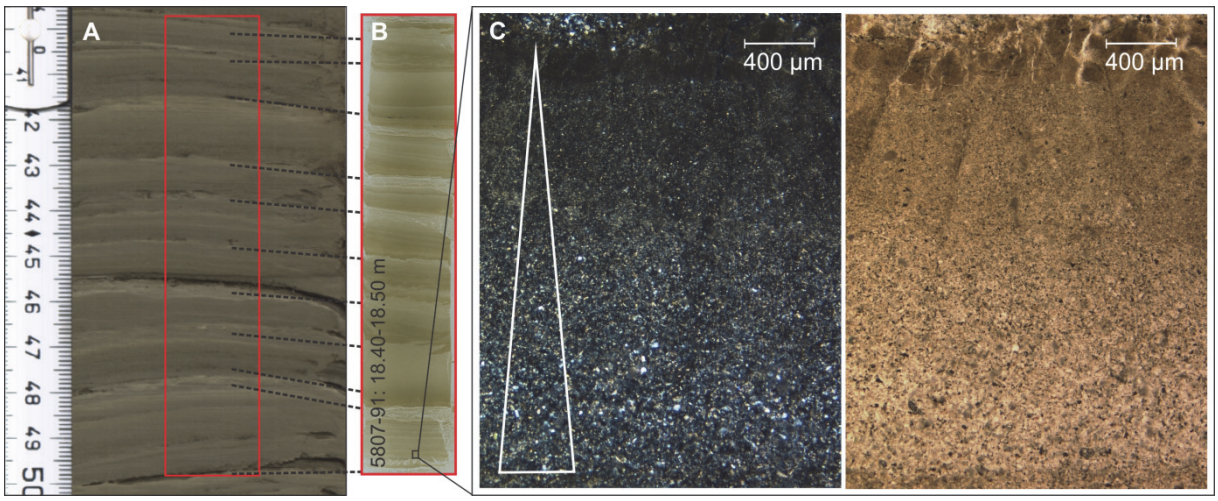

Fig. 2.5: Core scan photo (A) with correlated thin section (B) and a magnified detail of the normal grading structure of the lamination (C) is shown under crossed nicols (left) and plain polarized light (right).

For small thin section embedding (4 x 2.5 cm) of two ash layers at the Institute of Geosciences Jena, sediment pieces were cut from the core and inserted into folded aluminum boxes. The air-dried samples were impregnated as stated above. After all sediment pores were saturated, the samples were put under vacuum. After five days the samples were hardened and the aluminum box removed. The samples were polished on one side and a microscope slide was fixed on this polished surface. Then, the samples were cut and polished to 30 µm thickness.

2.2 Geophysical survey

2.2.1 Total field of magnetic intensity and magnetic susceptibility

In order to investigate the intensity of the Strohn lava flow total magnetic field anomaly, a magnetic survey was carried by T. Lange, diploma student at the Institute of Geosciences Jena (Lange 2014). Background of the measurement is that the lava flow containing olivine, augite, nepheline, hauyn and magnetite minerals (Hopmann et al. 1960) has a higher volume-magnetic magnetic susceptibility (4000-6000*10^{-6} SI, this study) in contrast to the Devonian bedrock (1000-2000 · 10^{-6}, this study). The total magnetic field anomalies over the lava result from its higher magnetization of ferrimagnetic magnetite minerals caused by both natural induction of the magnetic field of the earth and by natural remanence (Thompson and Oldfield 1986).

In 2014, the Strohn lava flow was measured in transects (2326 data points) with a horizontal measuring point distance of ~ 40 m using the proton magnetometer GSM-19 (GEM-Systems, Canada) after Telford et al. (1991) with a magnetic measurement accuracy of ± 0.2 nT (GEM systems) and a GPS accuracy of ± 3-5 m (Fig. 2.7). For drift correction, another proton magnetometer was utilized as base station. The data were pole-reduced by M. Queitsch after Baranov and Naudy (1964) as remanence is in direction of the magnetic field of the earth, using the declination- and inclination-calculator from IGRF2010 (Finlay et al. 2010) in combination with the software *Oasis montaj* by *geosoft*.

2.2.2 Shear wave seismics

The shear wave reflection seismic survey was carried out by Dr. U. Polom and co-workers from the Leibniz Institute for Applied Geophysics, Hannover, in three phases in August 2007 (P1), September 2007 (P2), and March 2008 (P3), Fig. 2.7. The three profiles were measured using the microvibrator ELVIS version 4.0 as seismic source (Rode and Cramm, 2007, Druivenga et al. 2005). The electrodynamically-driven horizontal shaking unit of this vibrator was mounted below a wheelbarrow frame carrying the battery pack which acts as primary hold-down force, supported by the operators' weight. Using a shaking direction perpendicular to the seismic profiling it emits horizontally-polarized shear waves (SH-waves). For data recording, a land streamer unit was used consisting of 120 horizontal geophones (SH configuration, type SM6 10 Hz resonance frequency) in 1 m intervals attached to a GEODE (Geometrics Inc., San Jose, CA, U.S.A.) recording system. Source interval was set to 4 m due to the observed data quality during the survey, resulting in an average Common Mid Point

(CMP) coverage of 15-fold. A linear sweep of 10 s duration with 30-240 Hz was used as source signal. At each source location two source excitations of alternating polarity were applied and stacked vertically subsequent to the vibroseis correlation process. Recording duration was set to 12 s resulting in 2 s listen time after correlation. Main steps of data processing included the application of an Automatic Gain Control (AGC), band pass filtering, Normal Move Out (NMO) correction, CMP stacking, Finite Difference (FD) time migration and depth conversion using a velocity field derived from NMO stacking velocities, which was evaluated by the results of the well 5807-70 (GWM1), see also Krawczyk et al. (2013).

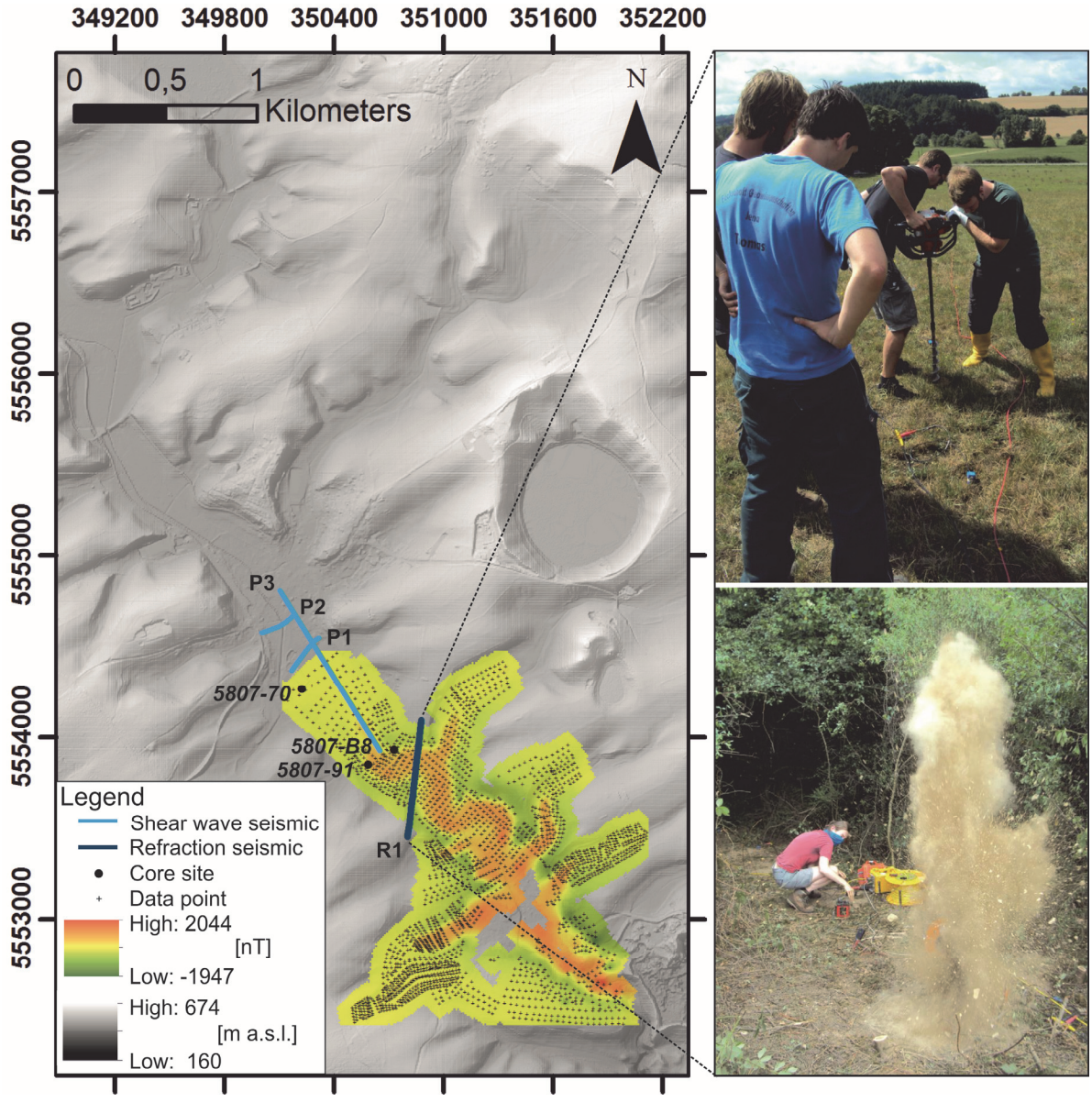

Fig. 2.6: Study area showing the four seismic profiles (shear wave seismic: P 1-3; refraction seismic: R1) and points of pole-reduced total magnetic field data (Lange 2014). Photographs display field work from refraction seismic survey. DEM source: ©GeoBasis-DE /LVermGeoRP (2014).

2.2.3 Refraction seismics

The refraction seismic survey was realized in a field campaign of nine members (students, PhDs, Postdocs) under coordination and assistance of M. Paschke and L. Eichhorn in summer 2015. Here, a 672 m long cross profile (R1, Fig. 2.7) was measured between the towns Strohn and Gillenfeld using the Seismic Impulse Source System (SISSY) (Geosym GmbH, Germany) and a seismograph system (Geometrics, U.S.A.) consisting of 336 geophones à 10 Hz. The investigation was carried out using a seismic source (Dynergit, 20 x 67 mm, 28 g NC-Basis) every 10 m, which detonated in boreholes at ~ 0.5 m depths. The source was recorded over 3 s with a sampling interval of 0.5 ms at all geophones aligned at a horizontal spacing of 2 m. Data processing for travel time tomography was carried out by the diploma student M. Henschen in 2016. Therefore, bandpass filtering at boundaries 0, 20, 150, 220 Hz was done to better identify the *P*-wave first arrivals that were picked using the software *zplot* (Zelt and Barton 1998). The inversion was applied to data of clear first *P*-wave arrivals using travel time tomography with the software *fast*. Using the results of the first inversion, synthetic data were processed from forward modelling in *zplot* in order to identify first arrivals in greater offsets which were used for a second inversion (Zelt and Barton 1998).

2.3 GIS modelling

GIS modelling was realized in cooperation with J. Engelhardt between 2014 and 2016. In order to reconstruct the Alf Valley to the end of the Wartgesberg eruptions which is the starting point for the river impoundment and the main lake stage including the initial lake bathymetry, and to determine the Strohn lava and Paleolake Alf sediment volume, a 3D model was created using ArcGIS (ArcMap, ArcCatalog, ArcScene) Version 10.2 (ESRI, U.S.A.). The input parameters for this model were (Fig. 2.8):

(1) Digital elevation model (DEM): 5 m x-,y-resolution from the State Office for Land Survey and Geobasis Information Rhineland-Palatinate

(2) Geophysical surveys: Shear wave seismic: Dr. U. Polom (2007/2008)
Total magnetic field intensity data: T. Lange (2014)
Refraction seismic: M. Henschen (unpublished data)

(3) Core lithologies: State Office for Geology and Mining in Rhineland-Palatinate, Mainz; State Office for Mobility Rhineland-Palatinate, Trier and Gerolstein; Water Supply Company Cochem-Zell; Engineering company “Wasser und Boden”, Boppard; Straka (1975)

(4) Eruption centers and tephra distribution after the volcanological map of Büchel (1994)

(5) Elevations of the Wartgesberg Volcano Complex before the Wartgesberg quarry activity after the topographic map (Reichsamt für Landesaufnahme 1936).

2.3.1 Surface reconstruction

The reconstruction of the Alf Valley (I) with the dam consisting of the Strohn lava flow (V) and scoria of the Wartgesberg Volcano Complex (IV) starts below the 410 m contour line which marks the assumed (see Chapter 3 for arguments) maximum lake level (Fig. 2.8). The infill was extracted from the DEM by deleting the inner valley contour lines. In addition, the recent contour lines from Mürmes Maar (II), Pulvermaar- Römerberg Complex (III) and Wartgesberg Complex (IV) were eliminated (see Fig. 2.8).

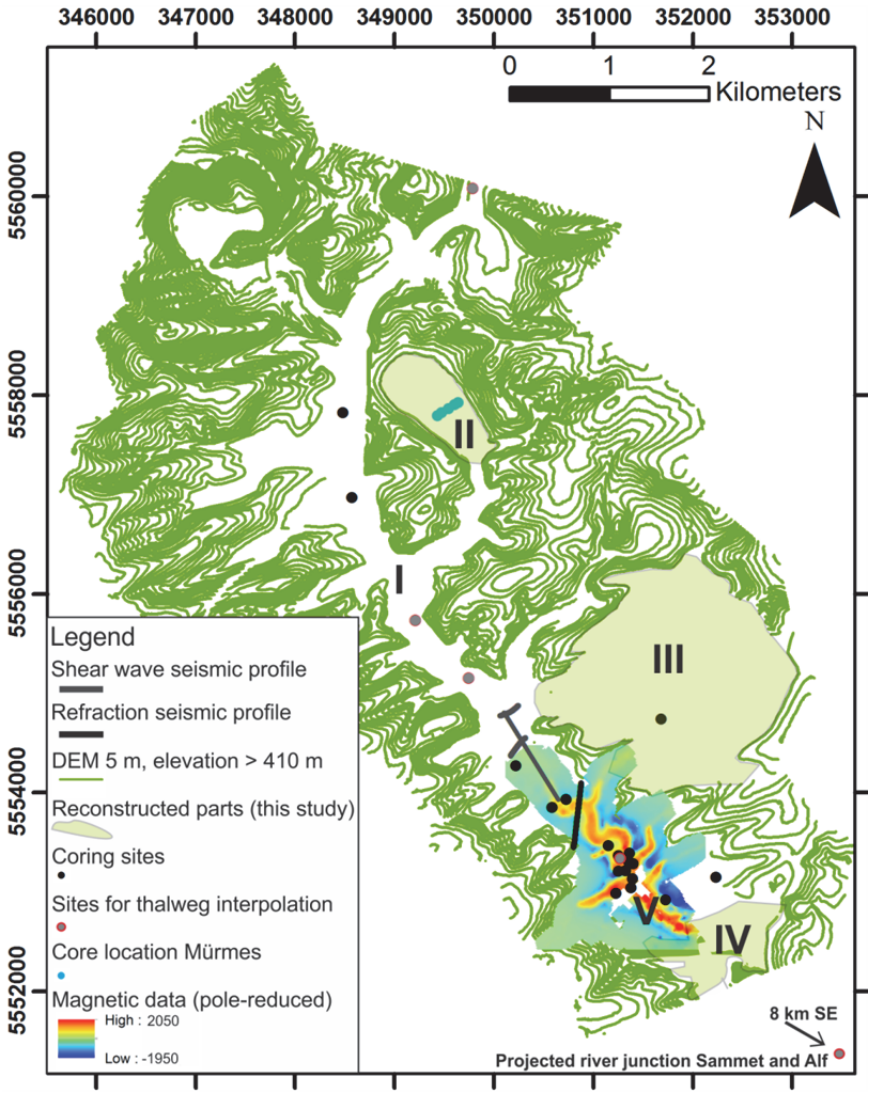

Fig. 2.7: Input parameters for the 3D reconstruction are dispalyed: (1) DEM with 5 m horizontal resolution, (2) total magnetic filed intensity data (Lange 2014) and (3) coring sites with lithologies from Alf Valley, Pulvermaar and Mürmes Maar (Straka 1975) including sites for thalweg reconstruction. Roman numerals mark the reconstructed parts: I-Alf Valley, II-Mürmes Maar, III-Pulvermaar-Römerberg Complex, IV-Wartgesberg Complex, V-Strohn lava flow. One point is situated out of the map at the junction of the rivers Sammet and Alf (x = 354202.7188; y = 5545033.4362).

Reconstruction Part I: Alf Valley

First, all “big” artificial constructions like highways were eliminated from the recent DEM above 410 m.

The reconstruction of the Paleo Alf thalweg shape was conducted using magnetic data of the Strohn lava flow (village Strohn and 2.5 km to the north) as it can be assumed that the lava traced the pre-dammed thalweg. This Strohn lava flow was determined by Cipa (1958) and Wienecke (1979), and was remeasured in a recent geomagnetic survey (Lange 2014). North of the Strohn lava flow, 16 core lithologies, refraction seismic data, shear wave seismic data and morphology information from the DEM were utilized to determine the thalweg shape.

To reconstruct the depth of the former Alf thalweg, the elevation of two points outside of the dammed lake area were taken (at Mehren and at the junction of river Alf and Sammet) where Devonian bedrock crops out (Büchel, pers. communication, 2015, Fig. 2.8). Further, Devonian bedrock information of the three core lithologies 5807-90, 5807-2 and 5807-26 was considered because these drillings are located close to the reconstructed thalweg. Then, the bedrock information of these five points was interpolated using the ArcGIS Geostatistical Analyst: *Inverse Distance Weighting, with the Power: 1*.

Both, the thalweg shape and depth information were transferred to 18 cross profiles which were drawn using the DEM from ridge or valley to ridge or valley vice versa (Fig. 2.9A). The spatial information of these cross profiles was extracted from ArcGIS and imported to CorelDRAW. By fitting the “Top Devonian bedrock” depths from the core lithologies in the profiles and under consideration of the reconstructed depth of the Alf thalweg and morphological indications like visible preserved erosion banks or slip-off slopes in the DEM, the initial shape of the dammed valley was reconstructed drawing polylines (Fig. 2.9B). In a next step, the reconstructed polylines were imported into MS Excel. Here, z-values from the recent DEM were replaced by new z-values that fit the reconstructed polyline (Fig, 2.9C, colored contour lines). Importing these new z-values into ArcGIS, values of similar height were connected by manually-drawing contour lines under consideration of morphology (Fig. 2.9C).

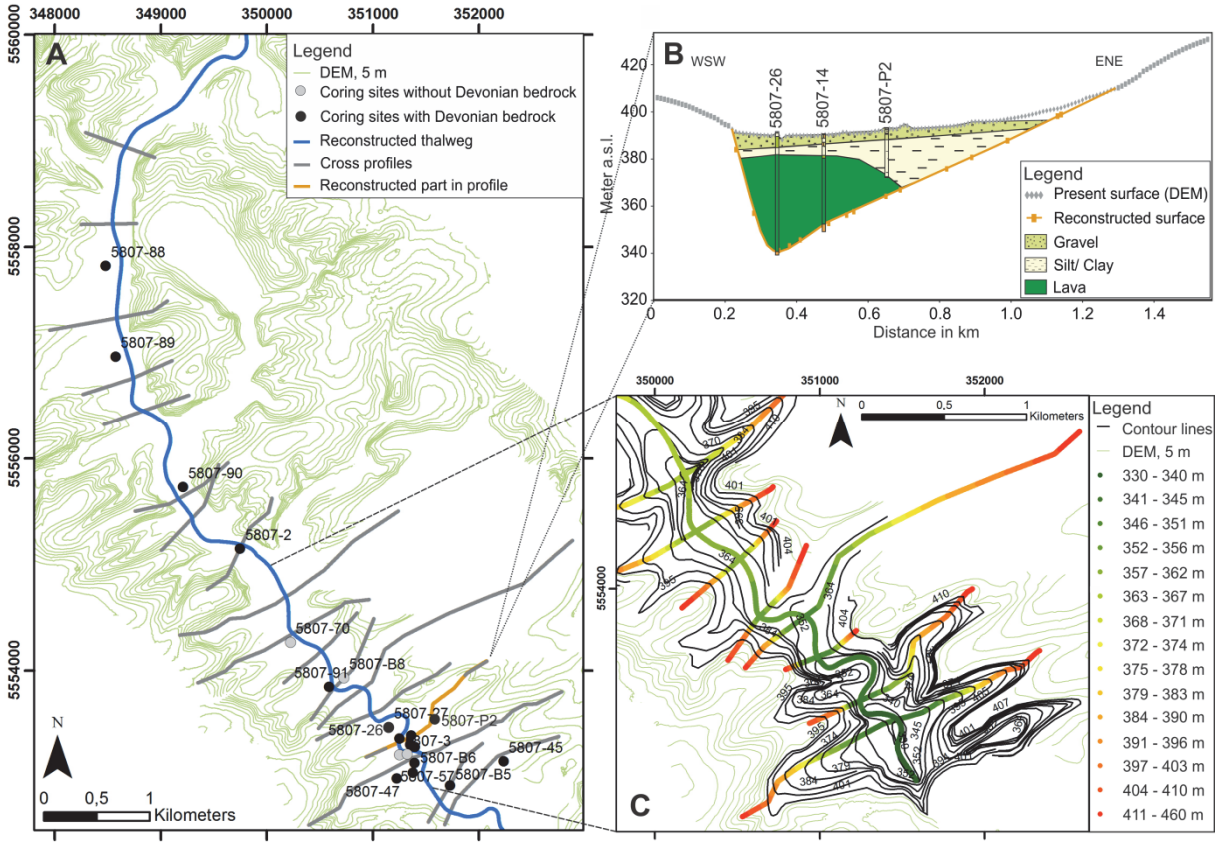

Fig. 2.8: Cross profiles are displayed with reconstructed thalweg after the end of the Wartgesberg eruptions and coring sites (A). One 2-dimentional cross profile with present surface beyond the valley floor (gray), reconstructed lower valley slope (orange) and core lithologies are presented in B. Resulting manually-drawn contour lines (black lines) from reconstructed cross profile depths are shown in C.

Reconstruction Part II: Mürmes Maar

The Mürmes Maar was reconstructed without sediments younger than 10 ka BP. Straka (1975) drilled at five locations into the Mürmes Maar sediment infill and described the uppermost six meters as peat with organic silt und fine volcanic particles. Conventional ^{14}C datings on Pollen grains revealed ages of ~ 12.5 ka BP for which reason this sequence was extracted from the current DEM. The underlying coarse volcanic tephra was considered as paleosurface for the 30 ka BP reconstruction model. Therefore, the depth information on the top of the coarse volcanic tephra was used and combined with cross profiles (Fig. 2.10). Then, present DEM z-values were replaced by the new z-values from the core lithologies, exactly as described for the main Alf Valley.

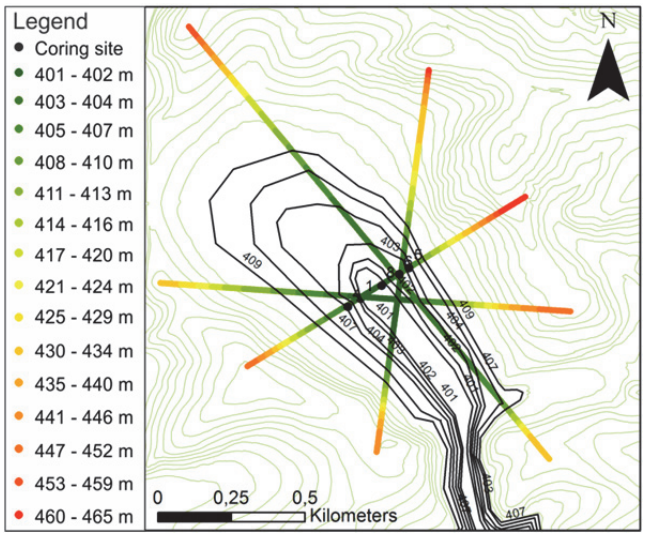

Fig. 2.9: Reconstruction shows the Mürmes Maar at the end of the Wartgesberg eruptions. Coring sites of Straka (1975) are shown with cross profile and manually-drawn contour lines (black lines).

Reconstruction Part III: Pulvermaar-Römerberg Complex

Due to the fact that the Pulvermaar-Römerberg Complex (Büchel 1984, Zöller and Blanchard 2009) is younger than the Wartgesberg Volcano Complex, the pre-eruptive morphology was reconstructed using Devonian bedrock outcrops from quarries, former tributaries and one core lithology. The grayish polygon in Fig. 2.11A indicates the boundary of the Pulvermaar ash deposits according to Linnebacher (1985). As the two northern depressions in the crater wall (Fig. 2.11A, 1) were documented as tributaries by Linnebacher (1985), Büchel and Lorenz (2016, pers. comm.), their thalweg downstream of their junction was placed through the deepest part of the present crater wall ending in the valley of the Römerberg. Due to the present valley-shaped depression north of the Römerberg (Fig. 2.11A, 2) the tributary was reconstructed straight through the recent eruption center of the Römerberg as it did not exist at ~ 31 ka BP. The manually-drawn contour lines (Fig. 2.11B) of the peneplain were created connecting the recent DEM altitudes with the point information (colored polygons and core lithology) in accordance to surrounding altitude information of the recent DEM.

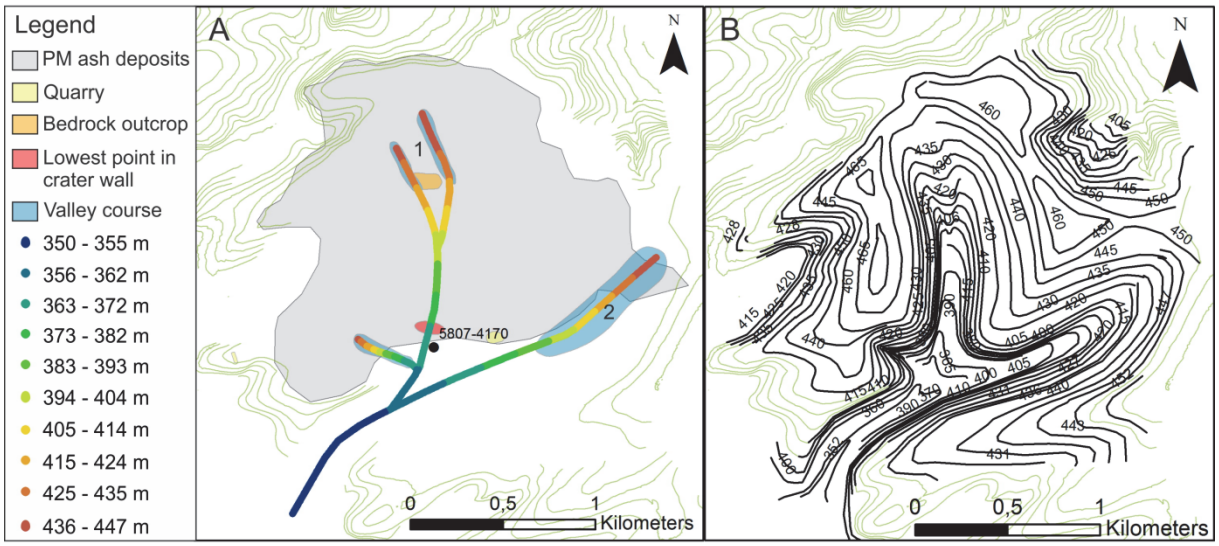

Fig. 2.10: Reconstruction shows the landscape before the eruptions of the Pulvermaar-Römerberg Complex: (A) presents core lithology with reconstructed valley courses and B shows the resulting manually-drawn contour lines (black lines).

Reconstruction Part IV: Wartgesberg Volcano Complex

The Wartgesberg Volcano Complex was reconstructed based on a topographic map 1: 25 000 (Reichsamt für Landesaufnahme 1936), field observations like scoria dipping from Krause (1984) and my own, and occurrence of red scoria, e.g., Büchel (1994). The topographic map of 1936 shows the Wartgeberg Volcano Complex before the present quarry with four major hills (Fig. 2.12A **a, b, c, d**). The hills **a** (known as Körperichberg)**, b** and **c** (part of the "Lange Klopp"), essential for the Alf impoundment, were interpreted as parts of two former eruption centers. Field observations revealed welded scoria at Körperichberg (**a**) and Lange Klopp (**c**) indicating direct proximity to the volcanic chimney, hill **b** does not exist anymore but was mapped by Büchel (1994) with welded scoria. Combining these obersvations with z-values from the topographic map, two eruption centers (Fig. 2.12B 1,2) were reconstructed with black contour lines.

Before reconstructing the lava flow, all reconstructed lines and the DEM contour lines above 410 m were merged into a raster using the ArcGIS tool *Topo to Raster* creating the Alf Valley at the end of the Wartgesberg Volcano eruptions just before the ejection of the Strohn lava flow.

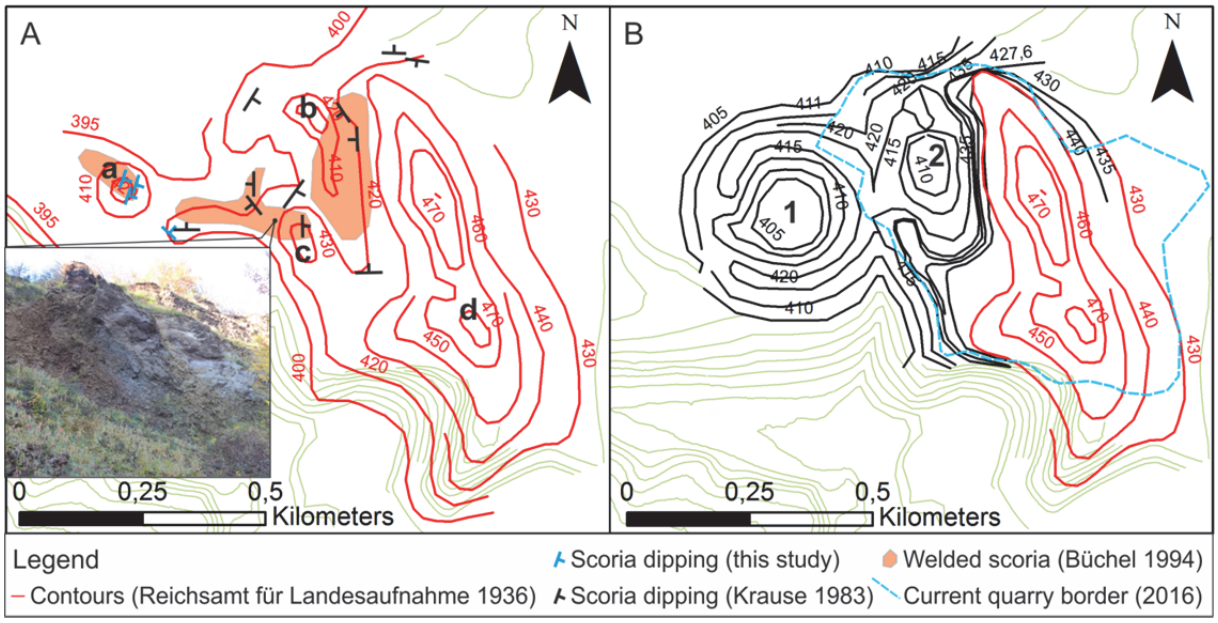

Fig. 2.11: Reconstruction shows the Wartgesberg Volcano Complex before the outflow of the Strohn lava flow. (A) displays contour lines from topographic map by Reichsamt für Landesaufnahme (1936) (red lines); scoria dipping information after Krause (1984) and own field measurements; and mapped areas of welded scoria (Büchel 1994). Foto (© G. Büchel 2015) shows welded scoria of the reconstructed eruption center in (B), taken from the Wartgesberg quarry in southwestern direction. (B) shows the resulting manually-drawn contour lines (black lines) of the reconstructed northernmost eruption centers 1 and 2 of the Wartgesberg Volcano Complex and parts of the contours from the topographic map (red lines). For orientation, the current quarry border was added.

Reconstruction Part V: Strohn lava flow

The Strohn lava flew upstream over a distance of > 1 km most likely due to a fissure that opened in the NW part of the scoria wall. For the reconstruction of the Strohn lava flow, the z-values “Top lava” of 16 core lithologies and the geomagnetic total field intensity data for lava extension were utilized to manually draw contour lines (Fig. 2.13).

In addition, the reconstructed valley contour lines had to be removed where contour lines of the reconstructed lava existed. Finally, all reconstructed lines were merged again creating a raster representing the former Alf Valley topography after the end of the Wartgesberg eruptions and after the outflow of the Strohn lava.

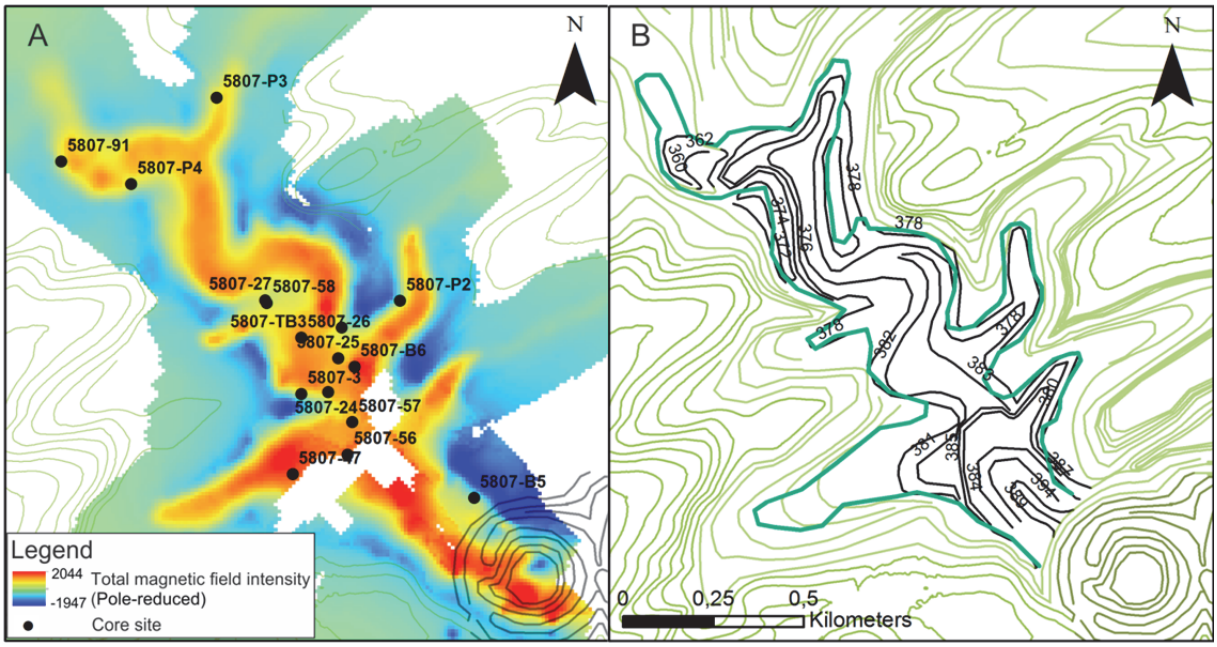

Fig. 2.12: Reconstruction of the Strohn lava flow is shown. Core sites and pole-reduced total magnetic field intensity data (Lange 2014) as input parameters are displayed in (A). (B) shows manually-drawn contour lines (black lines) of the reconstructed Strohn lava flow with border of total magnetic field intensity for orientation (cyan line).

2.3.2 Volume calculation

In order to define the volume of irregular bodies of, e.g., the Strohn lava flow and the Paleolake Alf sediment infill, two raster data sets can be subtracted from each other. First, the two raster data sets have to be of equal size by creating a new polygon using the ArcGIS tool *Clip*. Then, both raster data sets have to be transformed to a triangulated irregular network (TIN) using the ArcGIS tool *Raster to TIN* with a z-tolerance of 0.25 m. Finally, one TIN is subtracted from the other using the tool *Surface Difference* or *Extrude Between*.

Chapter 3

3. Basin architecture of lava-dammed Paleolake Alf (Quaternary West Eifel Volcanic Field) compared to modern reservoirs

Chapter 3 corresponds to a planned publication with the listed co-authors.

Luise Eichhorn[1], Michael Pirrung[1], Thomas Lange[1], Ulrich Polom[2], Bernd Zolitschka[3], Andreas Bauer[4], Karl-Heinz Köppen[5], Georg Büchel[1]

[1] *Friedrich Schiller University Jena, Institute for Earth Sciences, 07749 Jena, Germany,*
[2] *Leibniz Institute for Applied Geophysics, 30655 Hannover, Germany*
[3] *University of Bremen, Institute of Geography, 28359 Bremen, Germany*
[4] *Karlsruhe Institute of Technology, Institute for Nuklear Waste Disposal, 76344 Eggenstein-Leopoldshafen*
[5] *Engineering Company Wasser und Boden GmbH, 56154 Boppard-Buchholz, Germany*

Abstract

Dams can form temporal sediment traps used as paleoenvironmental archives but also bear natural hazards due to a sudden dam collapse. In this study, the lava-dammed Paleolake Alf, situated in the West Eifel Volcanic Field, is investigated in order to describe the lake basin architecture and how it compares to modern artificially-dammed lakes or reservoirs. In addition, the reason for the disappearance of Paleolake Alf is focused. Therefore, core lithologies are studied; grainsize is determined; sediment structures and ^{14}C-dates are analyzed. Sediments are predominantly composed of clastic catchment material including volcanic components reflected in the mineral composition. Fluvially-transported top- and bottomset sediments can be distinguished by coarser grainsizes at the Alf inlet and finer particles in the basin center, respectively. The lake persisted from ~ 33 cal. ka to minimum ~ 21 cal. ka BP. After that, Paleolake Alf most likely disappeared due to a combination of backward erosion and dam failure due to intense discharge event. This is indicated by an abrupt grainsize change, interpreted as hiatus, from silt-sized lacustrine sediments which are partially eroded to covering sand-sized fluvial sedimentation.

3.1 Introduction

Dams transform rivers into lacustrine ecosystems and affect the hydrological, physical, chemical and biological characteristics (Friedl and Wüest 2002). These lacustrine ecosystems can serve as paleoenvironmental archives but can also pose major natural hazards after a sudden dam collapse (Dunning et al. 2006, Vuichard and Zimmermann 1987). The persistence of dams depends on its volume, geometry, inflow rate and most importantly its material composition. Primary formed dams e.g. from glacier ice, ignimbrites, scoria or lava are solid and can resist erosion for a time span of months to thousands of years (Capra 2007). In contrast, dams built of secondary, reworked material like landslides, debris avalanches, lahars or moraines (Costa and Schuster 1988) mostly fail minutes to days after their formation because of their loose components (Clague and Evans 1994, Costa and Schuster 1988). In this study a fluvio-lacustrine sediment archive is presented, formed by a volcanic dam. This dam consists of agglutinates of the Wartgesberg Volcano Complex that erupted in a chain of eruption centers around 31±11 ka BP (Plateau age of $^{40}Ar/^{39}Ar$ on groundmass of low-SiO_2 lava, Mertz et al. 2015) during the Weichselian Middle Pleniglacial and immediately prior to the Last Glacial Maximum (LGM). Because of this dam, the Alf River was impounded leading to a dendritically-shaped lake. The composition of the dam built of lava and scoria and its geometry entirely filling the V-shaped valley are both preconditions for building a lacustrine archive that covers the Weichselian Middle to Late Pleniglacial. The basin is characterized by an elongated shape and a large catchment area compared to modern lakes in the West Eifel like the Holzmaar (2 km²) or Meerfelder Maar (5.8 km², Negendank and Zolitschka 1993) in the vicinity.

The focus of this investigation is a description of the basin architecture of Paleolake Alf and how it compares to modern reservoirs. Further, the reason for the disappearance of Paleolake Alf should be addressed. Therefore, the evolution of the sediment infill-process is reconstructed with regard to present-day mechanisms like flood events (Kämpf et al. 2012), the impact of drawdowns, and the evolution of prograding deltas in recent reservoirs (Snyder et al. 2006).

3.2 Material and Methods

In order to describe the basin architecture and to discover hints for the disappearance of Paleolake Alf, lithologies and descriptions of nine cores from the Alf Valley (5807-88, 5807-89, 5807-90, 5807-2, 5807-70, 5807-91, 5807-B8, 5807-26, 5807-B6) are analyzed. Further,

sedimentological structures (macroscopic from core scans and microscopic from small thin sections) as well as sedimentological (magnetic susceptibility, grainsize) and geochemical (C-analysis, XRF, XRD clay mineralogy) parameters are investigated of core 5807-91. Grainsize data of core 5807-91 is compared to core 5807-89 to discover distal and proximal sediment delivery. Sediment structure of core 5807-91 is compared to core 5807-B8 to distinguish the influence of slope transport into the lake basin. Radiocarbon age dating is applied to create an age model of the Paleolake Alf archive. Shear wave seismic is utilized to reconstruct the basin shape. All mentioned methods are described in detail in Chapter 2.

3.3 Results

In order to reconstruct the former lake extension, bedrock ridges were examined to detect lake terraces using a DEM in 5 m resolution. However, no terraces could be observed most likely due to continuing solifluction processes during the last glaciation and Holocene human impact. As a Devonian bedrock ridge northwest of the Wartgesberg Volcano Complex has a height of 412 m and water did not regressively erode into this neighboring tributary (Fig. 3.1) it is assumed that the paleolake level was at maximum 410 m a.s.l.. Using this assumption, the reconstructed Paleolake Alf had an estimated catchment area of 55 km², a maximum depth of 50 m and a lake surface area of estimated 8.2 km².

Basin architecture

The valley basin bedrock composes of Lower Devonian sand- and siltstones. Due to the Wartgesberg eruptions, the northern part of the paleo Alf Valley was partly filled by the Strohn lava flow that started with a thickness of ~ 58 m from a center south of Strohn and was flowing 2.6 km in northwest direction due to a dam further south as documented by core lithologies (5807-91, -26, -B6), an outcrop at the Strohner Mühle (Fig. 3.1, A) and a geomagnetic survey (Lange 2014). Around Strohn, this lava flow was covered by ~ 20 m of scoria, residual parts are still preserved at “Körperichberg” (Fig. 3.1, B) and “Lange Klopp” (Fig. 3.1, C).

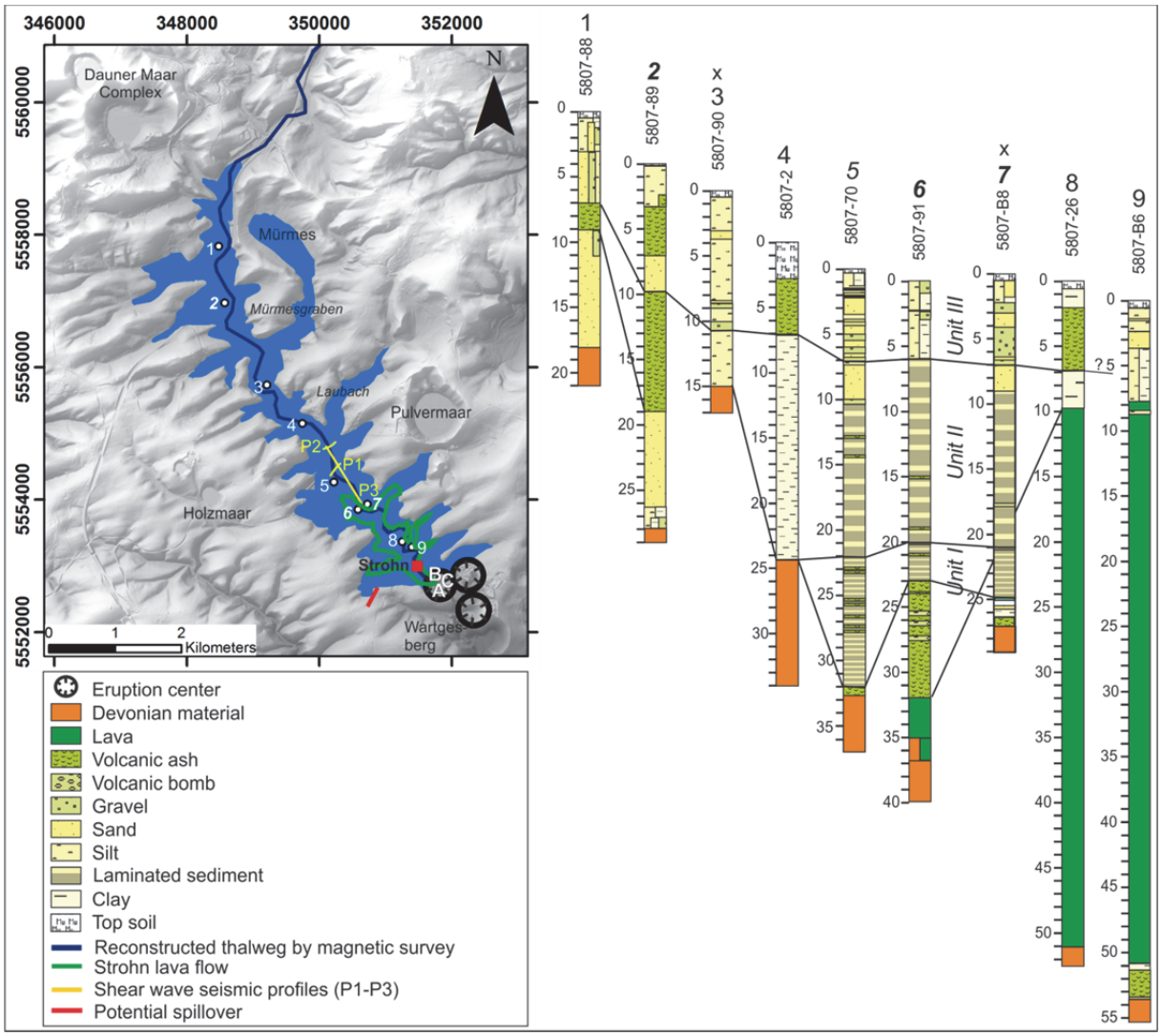

Fig. 3.1: Study area with the reconstructed Alf thalweg and the Paleolake Alf shore line at 410 m a.s.l. combined with core locations (white letters), shear wave seismic profiles and the Strohn lava flow. The volcanic dam is indicated by black circles. The core lithologies were displayed at the present ground level, "X" represents cores that are not located on the thalweg. Italic and bold numbered cores were studied in detail.

Close to the base of the dam, bedrock is covered by basaltic lava, redeposited ash and scoria (Fig. 3.2, Lithology bar). This volcanic material is overlain by clay-rich silt with a mean grainsize of ~ 6 µm (on average: 21 % clay, 78 % silt, 0.08 % sand) with (sub)millimeter laminae forming *Unit I*. This *Unit I* is intercalated by 30 cm-thick slump structures, silt extraclasts of up to 45 mm (Fig. 3.2D) and 30 mm-thick homogeneous sand layers. The thicknesses of *Unit I* differ from ~ 10 m in core 5807-70 and to ~ 3 - 4 m in cores 5807-91 and 5807-B8 (Fig. 3.1). *Unit I* is covered by silt-sized material containing ~ 0.8 cm thick laminae (dark: 10 µm and light: 6 µm grainsize) of *Unit II* (for more details, see Chapter 4). *Unit II* reveals a thickness of ~ 14 m in cores 5807-70, 5807-B8 and 5807-91 (Fig. 3.1). Both units contain illite/ smectite and kaolinite reflected in the clay mineralogy. The lamination is

interrupted by turbidity layers (Fig. 3.2B), debris layers (Fig. 3.2C) and redeposited distinct ash layers at depths of 14.5 and 18.3 m (Fig. 3.2E, F).

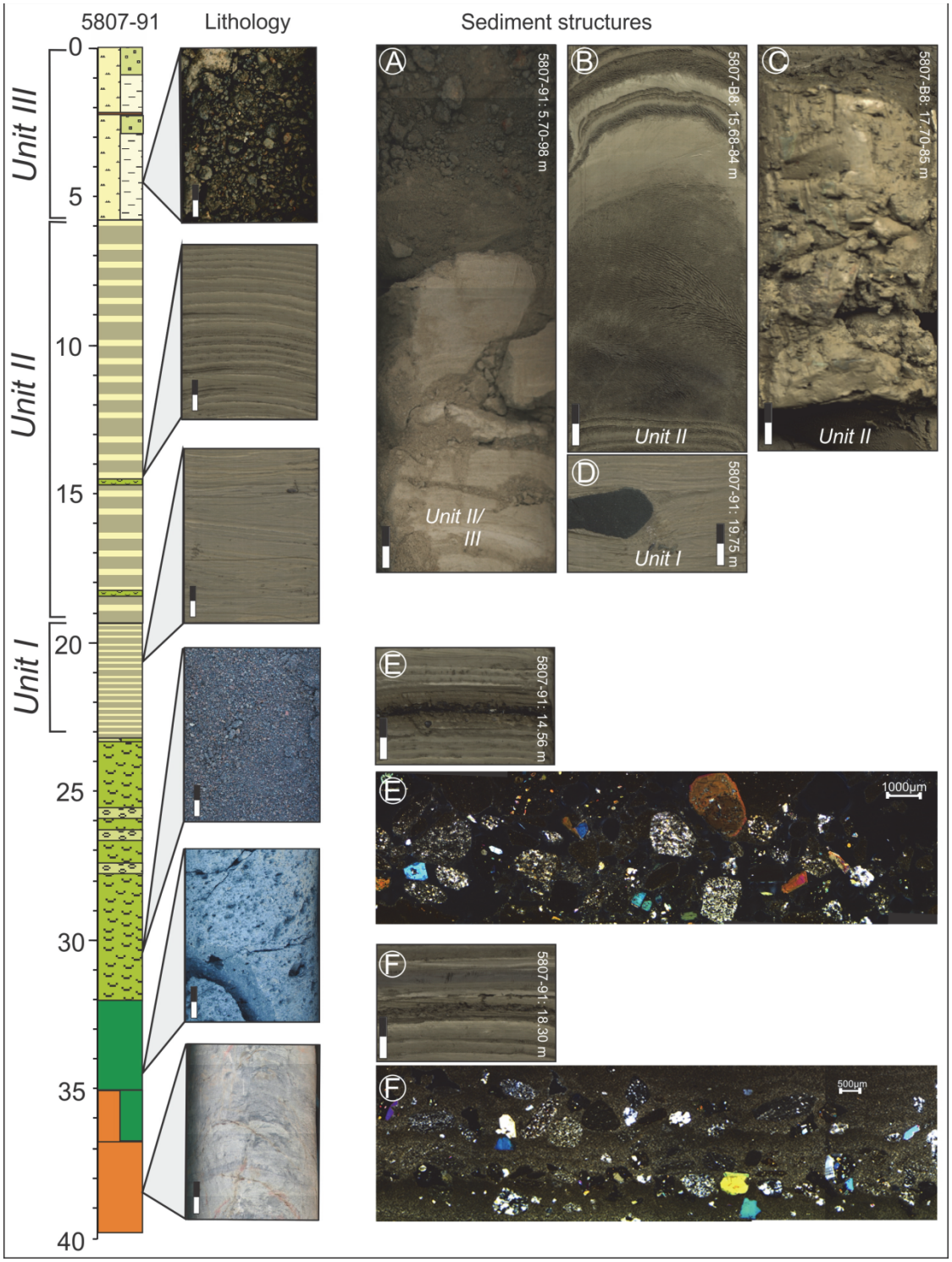

Fig. 3.2: Lithology of core Nr. 6 in Fig. 3.1 (5807-91) is presented with core photos and sediment structures of cores 5807-91 and -B8 showing: (A) transition from *Unit II* to *Unit III*, (B) turbidity layer, (C) debris layer, (D) drop stone, (E) ash layer at 14.5 m depth with pyroxenes, olivines, rounded silt clasts, and (F) ash layer at 18.3 m depth with pyroxenes, olivines, one polysynthetically-twinned plagioclase, rounded silt clasts of *Unit II*. For legend, see Fig. 3.1, black-white scale bar equals 2 cm.

These ash layers could be observed macroscopically, microscopically and with magnetic susceptibility. The mafic ash layer at 14.56 m depth is 0.5 cm thick and clearly delimited from the sediment by an abrupt grainsize, structure and color change. The magnetic susceptibility suddenly rises from 2000 to 4000 · 10^{-6} SI (Fig. 3.3). The ash layer consists of rounded Devonian sand- and siltstone clasts, angular to rounded basalt clasts with phenocrysts and macro minerals of 1100 to 1500 µm in average. Phenocrysts in the basalt clasts are predominantly pyroxenes (64 %, partly green core pyroxenes) and olivines (36 %), partly idiomorphic, matrix minerals are acicular pyroxenes. Single macro minerals are idiomorphic to hypidiomorphic and composed of olivines and pyroxenes (Fig. 3.2E).

The mafic ash layer at 18.305 m depth is 0.7 cm thick and clearly delimited from the sediment by an abrupt grainsize, structure and color change. Here, magnetic susceptibility suddenly rises from 2000 to 5600 · 10^{-6} SI (Fig. 3.3). This ash layer contains rounded Devonian sand- and siltstone clasts, angular to rounded basalt clasts with phenocrysts and macro minerals of 500 to 800 µm in average. Mineral phases of phenocrysts in the basalt clasts are predominantly pyroxenes (61 %, partly green core pyroxenes) olivines (36 %) and one polysynthetically-twinned plagioclase, partly idiomorphic. Single macro minerals are hypidiomorphic and composed of olivine and pyroxene (Fig. 3.2F).

The silt-sized sediments are predominantly clastic, composed of allochthonous material from the Lower Devonian sand- and siltstones and volcanic components, partly loess and autochthonous-precipitated calcite, ostracod valves and mussel fragments. Predominant minerals in the sediments are quartz, feldspar, transparent mica, chlorite, calcite and opaque oxides.

Higher K/coh ratios from XRF analysis in *Unit I* with an average of 0.4 indicate higher concentrations of feldspar and phyllosilicates which decrease to 0.3 in *Unit II* (Fig. 3.3). Microscopically observed calcites are predominantly rounded and a few of rhombohedral shape. Lower Ca/coh ratios of 0.2 were measured in *Unit I* which increase to 0.6 in *Unit II* indicating a higher contribution of redeposited loess components. TOC and TIC values in *Unit I* average both to 0.3 % (Fig. 3.3). In *Unit II*, TOC stays at 0.3 % whereas TIC values increase to 0.75 %. The transition from *Unit II* to *Unit III* is characterized by a sudden grainsize change from predominantly silt-sized sediments of *Unit II* to gravelly-sand of *Unit III* (Figs. 3.2A, 3.4B).

In *Unit III* a mixture of gravel-sized Devonian siltstones, quartz and volcanic material is embedded in a silty to sandy matrix. The transition from *Unit II* to *III* is shown in Fig. 3.2A.

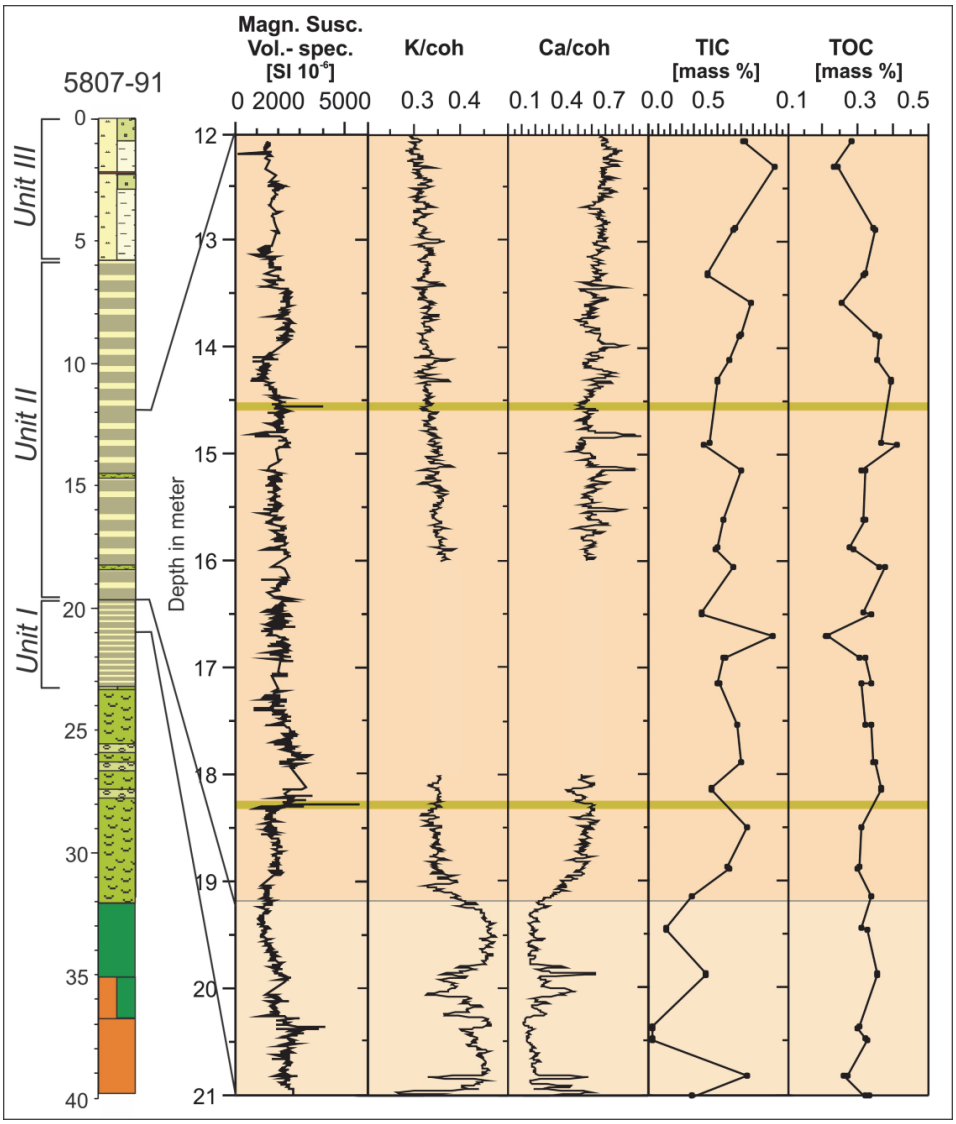

Fig. 3.3: Magnetic susceptibility and elemental ratios showing the transition between *Unit I* and *II* of core 5807-91. K/coh and Ca/coh are displayed as 5 point running mean, data was examined on undisturbed lamination, data gap between 16 and 18 m depth is due to turbidity layers. For legend, see Fig. 3.1. Volcanic ash layers are marked with green frames.

In the basin center, the lowermost sediment in core 5807-91 consisting of ash and scoria dominates in fine sand to fine gravel (Fig. 3.4B). Silt-sized sediments (*Units I* and *II*) prevail between 6 and 24 m below surface (Fig. 3.4B). This sequence is covered by 6 m thick gravelly sand-sized sediments (*Unit III*).

In the lower section of the proximal part of the lake, sand-sized sediments dominate with varying fine gravel content (Fig. 3.4A). Between 11 and 8 m below surface, sediments are characterized by an increasing silt content which coarsens again between 6 and 3 m. The uppermost 3 m are fine with dominating silt size.

Following the increasing and decreasing trends, *Units I* and *II* of core 5807-91 were correlated with the lowermost sequence of core 5807-89 ending at 19 m below surface. The uppermost sediments of core 5807-91 are coarser than in core 5807-89.

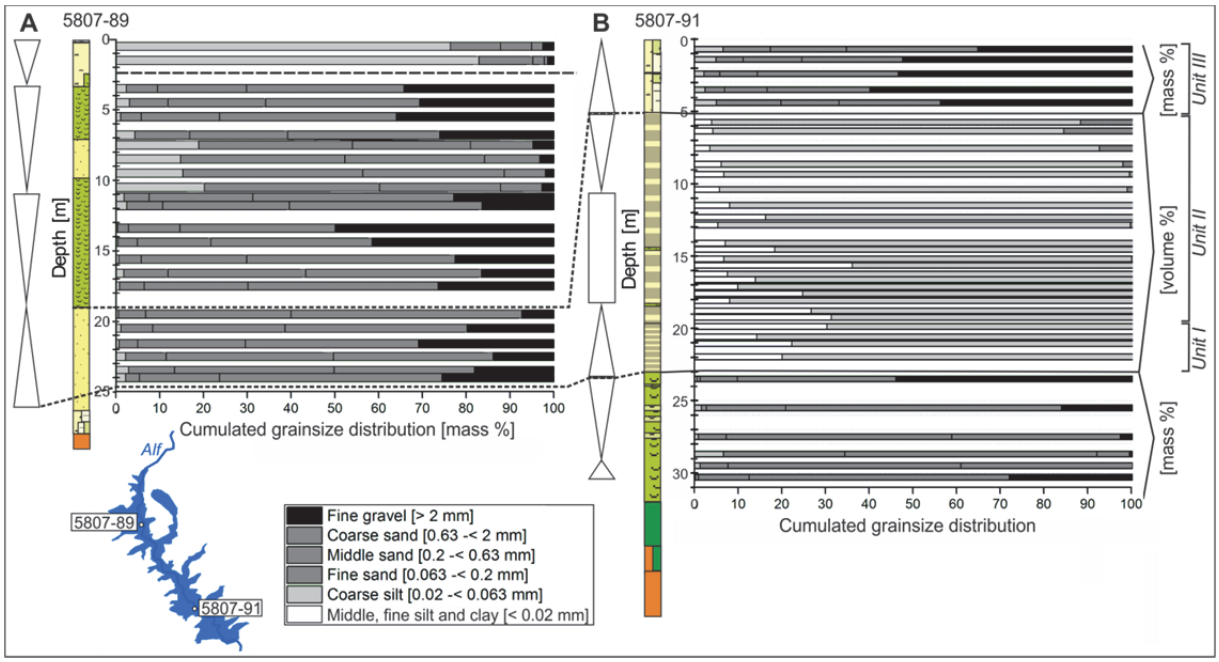

Fig. 3.4: Grainsize distribution of cores 5807-89 (A) and 5807-91 (B) given in volume % and mass %, as indicated, with inserted location in Paleolake Alf. Increasing and decreasing grainsize trends are symbolized with triangles. Fine dashed lines indicate correlated part of lake stages in the lower part of both cores. Upper dashed line in profile 5807-89 might indicate another lake stage described in the discussion part of this chapter. For legend, see Fig. 3.1.

When correlating core 5807-91 from the basin center with core 5807-B8 from the eastern Devonian slope using a distinct dark silt marker layer found in *Unit II*, laminae thickness in core 5807-B8 is lower by 24 % (Fig. 3.5, right side). In addition, in core 5807-B8 turbidity layers are thicker; more frequent and even debris layers occur (Fig. 3.2C).

Based on a correlation of sediment cores 5807-91, 5807-70 and 5807-B8 using lithology, magnetic susceptibililty humic acid AMS ^{14}C ages and the distinct dark silt lamina, an age-depth model was established (Fig. 3.5). *Unit I* of core 5807-91 was dated to between 33 and 30.6 cal. ka BP projecting ^{14}C dates of core 5807-B8 according to lithology. For dating of *Unit II*, core 5807-91 was correlated with cores 5807-70 (Pirrung et al. 2007) and 5807-B8 using one marker layer, magnetic susceptibililty and lithology revealing a time span between 30.6 and 21 cal. ka BP. The top third of *Unit III* was dated to 14.2-13.8 cal. ka BP in core 5807-70 (Pirrung et al. 2007), the Laacher See Tephra (LST) at 1 m depth in the same core indicates an age younger than 12.9 ka BP (~ 14 cal. ka BP) which is the age of the Laacher See Tephra determined by Brauer et al. (1999).

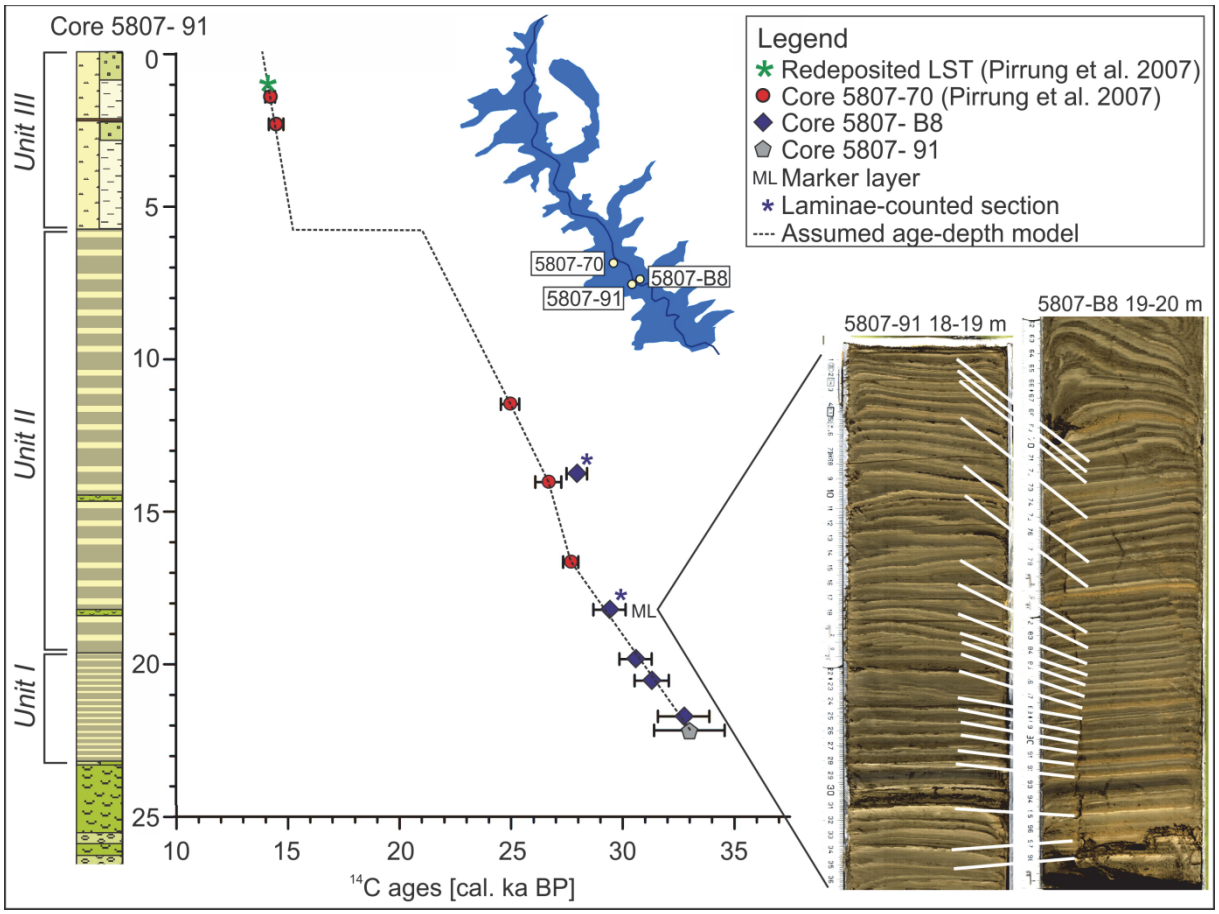

Fig. 3.5: Age-depth model of core 5807-91 is presented based on humic acid ^{14}C ages of cores 5807-70 (Pirrung et al. 2007) and 5807-B8 that were correlated according to lithology, magnetic susceptibility and a marker layer. For legend, see Fig. 3.1.

3.4 Discussion

The naturally-formed volcanic dam in the Alf Valley created a paleoenvironmental archive and caused a natural hazard due to a sudden dam collapse. Using core lithologies and sedimentological analysis it could be stated that the Alf basin architecture resembles that of modern reservoirs.

The lowermost sandy deposits in core 5807-89 are lacustrine deposits that were correlated to *Units I* and *II* of core 5807-91 and could be interpreted as the foreset region, as found in recent reservoirs, e.g. Englebright Lake in northern California (Snyder et al. 2006). Here, coarse gravel-sized river sediments deposit in the delta, topset and sand-sized material in the foreset region. The fine-grained clay and silt particles of *Units I* and *II* are interpreted as the bottomset area as reflected in recent reservoirs (Snyder et al. 2006; Fig. 3.4B). The sedimentation rate of 2.7 mm · a^{-1} in *Unit II* (core 5807-70) corresponds to climate reconstructions by Huijzer and Vandenberghe (1998) with increased peak discharges from snow melting around 27 ka (= 30 cal. ka BP). A similar sedimentation rate of 2 mm · a^{-1} is

documented from dry maar Auel (Brunck et al. 2016) which has a much smaller catchment area compared to Paleolake Alf.

The higher laminae thickness in *Unit II* of core 5807-91 compared to the same unit of core 5807-B8 from the eastern slope is resulting from predominant sediment delivery along the former thalweg. The higher abundance and thickness of turbidity sequences in the same unit of core 5807-B8 and the occurrence of debris layers in *Units I* and *II* indicate slope processes like soli- or gelifluction shown as solifluction lobes in the shear wave seismic cross profile P1(Fig. 3.6).

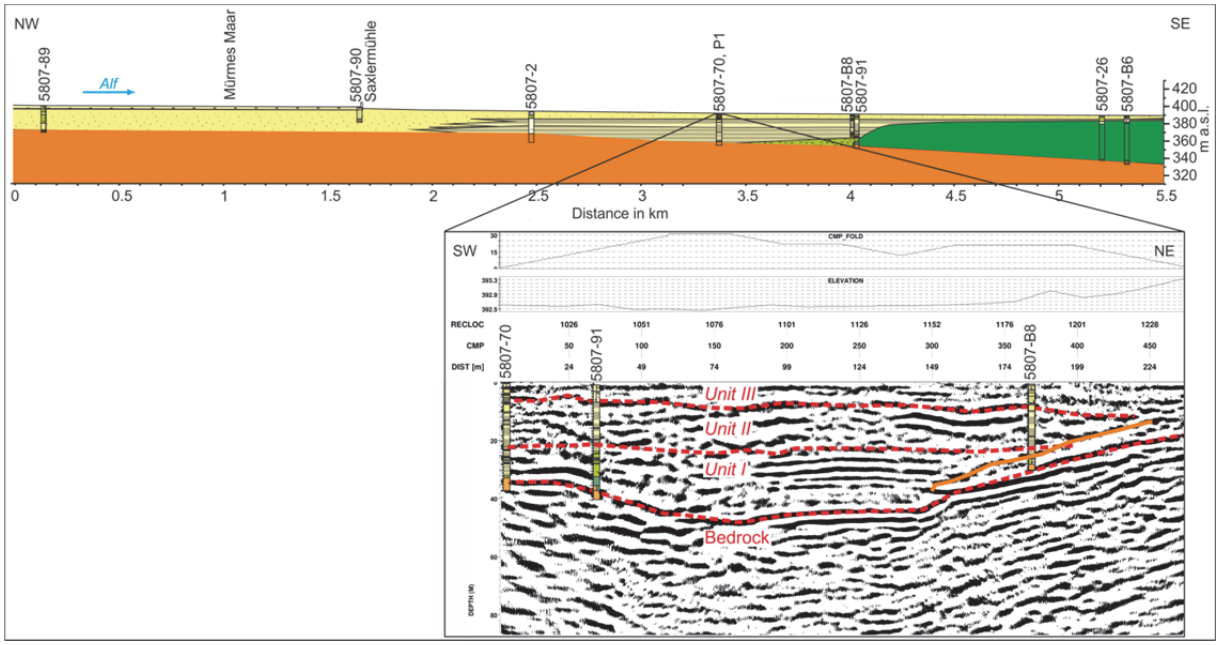

Fig. 3.6: Above: Longitudinal (NW-SE) profile is shown with interpreted sediment infill between the cores. Below: Seismic shear wave cross profile P1 (SW-NE, for location and legend, see Fig. 3.1) with projected lithologies of cores 5807-70 of 110 m, and 5807-91 and B8 of 760 m distance showing reflections at the lithological boundaries of *Units I*, *II* and *III* indicated by red dashed lines. Dipping reflectors (orange line) were interpreted as resulting from solifluction lobes from the slope.

The calcium increase in *Unit II* of core 5807-91 (Fig. 3.3) towards 24 ka may be explained by drier climatic conditions which fits to the NGRIP Greenland Stadial 3 (Andersen et al. 2006, see Chapter 4) and enhanced eolian activity as interpreted for the Eifel by Sirocko et al. (2016) in the landscape evolution zone 4 (Polar desert). Clay mineralogy reveals illite, smectite and kaolinite. Illite derives from Lower Devonian silt- and sandstone bedrocks (Felix-Henningsen 1990), and smectite most likely from weathered olivines and pyroxenes of the volcanic ashes as described by Blümel et al. (1985) from the S-Shetlands/West-Antarctic. Kaolinite is a relict from intense subtropical Tertiary weathering of bedrock chlorite (Felix-Henningsen 1990) which was detected in the lacustrine sediments (see Chapter 4), and derives

from i.e. paleosoils. Due to the fact, that these clay minerals occur in both units, the sediment source did not change.

The redeposited ash layers in core 5807-91 at 18.3 m depth could be associated with a maar eruption due to the high amount of bedrock. The occurrence of plagioclase minerals was detected in lapilli from two eruption centers in the vicinity of the Alf Valley which fit considering eruption time: Holzmaar (WGS84 32U E:348240, N: 5554350) and Wartgesberg (WGS84 32U E:352377, N: 5552712). Holzmaar ash cannot be considered as hornblende and sanidine minerals (Hopmann et al. 1960) should occur as well and olivine and pyroxene mineral phases do not occur in observed portion (own observation). Wartgesberg lapilli contain more olivines (55 %) than pyroxenes (45 %). Regarding the olivine: pyroxene portion, the Sprinker Maar (WGS84 32U E: 352498, N: 5552386), with < 10: 65 % and the Gemündener Maar (WGS84 32U E: 346003, N: 5560967) from the Dauner Maar Complex with 25: 75 % are best fitting. The same applies to the ash layer at 14.5 m depth.

Considering the transition from *Unit II* to *Unit III*, e.g., in core 5807-B8 section 9-10 m, sediments become coarser but show lamination which abruptly disappears at section 8-9 m. The same is observed in core 5807-91 where sediment deeper than 5.8 m contains clay which suddenly disappears. A different sedimentation is observed in core 5807-70, where lacustrine sections appear and suddenly disappear between coarser sections. The abrupt disappearance of lamination implies a hiatus and is interpreted as a sudden change from a lacustrine to a fluvial environment. This change is probably induced by river progradation which is the result of lake level lowering - a drawdown. Sedimentation of regulated drawdowns at Englebright Lake (Snyder et al. 2006) shows that the delta front prograded into the basin, reworking and winnowing already deposited coarse material from top- and foresets which then overlie bottomset deposits. Drawdowns can be caused by several reasons: (a) silting-up by, e.g., high sediment delivery, (b) lower availability of water by lack of precipitation or by leakage of the dam due to backward erosion, or (c) dam failure causing flooding events by, e.g., increased streamflow during periods of intense rainfall or snowmelt or earthquakes (Claque and Evans 1994). For Paleolake Alf, a combination of (b) and (c) with erosion of parts of the lacustrine sediment is most likely (Fig. 3.7).

Before the Wartgesberg Volcano eruption, River Alf had an ideal river profile which is linear in the displayed section (Fig. 3.7A). After the Wartgesberg Volcano eruption ~ 31±11 ka BP (Mertz et al. 2015), River Alf was impounded (Fig. 3.7B). Volcanic ash and scoria covering the slopes around the eruption center were transported into the young lake basin. Coarse, frost weathered material from the solifluction-covered ridges formed fans at the inlet of tributaries

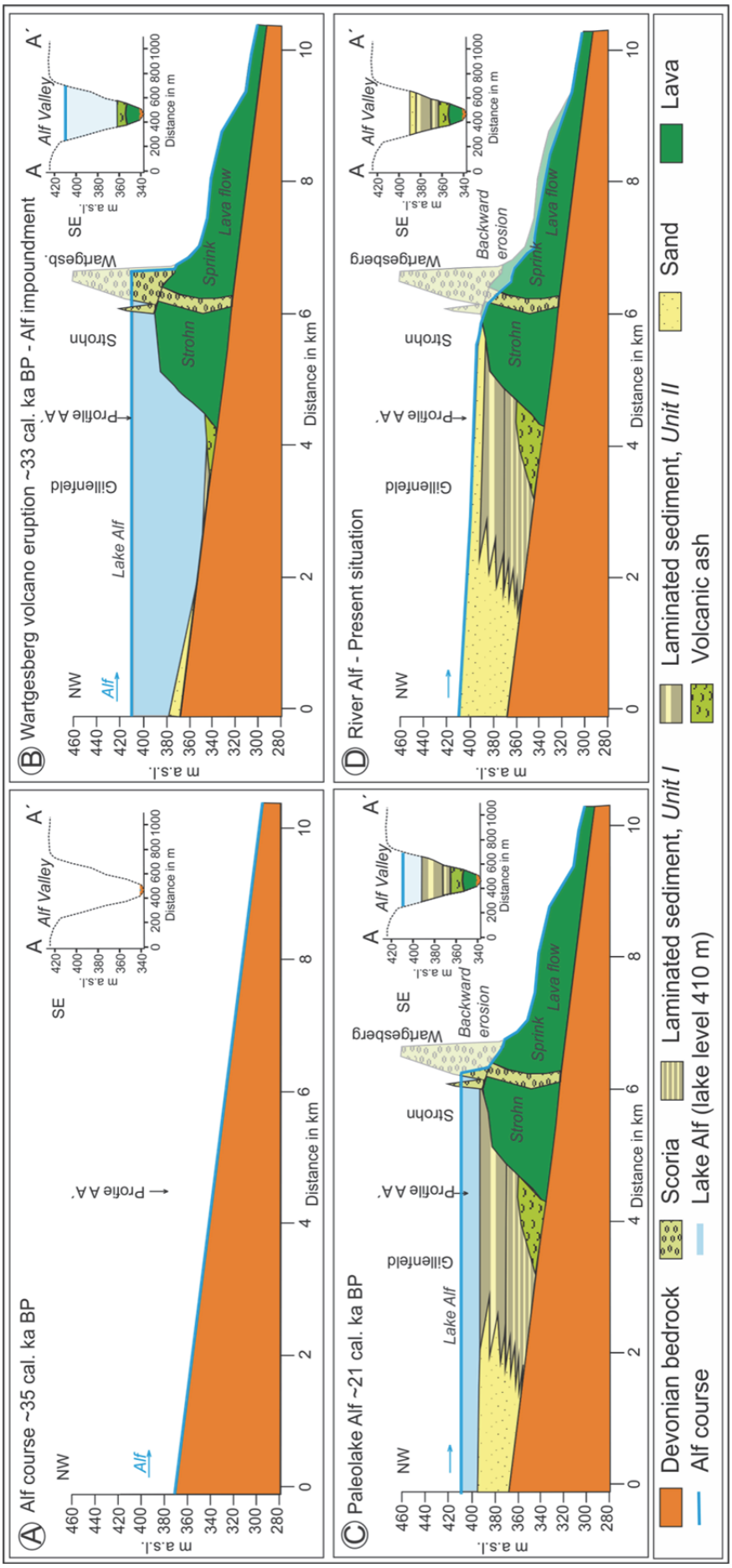

Fig. 3.7: Valley evolution is displayed between 35 ka BP and today: Pre-volcanic Alf Valley (A); Wartgesberg eruptions impounding the Alf River forming Paleolake Alf (B), lake basin sediment infill (C), and dam collapse with hiatus – partial erosion of lacustrine sediments (D).

(see Chapter 4). At the Alf inlet this material built the top- and foresets of a delta. Silt to clay-sized particles accumulated in the basin center forming *Units I* and *II* (Fig. 3.7C). Assuming that Paleolake Alf leaked by water penetrating along the contraction-joint surfaces of the lava flow, frost-thaw changes were able to disintegrate and erode the volcanic dam which caused incision (Fig. 3.7C) as described by Claque and Evans (1994) from natural dams in the Canadian Cordillera.

At the end of the lake stage just prior to the dam failure, the Pulvermaar must have been erupted because the lacustrine sediments do not contain any primary ash deposits. Around 15 cal. ka BP (~ 13.5 ka BP) – during the Mecklenburg Phase of the Weichselian, the dam failed most likely with a hazardous flood wave and ~ 6 m of the lacustrine sediments were eroded including primary deposits from the eruptions of the Pulvermaar-Römerberg Complex which are assumed between 15 and 20 ka BP (Büchel 1984). When the IVEX dam in northeast Ohio failed, ~ 9 to 13 % of the original reservoir infill was mobilized (Evans et al. 2000). The abrupt lowering of the lake level due to dam failure caused remobilization of the top- and foreset material which might represent parts of *Unit III* in core 5807-91 as these sediments are coarser than the correlated section of core 5807-89. The upper part of *Unit III* (core 5807-91) containing a mixture of silt, sand, gravel and redeposited ash from the Pulvermaar eruption is interpreted as fluvial deposits from the proximal tributary Laubach (Fig. 3.1). Even Mürmes Maar deposits must have been mobilized from the dam failure.

Due to the lake water drainage and the load of the overlaying fluvial deposits, the silty sediments settled and compacted. Therefore, the fluvial sediments accumulated in the basin and were not immediately eroded (Fig. 3.7D). At the same time, sediments started to accumulate in the Mümes Maar (Straka 1975) and the LST was transported from the slopes and redeposited into the basin.

Sediments in core 5807-89 become finer in the upper part which might be related to the Saxler Stausee built by humans during the Mesolithic who impounded the Alf River at Saxlermühle (Löhr and Neyses 1997). The resulting silt-sized sediments are documented in core 5807-89 in the uppermost 2 m (Fig. 3.4). Today, River Alf is regressively eroding the Strohn lava flow and *Unit III* in order to someday regain its ideal river profile.

Chapter 4

4. Pleniglacial sedimentation process reconstruction on laminated lacustrine sediments from lava-dammed Paleolake Alf, West Eifel Volcanic Field (Germany)

Chapter 4 corresponds to a manuscript for resubmission to the journal of Quaternary Science Reviews with the listed co-authors.

Luise Eichhorn[1], Michael Pirrung[1], Bernd Zolitschka[2] and Georg Büchel[1]

[1] *Friedrich Schiller University Jena, Institute for Earth Sciences, 07749 Jena, Germany*
[2] *University of Bremen, Institute of Geography, 28359 Bremen, Germany*

Abstract

Differentiating between regularly seasonal, irregular and event-based clastic sedimentation is difficult if sedimentation structures resemble and dating methods are imprecise. In this study, clastic light and dark laminae from lava-dammed Paleolake Alf in the Quaternary West Eifel Volcanic Field are analyzed to clarify how they formed and if they are of annual origin and comparable to assumed periglacial varves from neighboring Lake Holzmaar. Therefore, a multiproxy approach is applied combining sediment thin section analysis which focuses on composition and structure with ^{14}C dates. The results are compared to recently-formed annually-laminated clastic sediments from lakes of, e.g., the High Canadian Arctic. Observed sedimentation structures reveal sediment delivery by over- and interflows and deposition from suspension forming two characteristic microfacies: *Type I* graded laminae and *Type II* laminae with graded sublayers. Additionally, erosional bases and event deposits indicate episodic underflows. Thus, lamination is potentially seasonal but is significantly veiled by extreme runoff causing erosion and resuspension processes or a mixed water body preventing sediment delivery into the lake basin. However, sedimentation processes between watershed and lake could be reconstructed by comparing recent and paleosediment structures.

4.1 Introduction

High resolution lacustrine sediment archives that preserve information about Middle (40-26 ka BP) to Late Pleniglacial (26-13.7 ka BP) sedimentation processes in Germany are rare as these deposits were mostly eroded during Holocene. Prominent archives covering this time period like Holzmaar (Brauer 1994, Negendank 1989), Meerfelder Maar (Negendank 1989) or Dehner Maar (Sirocko et al. 2013) derive from maar lakes of the West Eifel Volcanic Field.
From the West Eifel, periglacial varves meaning annuals deposits (De Geer 1912) are documented from, e.g., Holzmaar (Brauer 1994, Vos et al. 1997). These clastically-varved sediments provide information about sediment delivery processes generally related to either event-related deposition, e.g. rainfall events or slope instabilities, or to seasonal snow/glacier melt forming annually laminated sediments (Brauer 1994, Lamoureux 2000, Ojala et al. 2012, Zolitschka et al. 2015).
In this study, fluvio-lacustrine sediments from Paleolake Alf, a volcanically-dammed lake situated in the WEVF, are investigated. They consist of alternating light and dark laminae which cover the Weichselian Middle to Late Pleniglacial immediately prior to the Last Glacial Maximum. As this Paleolake Alf differs from maar lakes due to its elongated shape, a main inlet and a bigger catchment area, it provides an important supplementary archive of this time.
The focus of this study is to give an explanation of the depositional processes that formed the lamination and to examine whether the clastic light and dark laminae couplets of Paleolake Alf can be interpreted as varves.
Therefore, the observed laminated sediment structures are compared to modern monitoring studies from glacial or periglacial environments like the Canadian High Arctic or Svalbard (Cook et al. 2009, Guilizzoni et al. 2006, Leonard 1997, Zolitschka 1996) to understand related depositional processes.

4.2 Material and Methods

In order to reveal the structure and composition of the lamination, sediments of core 5807-91 are analyzed for micro remains (7 samples between 12.5 and 22.2 m), grainsize (11 samples between 19.79 and 22.97 m from *Unit I,* 15 samples laminae-wise between 18.72 and 18.79 m and between 16.64 and 16.72 m from *Unit II*), mineralogy (XRD, 15.3; 15.4 m, *Unit II*) and geochemistry (XRF, 15-16 m, *Unit II*), Fig. 4.1. For the question if the lamination is seasonal or not, thin section microscopy on core 5807-91 (18.48 and 18.90 m from *Unit II*) and age determination on cores 5807-91 (^{14}C, 22 m, *Unit I*) and 5807-B8 (^{14}C, 15.3, 19.9 m, *Unit II* and 20.9, 21.8, 23.8 m, *Unit I*) are applied.

Sampling sections in core 5807-91 differ because of differing sediment quality, e.g., occurrence of folding or turbidity sequences. For detailed methodological descriptions please refer to Chapter 2.

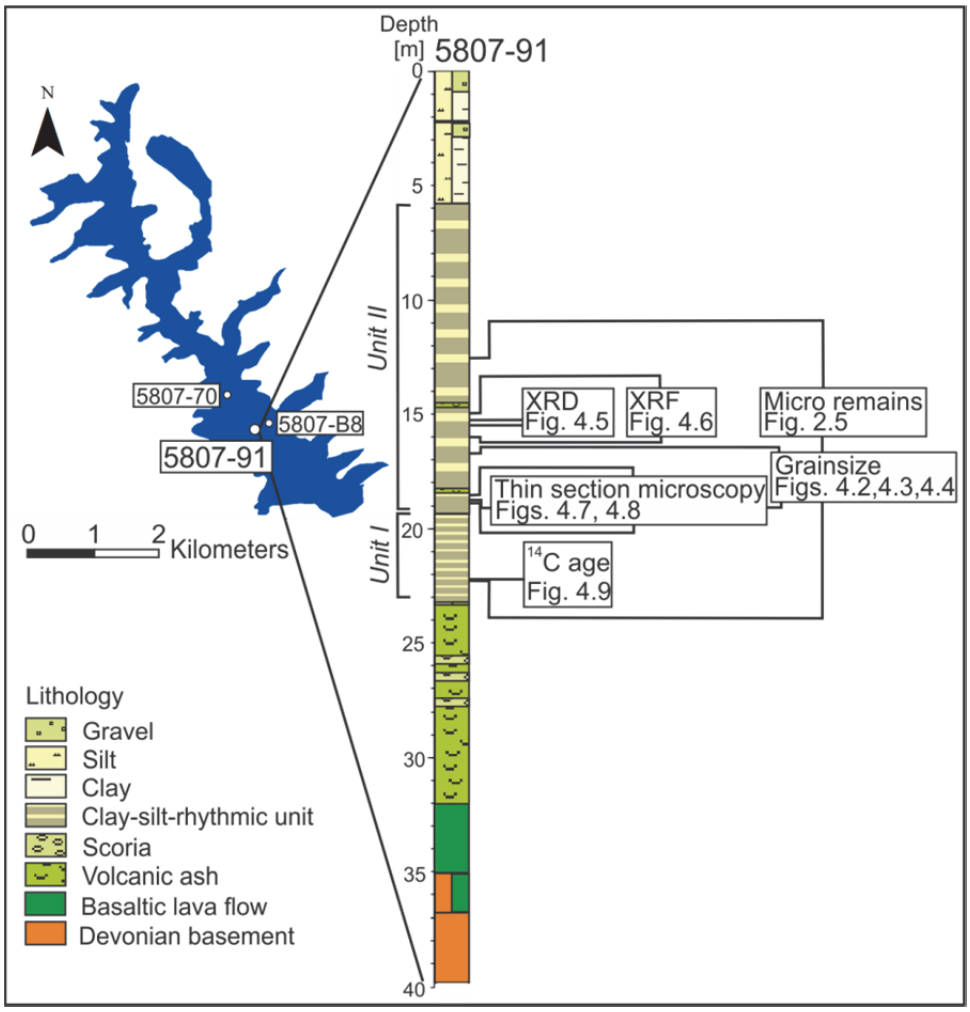

Fig. 4.1: Location and lithology profile of core 5807-91 is displayed combined with applied methods: X-ray diffraction (XRD), X-ray fluorescence (XRF), micro remains, grainsize, thin section microscopy and ^{14}C age.

4.3 Results

Mineralogy and micro remains

Generally, the lacustrine sediment of Paleolake Alf mainly consists of quartz, feldspar, transparent mica, chlorite, calcite and opaque oxides. In addition, single idiomorphic, rounded and silt-sized (200 µm) olivine, pyroxene and plagioclase crystals as well as basaltic clasts occur sporadically either isolated or as layers in a fine-grained matrix. Isolated siltstone extraclasts of up to 45 mm were found in the silt-sized sediments, which show hardly any deformation of the underlying sediment. Apart from its mineralogical components, the sediment contains parts of insects, seeds, mussel fragments, ostracod valves and pollen

(H. Schneider 2015, pers. com.). The ostracod species *Candona neglecta* and *Cytherissa lacustris*, identified by P. Frenzel (University of Jena, pers. com. 2015), were only observed at depth between 12.5 and 18.3 m.

Sedimentary units

Core 5807-91 contains Lower Devonian bedrock at its base from 40 to 35 m depth, followed by mafic lava between 35 and 32 m and a mix of scoria and volcanic ashes between 32 and 23 m (Fig. 4.1). The overlying lacustrine sediments were visually and geochemically separated into *Unit I* (23-19.2 m) and *Unit II* (19.2-5.8 m). The topmost 5.8 m display a mixture of clay- and silt- to gravel-sized sediments interpreted as fluvial deposits (Fig. 4.1). Focusing on the laminated lacustrine sequence, *Unit I* is composed of clay-rich silt (on average: 21 % clay, 78 % silt, 0.08 % sand) with a mean grainsize of 6 µm. This unit is predominantly characterized by a (sub)millimeter lamination with intercalated slump structures showing a 30 cm-thick folded section with extension faults between 21.00 and 21.30 m, a 45 mm-sized extraclast at 19.75 m and two 30 mm-thick homogeneous sand layers at 20.81 and at 20.97 m depth.

Unit II is composed of light and dark couplets averaging 8 mm in thickness. The light laminae have a mean grainsize of 6 µm and are clay-enriched (18 % clay, 81 % silt, 0.3 % sand) whereas dark laminae with a mean grainsize of 10 µm contain a higher content of silt particles (9 % clay, 90 % silt, 0.07 % sand, Fig. 4.2). Within the lamination two volcanic ash layers at 14.56 and 18.31 m are intercalated.

Two graded beds with thicknesses of 4 and 70 mm fining upwards occur with concordant bases from 16.09 to 16.13 m and from 16.65 to 16.72 m. They are interpreted as event-related deposits, i.e. as turbidity layers. As an example, the grainsize distribution of the 70 mm event layer marks a clear fining-upward grainsize evolution typical for a turbidity layer (Fig. 4.3).

The basal sandy silt layer has very low clay content and fines upward via a silty central part to a clay-rich top (clay cap) containing highest clay and lowest silt and sand content. Additionally, the grainsize distribution shown as cumulative curves reveals the light and dark laminae and the event deposit (Fig. 4.4).

The curves for dark laminae are shifted by 4 µm towards coarser grainsizes. However, light as well as dark laminae show a similar slope and good sorting, which indicates suspension fall out through a several meter thick water column. The top and middle sections of the event deposit are similarly well-sorted, only the basal layer has a fine tail indicating erosional reworking of the underlying clay layer at the base of the turbidity current. In addition, distal and proximal turbidity sequences of Meerfelder Maar (MFM) are displayed for comparison.

The distal turbidity layer of MFM shows a higher clay content than the light laminae of Paleolake Alf whereas the proximal turbidity layer of MFM contains much more sand.

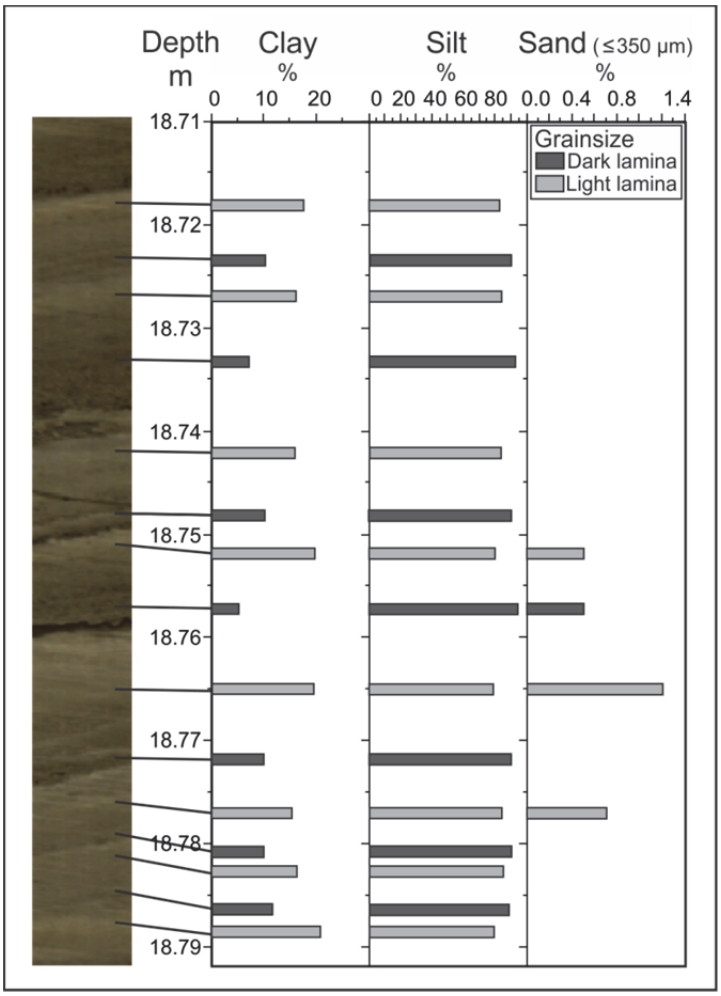

Fig. 4.2: Grainsize distribution is presented in volume percent. Sediment was sampled laminae-wise (light and dark separately) between 18.718 and 18.789 m depth from core 5807-91. Light and dark laminae are implied by bright and dark gray boxes, respectively.

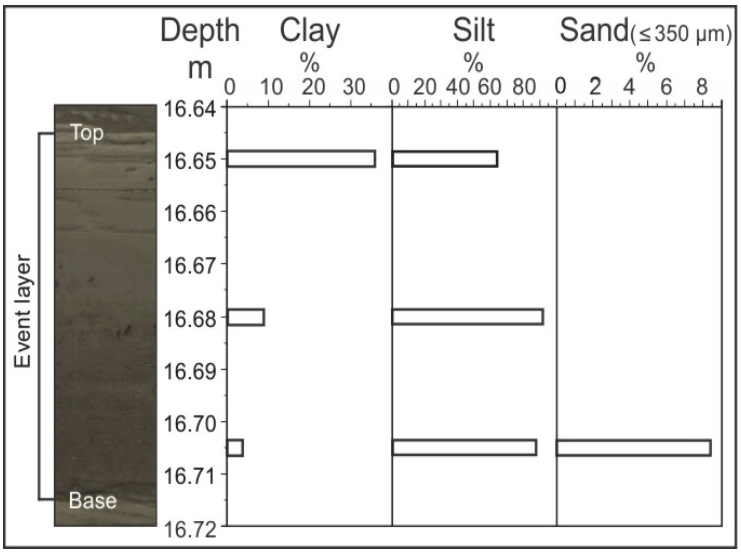

Fig. 4.3: Grainsize distribution presented in volume percent of the 70 mm thick graded event-layer between 16.645 and 16.715 m depth of core 5807-91.

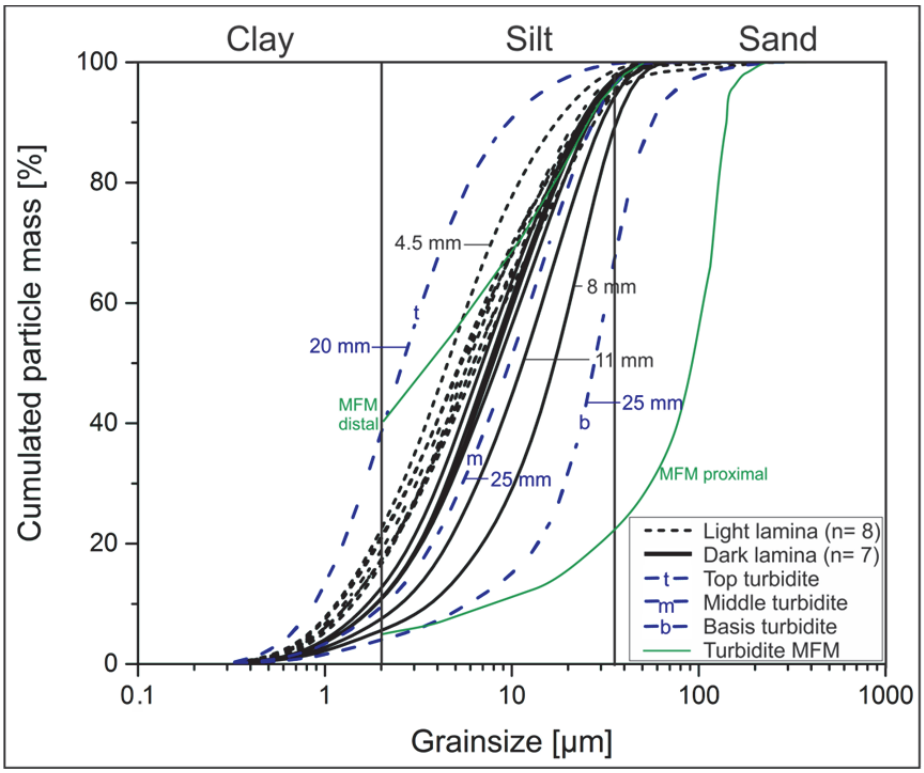

Fig. 4.4: Cumulative grainsize curves showing light and dark laminae (light laminae from core depths 18.718-18.789 m, dark laminae from 18.723-18.786 m, cf. Fig. 4.2) and one event deposit from core 5807-91, cf. Fig. 4.3. The labels reveal layer thicknesses in mm. Green lines show grainsize distributions of proximal and distal turbidity layers from Meerfelder Maar (MFM) for comparison (Drohmann and Negendank 1993).

Mineralogy and geochemistry of light and dark laminae

XRD-data of the light (15.445 m) and dark laminae (15.375 m), taken from *Unit II*, show that the main mineral phases are quartz, muscovite and chlorite as identified by diffraction reflexes (Fig. 4.5). Although the mineral phases of both laminae are almost identical, their proportions vary: the light lamina is enriched in phyllosilicates, whereas in the dark laminae quartz dominates. XRF-data from a sediment section of *Unit II* (15.35-15.60 m, Fig. 4.6) display a higher K/Ti ratio in the light laminae compared to the dark laminae indicating a higher content of mica in the fine-grained light laminae. The Ca/Ti ratio is generally higher in the dark laminae (Fig. 4.6), which points to the presence of calcite. It is microscopically visible but present in too small proportions to be verified with XRD. In the thick dark and light couplet (15.55-15.565 m), a gradation is indicated by arrows, i.e., Ca-enrichment at the base of the dark laminae and K-enrichment towards the clay top.

Sedimentary microfacies

Microfacies analysis was carried out by a microscopic investigation of thin sections from *Unit II*. For *Unit I* this was impossible, because thin sections cracked during drying due to the

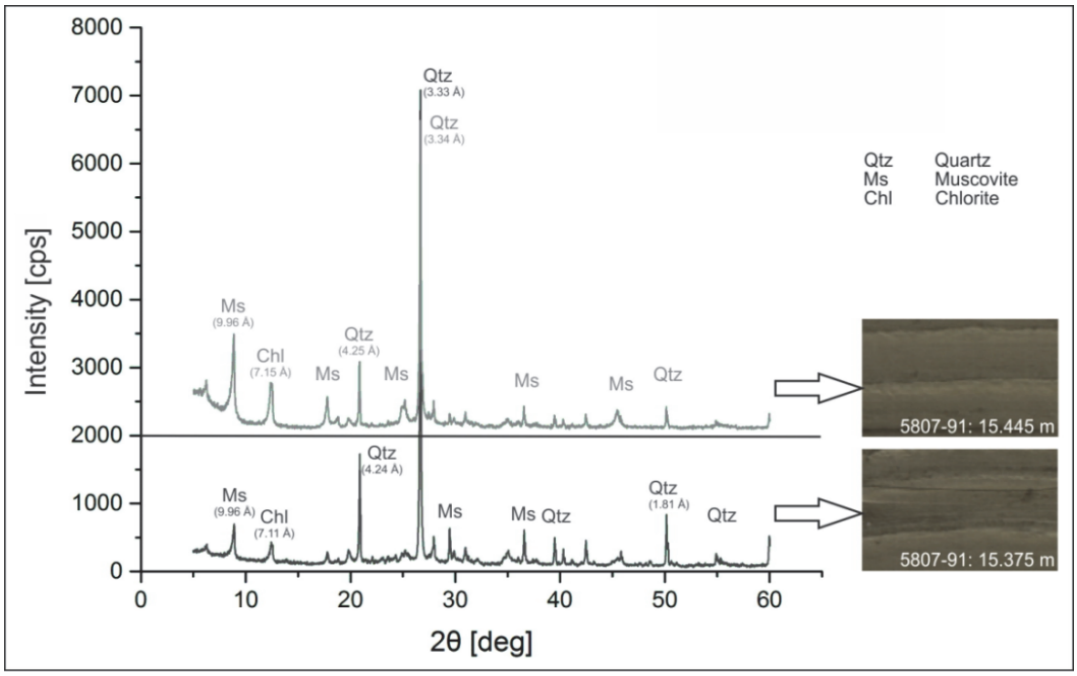

Fig. 4.5: X-ray diffraction pattern of the light, clay-enriched (top) and the dark, silt-sized lamina (bottom). Their position in the laminated sediments is indicated by the arrow next to the core image. Note that the upper pattern is shifted by an intensity value of 2000 cps for better visibility.

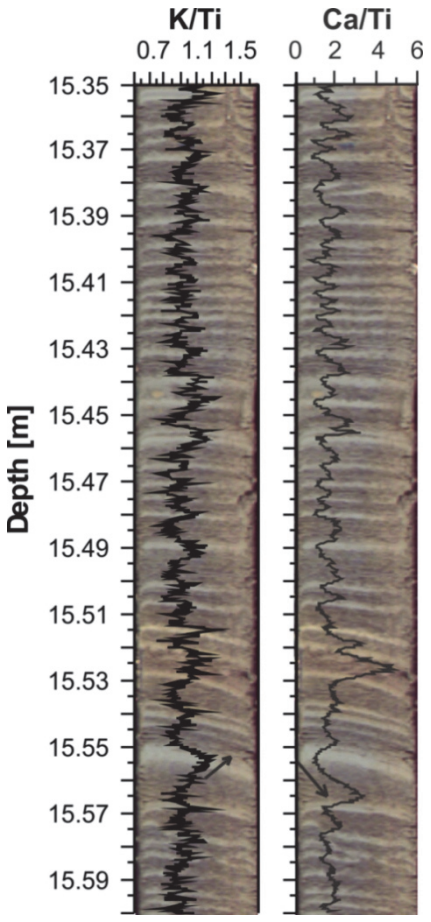

Fig. 4.6: XRF-data (interpolated 5 point mean) of *Unit II* analyzed with 200 µm vertical resolution plotted on the core image demonstrating K-enrichment in the light laminae and Ca-enrichment in the dark laminae.

higher amount of clay. The thickness of the dark and silt-enriched laminae varies between 0.4 and 18.6 mm with a mean of 5.9 mm (n = 74), whereas the thickness of the light and clay-enriched laminae varies between 0.2 and 8.0 mm with a mean of 1.9 mm (n = 78). Deformation of sedimentary structures by bioturbation was not observed.

The following two microfacies types are differentiated. Both are randomly distributed throughout the investigated section of *Unit II*.

Microfacies *Type I*: Lamination with normal grading

Type I (19 % occurrence) is characterized by grain-supported coarse-grained basal silt which fines up towards the clay top. The transition from dark to light laminae is gradational indicated by a smoothly rising clay content (Fig. 4.7, A). The typical dark lamina thickness of this type varies between 0.6 and 14 mm (n = 14).

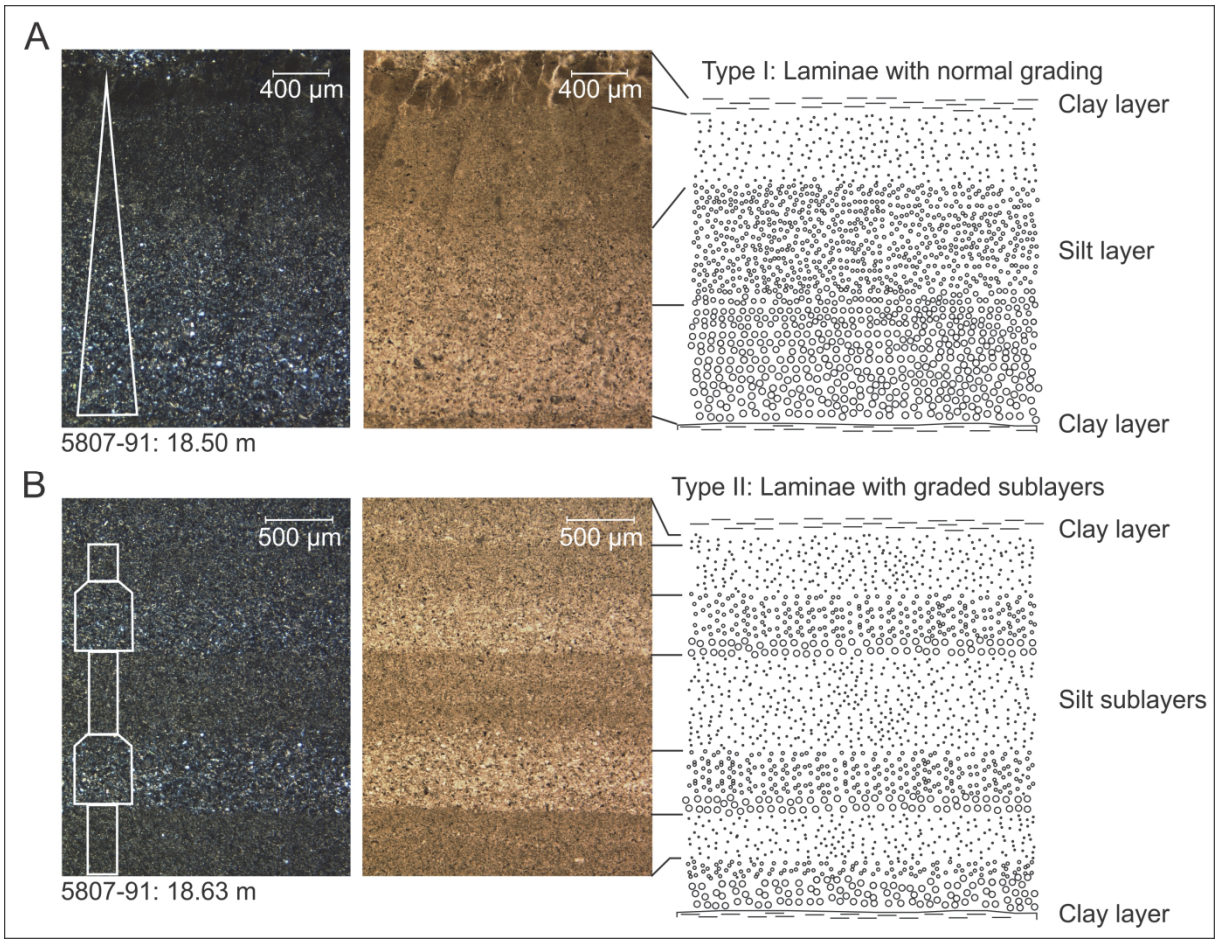

Fig. 4.7: (A) shows microfacies *Type I* - normal grading of a dark lamina shown under crossed (left) and plain (center) light. (B) displays microfacies *Type II* – laminae with graded sublayers shown under crossed (left) and plain (center) light. A complete lamina of *Types I* and *II* including the light lamina is also schematically displayed (right). Please note: in contrast to microscopic images, in core scan images the lower coarser part is dark, the upper fine part is light. This core scan nomination is applied throughout the text.

Microfacies *Type II*: Lamination with graded sublayers

Laminae with graded sublayers are more frequent (81 % occurrence). The coarse basal layer is characterized by grain-supported silt (20-60 µm). The upper part of the dark laminae is characterized by graded transitions from silt to clay-sized sublayers (Fig. 4.7, B). This pattern repeats until the upward fining ends in a distinct light lamina. The typical dark lamina thickness varies between 0.4 and 18.6 mm (n = 60).

Clay caps with isolated grains

Often, the lower parts of the clay-enriched light laminae of microfacies *Types I* and *II* contain dispersed coarser and isolated silt-sized minerals (Fig. 4.8, A-C). These dispersed coarse silt grains have the grainsize of the overlying dark lamina, rarely they are coarser. The upper part of the light lamina is often undulated, parts of the clay layer are sheared-off or laminae-thickness variations indicate erosional bases of the overlying sediment (Fig. 4.8, D-F).

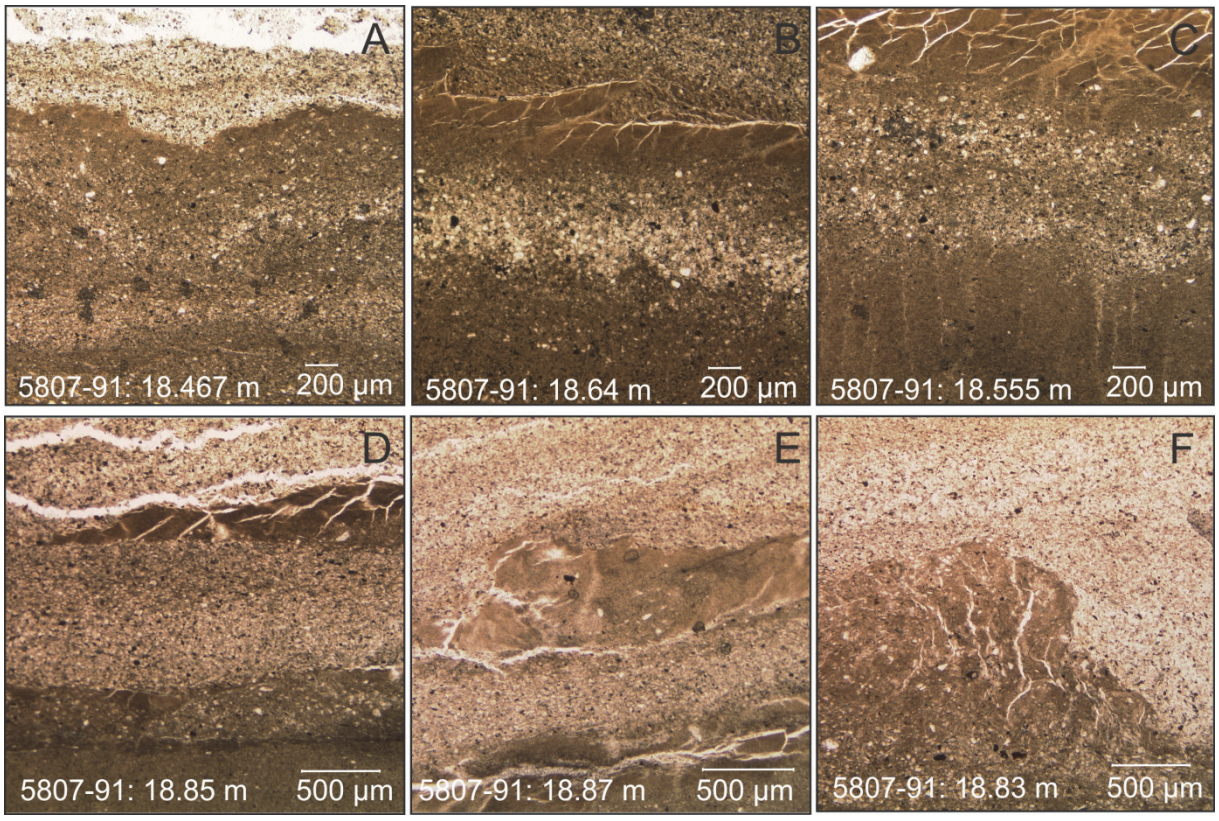

Fig. 4.8: Microphotographs (plain light) of light laminae show dispersed mineral grains and intercalated silt bands of *Type II* (A-C). Photos (D) and (E) show the transition from light to dark lamina with ripped-off clay fragments embedded in the silty matrix. Clay thickness variations in photo (F) indicate an erosional base on top of the light lamina.

Chronology

Based on a correlation with the two neighboring sediment cores 5807-70 and 5807-B8 (Chapter 2), an age-depth model for core 5807-91 was established (Fig. 4.9). By correlating ^{14}C dates (Appendix B.1) and lithology of core 5807-B8, *Unit I* of core 5807-91 was dated between 33 and 30,6 cal. a BP. For the age of *Unit II*, core 5807-91 was correlated with cores 5807-70 (Pirrung et al. 2007) and 5807-B8 using a marker layer, magnetic susceptibility and lithology revealing a time span between 30,558 and 20,837 cal. a BP which represents approx. 9721 a.

Assuming that one light-dark couplet represents one year, the couplet-counting between 15.35 and 19.90 m depth on core 5807-B8 (projected section marked with a blue star is shown in Fig. 4.9) revealed 591 couplets, whereas the ^{14}C dates for the same interval covers a time span of 1460 a.

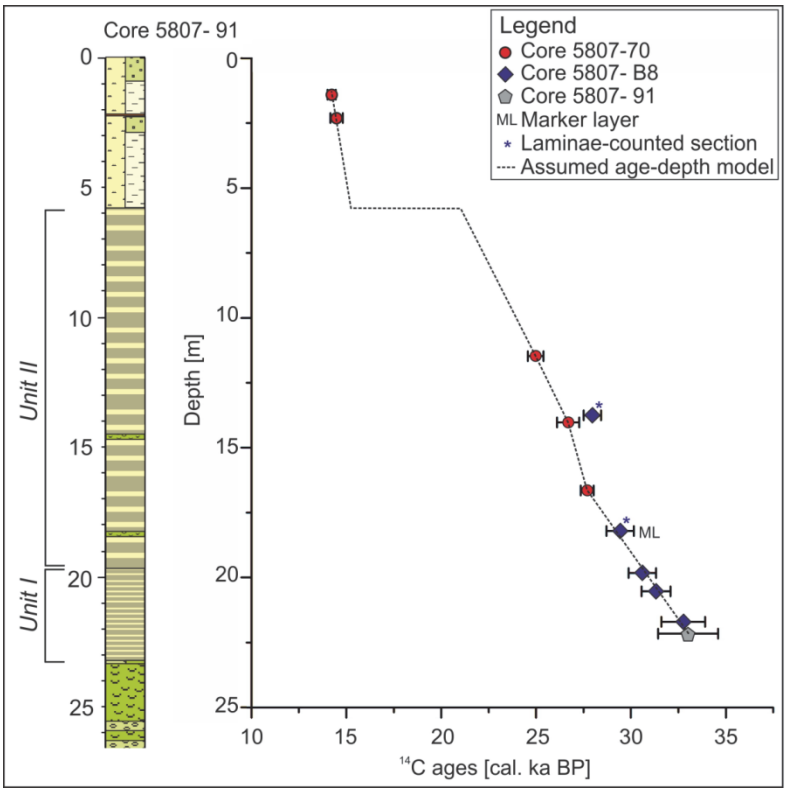

Fig. 4.9: Age-depth model of core 5807-91 is presented. ^{14}C ages of the neighboring cores 5807-70 (Pirrung et al. 2007) and 5807-B8 were projected on core 5807-91 following core correlation, see Fig. 2.4.

4.4 Discussion

Clastic lamination can be formed by fluvial processes (Retelle and Child 1996), gelifluction (Doran 1993), drifting ice (Francus et al. 2008), reworking by waves (Geirsdóttir et al. 2009)

and/or eolian input (Antoine et al. 2009). In Paleolake Alf, clastic lamination is predominantly formed by fluvial processes. Sediment delivery into Paleolake Alf is supposed to have been dominated by runoff from snow melt and precipitation. This is supported by the fact, that the predominant mineral composition of the lacustrine sediments (chlorite, mica, quartz, siltstone extraclasts) resembles that of weathered Lower Devonian bedrock (Felix-Henningsen 1990) by more than 90 %. Sparsely occurring olivines and pyroxenes are typical minerals for basanite volcanism as documented from surrounding maars and scoria cones (Becker 1977, Shaw and Eyzaguirre 2000). Certainly, these components entered the lake basin as reworked material. This applies also to the two ash layers which contain mostly subrounded fragments and lack of glass shards (Thor Thordarson, University of Iceland, 2014, pers. com.). Neither in Holzmaar, Meerfelder maar nor Auel maar these two ash layers were described but flood events from that time from Auel maar (Brunck et al. 2016) which supports the assumption that the ash layers were reworked. Single calcite grains of predominantly rounded and the only few calcites of rhombohedral shape implicate a mixture of (1) calcite precipitation in the water column, like they are triggered by algae blooms in recent lakes (Koschel 1997), and (2) detrital origin as reworked eolian input as documented in a reconstructed high-resolution dust record from Eifel maar lake sediments – the Eifel Laminated Sediment Archive (ELSA) stack (Schaber and Sirocko 2005, Seelos et al. 2009) and the Holzmaar sediment record (Zolitschka et al. 2000).

The high abundance of fine to middle-silt fraction in the Paleolake Alf laminated sediments can be explained by multiple freeze-thaw cycles that weather quartz grains and disintegrate bedrock, as, e.g., documented in a study from Siberia (Schwamborn et al. 2012). Loess can also explain the silt size as documented from the former crater top of the Wartgesberg quarry. Additionally, the volcanic activity in the catchment area of Paleolake Alf provided a high amount of disintegrated bedrock because especially maar eruptions promote up to 90 % of country rocks (Zimanowski 1986). Kaolinite most likely deriving from Tertiary relict soils was found in the clay fraction as well (see Chaper 3 of this study).

During the Wartgesberg eruptions, the southern part of the Alf catchment area was covered by ash and scoria. This volcanic material was eroded and immediately transported into the young lake basin as indicated by the 9 m-thick mix of ashes and scoria on top of the lava flow documented in core 5807-91.

During melting season, catchment sediments were transported to the lake basin: the transport capacity caused a near shore and within-tributary deposition forming subaquatic alluvial fans of coarser sediments near the inlets of rivulets (Fig. 4.10) whereas silt-sized particles settled

from suspension in the center of the lake basin forming *Unit I*. After the water level reached its final elevation of 410 m a.s.l., Paleolake Alf might also have had a spillover acting like a continuous sediment pull current, probably comparable to observations of the recent spillover at Lehnmühle reservoir (Kämpf et al. 2012). From correlation of the Paleolake Alf Ca/coh curve with the Greenland NGRIP Ca^{2+} curve, *Unit I* formed during Greenland Interstadial 3 (see Chapter 6). The higher amount of precipitation during interstadials is reflected in an increased occurrence of slumping indicated by folding structures and event layers in *Unit I*. At around 26,300 ka BP, the amount of calcium increases in both records indicating a cold spell - the Greenland Stadial 3 - with enhanced dust accumulation as described by Schaber and Sirocko (2005) and Seelos et al. (2009), forming *Unit II*. Due to the same mineral composition of the light and the dark laminae, the varying silt content can only be associated with seasonal sediment delivery. During the snowmelt season, the high transport energy carried silt-sized, carbonaceous loess that was accumulated in the catchment into the lake basin as indicated by the slightly higher mean grain size of 10 µm and calcite enrichment in the dark laminae.

During winter when the lake was ice-covered, still-water conditions caused suspension settling and the 6 µm-sized particles of the light laminae were deposited. Effectively, grain size and grain shape caused a mineral fractionation in favor of more isometric quartz grains in the dark laminae whereas foliate chlorite and mica grains, due to their higher surface causing uplift, dominate in the light laminae. The 45 mm-sized extraclast and isolated coarse silt grains in the light laminae might indicate a seasonal ice-cover when meltwater slush accumulated on the lake-ice surface as described by Retelle and Child (1996) for Lake C2 in Canada. Load fractures on the ice might have stimulated the meltwater path inducing ice-brake-off. Wind could then have drifted ice floats around the lake in early summer as described by Francus et al. (2008) from Sawtooth Lake in Canada. As documented in core 5807-91, a similar process might have released extraclasts in the center of Paleolake Alf (Fig. 4.10). Silt bands in the light laminae are interpreted as wind-blown loess deposition on the ice cover.

A further indication for an at least seasonally ice-free lake surface is the abundance of ostracod valves (Fig. 4.10). The ostracod species *Candona neglecta* and *Cytherissa lacustris* were only observed in *Unit II*. *Cytherissa l.* is a glacial species that lives in the littoral and profundal zone of lakes and is not recently living in middle Europe but fossil in shallow glacial and interglacial lake sediments (Fuhrmann 2012, Meisch 2000). *Candona n.* is oligothermophil recently occurring in North West Saxony in permanent or slow-flowing water

(Fuhrmann 2012). Both species were also found in the Dehner dry maar in depths between 7 and 34 m (Adams 2010) equaling a time span between 15,000 and 34,000 a b2k (Sirocko et al. 2013).

The question if these laminations are varves, meaning annual deposits (De Geer 1912), is difficult to answer as processes that drive the formation of theses sedimentary structures are complex. As this clastic lamination is drainage-controlled it depends on whether seasonal discharge took place or not, when and if it appeared once or several times a year. This information is important to ensure a continuous record. Further, it is essential to know if the lake waterbody was stratified to transport the sediment suspension along the thermocline into the lake basin or if the lake water was mixed. The two randomly occurring micofacies types forming laminae with normal gradation (*Type I*) and laminae with graded sublayers (*Type II*) suggest single and multiple discharge events under stratified lake conditions. Microfacies *Type I* could have been formed by suspension fall out of an over- or interflow reaching the basin center (Fig. 4.10). Such conditions are promoted by an early-season discharge when the lake is still stratified due to temperature- and density-differences between the inflowing river and the lake's epilimnion as described by Menounos and Clague (2008) from the Canadian Cheakamus Lake. Microfacies *Type II* suggests repeatedly occurring melting events during summer and/or enhanced precipitation events, as described by Chutko and Lamoureux (2008) for the Canadian Arctic, forming stacked graded sublayers as described by Brauer (1994) for Holzmaar.

The up to several centimeter thick graded beds are interpreted as event-related turbidity layers in analogy to studies by Mulder and Alexander (2001) that might have formed during mixed lake conditions. These high energy hyperpycnal turbidity currents distribute as concentrated density flows or underflows during the late melt season due to the missing stratification as described by Menounos and Claque (2008) from Cheakamus Lake or if the inflowing river suspension is denser than the lake water. They are triggered by peak water discharge, slope failure or delta front collapse as described by Zolitschka (1996) from Lake C2 on northern Ellesmere Island, Canada. A higher amount of clay in the event layers indicates resuspension of formerly deposited light laminae and a higher amount of sand suggests a more proximal origin of the density current and a higher transport energy, most likely originating from neighboring slopes. The reconstructed climatic conditions for Central Europe during the Pleniglacial reflect similar conditions as presently occurring in the Canadian Arctic at, e.g., Iqaliut in Nunavut (WMO ID: 71909, Canadian Climate Normals 1981 – 2010) with cold winters, short summers and prevailing permafrost (Huijzer and Isarin 1997, Kasse et al. 1998,

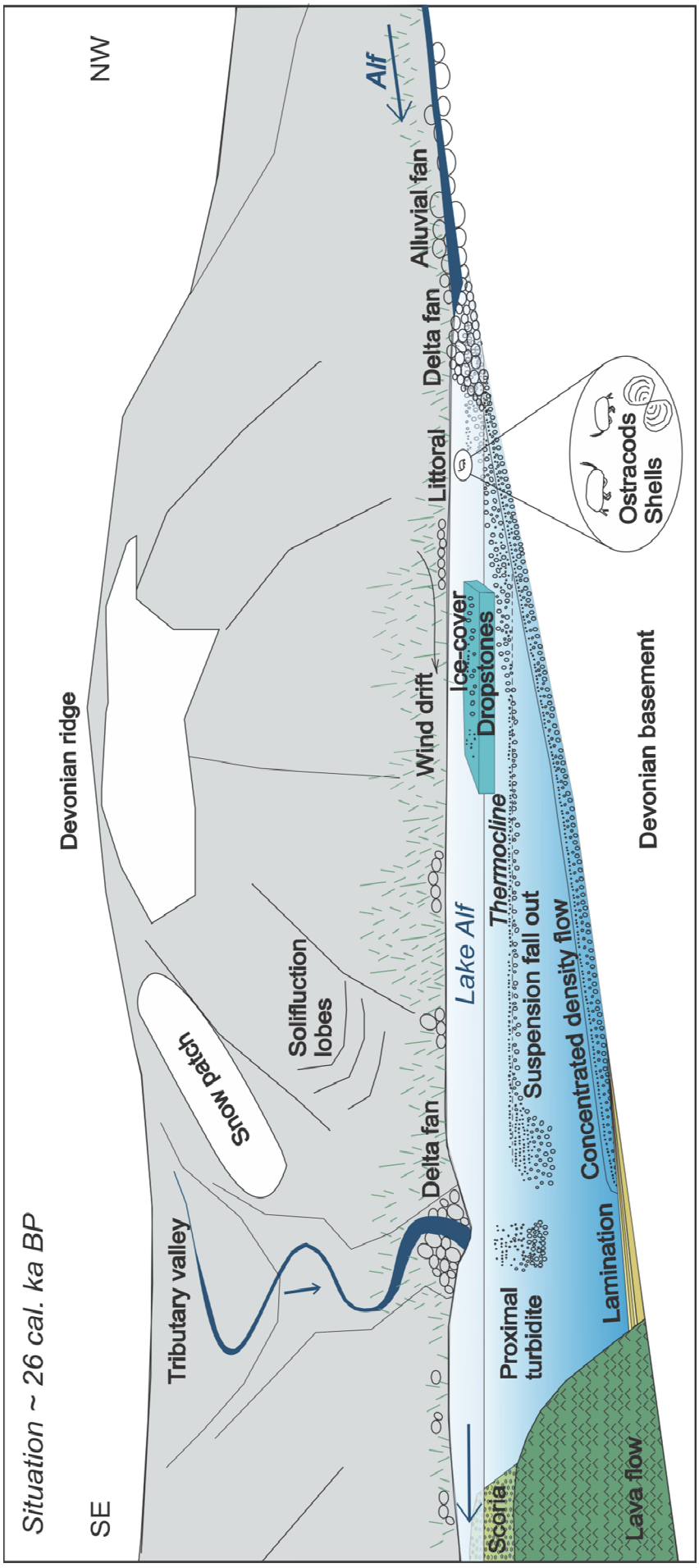

Fig. 4.10: Conceptual model showing Pleniglacial landscape with erosional and sedimentation process reconstruction from sediment structure and component analysis.

Vandenberghe 1993) except for, e.g., differing insolation. Therefore, most studies for comparison were chosen from this region. During the short summer period of five months, we assume melting conditions with sediment erosion and transport. For the other seven months the environment is under snow and ice cover leading to suspension fallout from the lake water column. Due to the more southern location of Germany and the associated higher solar radiation it is suggested that the ice-cover of Paleolake Alf disappeared every summer. Taking these assumptions into account there should be a seasonal signal in the sediments and it is assumed that the lamination is seasonal. The regularity and the good sorting of the laminae of Paleolake Alf support this argument. Also the sedimentation pattern of gradation and stacked graded silt layers are described as being related to varves by studies from Holzmaar, Quaternary West Eifel Volcanic Field in Germany (Brauer 1994) and Lower Murray Lake, High Arctic of Canada (Cook et al. 2009). However, main concerns about an annual mode of deposition are the discrepancy between ^{14}C dating and counted dark-light couplets. An explanation for this could be that not every seasonal sediment delivery has reached the lake basin at the core position so there is a seasonal but irregular deposition. Another possibility might be errors in layers counting as this was only done on high-resolution core scan pictures of 5807-B8 where the ^{14}C measurements were taken from as well.

Since the time span of ^{14}C ages is two to three times higher than the amount of counted couplets, the ^{14}C dating itself might also be questioned because there is hardly any organic matter (humic acid: 1.1-1.5 mg C) preserved for dating under pleniglacial climate conditions. Another option is resuspension of the rare organic matter either by waves eroding old material from the lake shores as described by Geirsdóttir et al. (2009) from Lake Haukadalsvatn, Iceland, or by density flows incorporating older and already deposited lake sediments.

However, as ^{14}C dating of minerogenic, organic carbon poor sediment is always difficult, the key to a better understanding the formation of laminae in Paleolake Alf cannot be obtained until further techniques like magneto- and pollenstratigraphy or luminescence dating have been applied successfully in the future.

Chapter 5

5. Surface reconstruction for lava and sediment volume calculations using ArcGIS demonstrated on a case study of the Alf Valley, Quaternary West Eifel Volcanic Field.

Chapter 5 corresponds to a planned publication with the listed co-authors.

Luise Eichhorn[1], Jörn Engelhardt[1], Thomas Lange[1], Michael Pirrung[1], Marcel Henschen[1], Georg Büchel[1]

[1] *Friedrich Schiller University Jena, Institute for Earth Sciences, 07749 Jena*

Abstract

The reconstruction of paleosurfaces is essential for landscape evolution visualization and volume calculation of bodies with irregular shapes, e.g., sediments from a dammed lake to estimate the reservoir lifetime combined with an age model.

In this study, a 3D model is established using GIS to reconstruct and visualize the Pleniglacial landscape of the volcanically-dammed Alf Valley situated in the West Eifel Volcanic Field. Specifically, the pre-eruptive morphology of the Pulvermaar-Römerberg Complex, the northern eruption centers of the Wartgesberg Volcano Complex including the Strohn lava flow and the Alf valley without sediment infill were reconstructed. The main aims are to calculate the volume of the Strohn lava flow and the fluvio-lacustrine sediment infill, a calculation of a realistic Pleniglacial denudation rate and the Paleolake Alf lifetime. The calculated Strohn lava volume represents 18 Mio. m³ and the Pleniglacial denudation rate between 33 and 21 cal. ka BP amounts to ca. 37.5 mm · ka^{-1}.

The model is based on line input data from, e.g., cross sections and contour lines, and point information from sediment cores. Due to the variable morphology of the catchment area, computer-based interpolation between profiles would have been very imprecise. Therefore, contour lines are manually-drawn.

5.1 Introduction

Most of the continental bedrock is covered by, e.g., sediments, lava or glaciers. In some depositional environments, this coverage in combination with an age model of the cover material involves essential information about, e.g., denudation rates triggered by climatic variations (Amato et al. 2003, Schrott et al. 2003). The latter are important for hydraulic engineers in order to calculate artificial reservoir lifetimes (Einsele and Hinderer 1997). The knowledge about the volume of stored water masses in glaciers is necessary in terms of future water availability (Linsbauer et al. 2009).

In order to model the volume of bodies with irregular shape, a precise underlying bedrock topography is necessary. Previous models that refer to bedrock depths were usually generated from, e.g. geophysical surveys along profile-based transects (Schrott et al. 2003) or point-wise information from core locations. This information is interpolated with the recent $DEM_{surface}$ to create a $DEM_{bedrock}$. However, if the space between the profiles or points is too big and the morphology is highly variable, e.g., in terms of multiple tributary junctions, undercut and slip-off slopes, mathematical interpolations do not result in a realistic model of the underground situation.

For areas with a highly variable morphology, a new technique was developed by combining cross profiles and manually-drawn contour lines under consideration of morphology. The method was applied at the Alf Valley situated in the Quaternary West Eifel Volcanic Field, a middle mountain area, with a medium-sized watershed of 55 km², where lava flows and scoria impounded the Alf River creating Paleolake Alf. Here, all periglacial erosion material was trapped. In this study a precise volume calculation of the Strohn lava flow and the fluvio-lacustrine sediment infill is presented.

The main objectives of this study are:

(i) to reconstruct the surface to the point after the end of the Wartgesberg eruptions just before the lake stage as this is the starting point for lake sediment deposition forming an important archive (Wartgesberg volcano buildup, lava flow reconstruction and elimination of younger volcanoes)

(ii) to determine the lava flow volume

(iii) to determine the Pleniglacial denudation rate by quantifying the sediment volume.

Denudation is here defined as the average ground lowering calculated from the stored sediment volume related to the size of the catchment area.

5.2 Material and Methods

In order to handle the main objectives of the study by creating a 3D model, assumptions have to be formulated.

In this model it is assumed that the catchment topography hardly changed during the last 30 ka years due to the sudden rise of the erosional base level caused by the dammed lake. The trapped predominantly silt-sized sediments contain frost-weathered Devonian silt- and sandstone bedrock, loess, and kaolinite most likely deriving from relict soils originating from Tertiary weathering of Devonian bedrock. In addition, the catchment area was covered by pyroclastic deposits of variable thickness deriving from eruptions of the Mürmes Maar, Dauner Maar Complex, Holzmaar and Wartgesberg Volcano Complex, in parts preserved until present day (Büchel 1994). Further, the Paleolake level was at maximum 410 m a.s.l. as the present height of the Devonian ridge west of Strohn is 412 m. If there had been an overflow over that ridge, the present thalweg of the Alf River would not pass the village Strohn (Fig. 3.1).

The Mürmes Maar was reconstructed because it is much older than 30 ka BP justified by the flat morphology of the maar crater wall (Büchel, pers. com. 2016). Straka (1975) drilled at five locations into the Mürmes Maar and described the uppermost six meters as peat with organic silt und fine volcanic particles. ^{14}C datings on Pollen grains revealed ages of ~ 12.5 ka BP for which reason this sequence was extracted down to the top of the underlying coarse volcanic tephra (Straka 1975). The pre-eruptive morphology of the Pulvermaar-Römerberg Complex was reconstructed because the Pulvermaar crater morphology appears younger than Paleolake Alf (around 15 to 20 ka BP) due to steep flanks and an intact crater wall (Büchel 1984, Büchel und Lorenz 1983). The Wartgesberg Volcano Complex, at present hosting a huge quarry, was reconstructed from a map of the year 1936, presenting a pre-mining situation. The reconstruction of the two northernmost eruption centers of Wartgesberg Volcano Complex with the Strohn lava flow representing the volcanic dam is the starting point for the river impoundment and subsequent lake stage.

The input parameters for applying the reconstruction in a 3D GIS model were:

- Digital elevation model (DEM): 5 m horizontal resolution from the State Office for Land Survey and Geobasis Information Rhineland-Palatinate (2014)
- Shear wave seismic: U. Polom (2007/2008)
- Total magnetic field intensity data: T. Lange (2014)
- Refraction seismic: M. Henschen (unpublished data)
- Core lithologies

- Eruption centers and tephra distribution after the volcanological map (Büchel 1994)
- Elevations of the Wartgesberg Complex before the Wartgesberg quarry activity after the topographic map (Reichsamt für Landesaufnahme 1936).

In the flow chart of Fig. 5.1, the applied method is summarized. For further details please read Chapter 2.3.

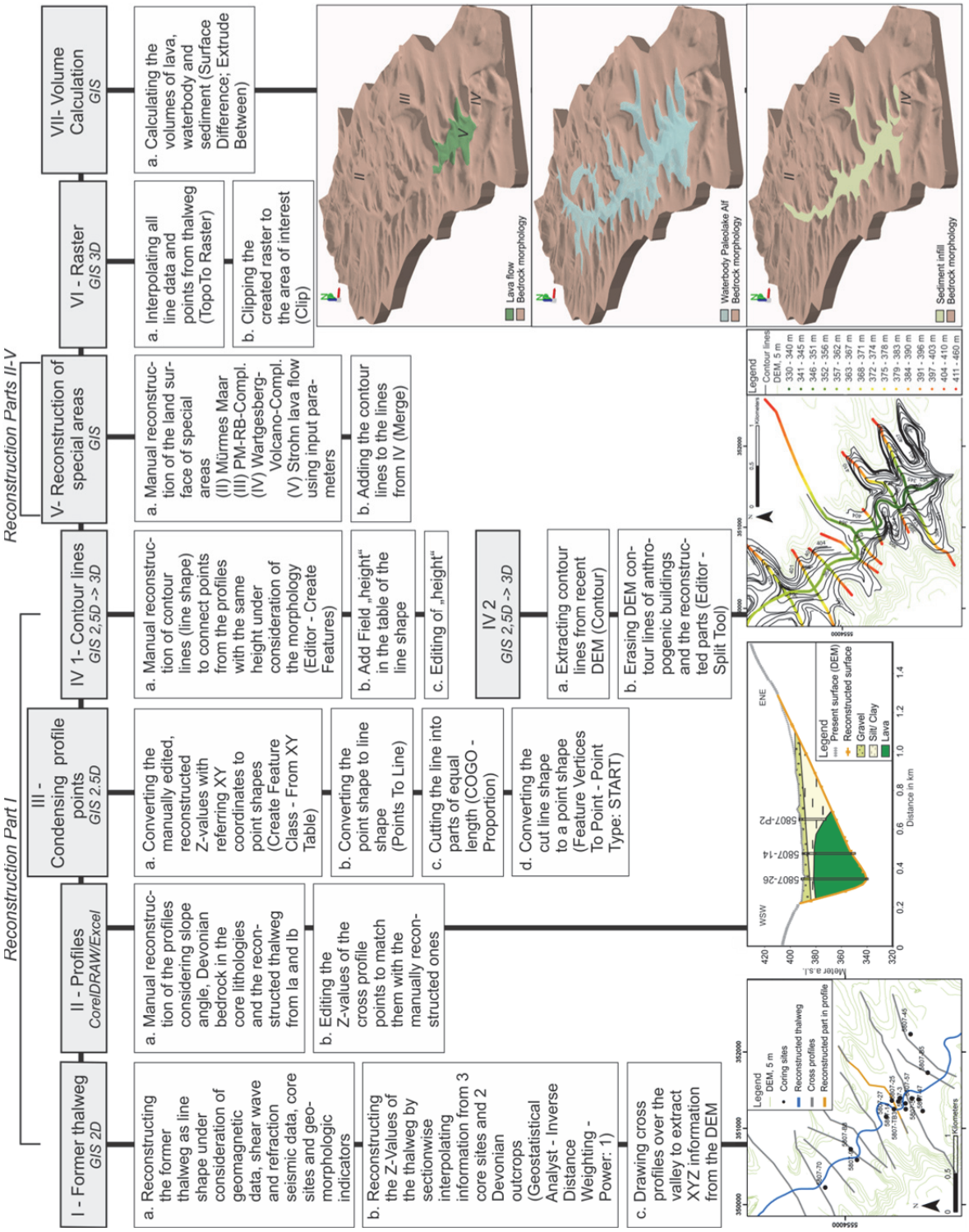

Fig. 5.1: Schema for surface reconstruction and volume calculation using GIS (ArcCatalog, ArcMap, ArcScene), CorelDRAW and Microsoft Excel.

5.3 Results

By using the recent DEM, geomagnetic data, core lithologies, field observations, literature and maps it was possible to reconstruct the Alf Valley after the end of the Wartgesberg eruptions including the Wartgesberg Volcano (IV) build-up (Fig. 5.2A) with the Strohn lava flow (V) (Fig. 5.2B) just before the lake stage. The northern part of Wartgesberg Volcano Complex was rebuilt containing two eruption centers that blocked the Alf Valley with their scoria walls. An argument for this assumption is that the Strohn lava flow could not enter the southeastern valley. According to this reconstruction, the Strohn lava flow derived from the western eruption center.

The Alf thalweg was reconstructed to ~ 332 m a.s.l. before the Wartgesberg eruptions at the position of the presently existing "Körperichberg". The deepest part of the reconstructed Paleolake Alf basin in front of the lava flow was at 336.5 m a.s.l. and the max. lava thickness accounts for ~ 58 m.

In addition, at the Pulvermaar-Römerberg Complex (III), younger than the lake establishment, the pre-eruptive landscape was reconstructed as a peneplain – based on the present existence of remains of the latter to the SW and SE of the dam - dissected by four tributaries (Figs. 5.2A, B). For comparison, Fig. 5.2C shows the present situation in the Alf Valley with the sediment infill, the Pulvermaar-Römerberg Complex and the Wartgesberg quarry.

According to shear wave and refraction seismics, and towards assumptions, the Alf Valley was not as narrow V-shaped as the neighboring Uess Valley (Krawczyk et al. 2013), but had a wider valley bottom possibly due to solifluction material stored at the lower valley flanks. At least in core 5807-70, 4 m of this material were documented.

The volume calculation of the Strohn lava flow from the emergence of the reconstructed eruption center amounts to 18 Mio. m³ which is more than the 15 Mio. m³ estimated by Cipa and much more than the estimated volume of 4-5 Mio. m³ by Wienecke (1979). The water volume of Paleolake Alf at maximum 410 m a.s.l. was calculated to 144 Mio. m³. Under current climate conditions - without evaporation which might have been low during Glacial winters and high during Glacial spring and summers - it would need 286 a (determined by the monthly average flow rate of 42021 m³, water gauge at Saxler Mühle, No. 26800207, Landesamt für Umwelt 2003) to get entirely filled. Most likely the entire filling of the basin took longer during the Pleniglacial as water discharge was dependent on meltwater season and arid climate conditions as reconstructed by Huijzer and Isarin (1997). However, surface runoff was probably higher than today due to permafrost preventing water penetration into the ground.

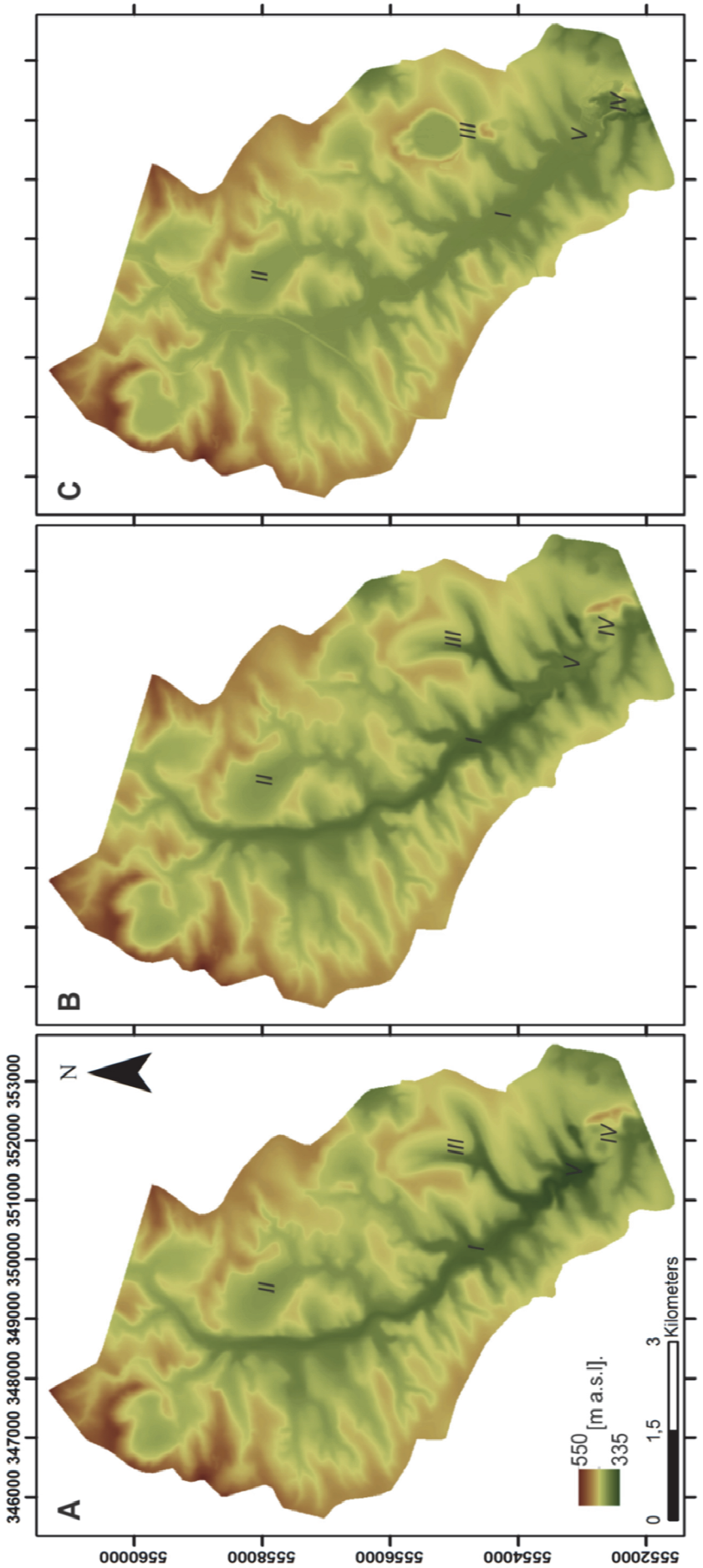

Fig. 5.2: Reconstructed Alf Valley with the pre-eruptive morphology of the Pulvermaar-Römerberg Complex and two eruption centers of the Wartgesberg Volcano Complex shortly after the end of the Wartgesberg eruptions without Strohn lava flow (**A**) and with reconstructed Strohn lava flow (**B**). The present Alf Valley is shown in **C** (DEM source: ©GeoBasis-DE /LVermGeoRP, 2014).

The calculated entire sediment infill composing of fluvio-lacustrine material amounts to 73 Mio. m³. In Chapters 3 and 4, a hiatus was interpreted between *Units II* and *III* at 385 m a.s.l. (~ 6 m below present valley floor) showing an abrupt change between laminated silt-sized lacustrine deposits and sandy fluvial material. In a further step, only the lacustrine sediment volume was calculated below the level of the hiatus at 385 m a.s.l.. Combining this calculated volume with the age model of core 5807-91, 25 Mio. m³ of lacustrine sediment was accumulated between 33 and 21 cal. ka BP. According to these values, a 0.45 m thick slice of land surface would have been denuded from the catchment area during that time.

5.4 Discussion

Paleosurface reconstruction

The reconstruction of the Wartgesberg Volcano Complex is based on a topographic map of 1936 before mining started which represents the minimum former height since erosion most likely reduced relief. The former wider extension of the scoria wall of the eastern Wartgesberg eruption center blocking the neighboring tributary valley is very likely because no lava was found in the core (5807-45, see Fig. 2.9, Chapter 2). The Körperichberg was reconstructed as part of the western eruption center. The dipping of welded scoria could be mapped but it was difficult to decide if the scoria is solid or a boulder. Further, the Körperichberg is anthropogenically overprinted because the scoria was used for millstone production and military activities; presently it is used as dump. Against assumptions from literature that the “Lange Klopp” is a scoria cone with the eruption center in the Alf Valley at the Strohner Mühle (for position, see Fig. 3.1, Chapter 3), e.g., Hopmann et al. (1960), in this study it was reconstructed as part of two eruption centers according to the dipping of welded scoria.

Paleo-denudation rate

Denudation rates are essential in order to understand landscape evolution. Generally, it depends on different parameters like relief, rock properties, type and temporal distribution of precipitation (water availability), isostatic rebound/ tectonic uplift, average temperature and temperature range, vegetation, soil genesis, dust input, the size of the watershed and the activities of humans in the catchment area (Harrison 2000, Hinderer 2001, Maccaire et al. 1997, Schaller et al. 2002, Peizhen et al. 2001). There are several methods to determine denudation rates like fission track analysis (Gleadow et al. 2000), cosmogenic ^{10}Be analysis (Meyer et al. 2010, Schaller at al. 2002), dissection of datable surfaces (Van Balen et al. 2000)

or from sedimentary records of natural closed basins (Macaire et al. 1997, this study). For comparing denudation rates of, e.g., similar climatic regions, it is necessary to consider the above mentioned parameters.

In this study, the Paleolake Alf archive revealed a Pleniglacial denudation rate of 37.5 mm · ka^{-1} between 33 and 21 cal. ka BP. This value includes an uncertain amount of loess which accumulated during the Pleniglacial in the WEVF as documented by Sirocko et al. (2016) or Löhr and Neyses (1997) but can be used at least for comparison with other values in this region. Frechen et al. (2003) describe Weichselian loess deposits of ~ 1.5 m thickness from the East Eifel at Schweinskopf (E: 387616, N: 5579852) and Tönchesberg (E: 282613, N: 5578848), 40 km NE of the Alf Valley.

Comparing the denudation rate calculated from Paleolake Alf with the Allier River basin in France, the Pleniglacial denudation rate of 40-56 mm · ka^{-1} is quite similar. This number was determined by ^{10}Be and ^{14}C ages from terrace sediments (Schaller et al. 2002) and represents the period between 29 and 16 ka BP. The denudation rate in the Allier River basin might have been increased due to a higher relief difference of 700 m compared to the Alf catchment with 160 m (390 to 550 m a.s.l.).

In contrast, mean Holocene periglacial denudation rate for the high arctic Linnédalen Valley were calculated from Lake Linnévatnet in Svalbard, Norway (Svendsen et al. 1989), located in a 36 km^2 sized catchment area of metamorphosed quartzite, mica-schist and sedimentary rocks. Here, the denudation rate was calculated from sub-bottom acoustic profiling (echosounding), core stratigraphy and ^{14}C age dating. It amounts to only ~ 15 mm · ka^{-1}. This deviation could be explained by a general smaller catchment whereof 6 % is glaciated.

In addition, Late Glacial to Holocene (12.6-8.5 ka BP) denudation rate calculated from sediment volume of Lake Tartaret in the Massif Central, France (Macaire et al. 1997) located in a middle mountain area within crystalline bedrock amounts to 79-120 mm · ka^{-1}. The high denudation rate could be explained by the higher relief difference of 960 m and the change from a glacial storage to gravity processes-dominated regime after 15.5 ka BP eroding especially volcanic rocks. Here, volume calculation was conducted using Descartes Modélisation program (IGA Tours) with an accuracy of ±10 % by combining core lithologies, electric sounding and magneto-telluric measurements.

As stated before, the given examples of denudation rate numbers can only be taken for comparison when the parameters and the methods accuracy are considered.

Regarding the sediment yield, the calculated ~ 97 t · km^{-2} · a^{-1} would suggest a reservoir lifetime of ~ 10 ka before silting up according to a calculation table by Einsele and Hinderer

(1997). According to the age model, Paleolake Alf persisted at least 12 ka before the volcanic dam collapsed.

Lava volume

The calculated mass of the Strohn lava flow in this model differs by 3 Mio. m³ from calculations by Cipa. This discrepancy could be explained because Cipa used the magnetic anomaly intensity for lava flow thickness (Cipa 1958) which was determined in cross profiles. Due to the distant interval of the cross profiles, interpolation between profiles is less precise compared to calculations of this study.

Model deviation and error analysis

In some cases the depth of the reconstructed 3D surface and the bedrock surface depth taken from core lithologies "Top bedrock" deviate by more than 5 m. These cases will be explained in the following by naming the coring points (Fig. 5.3). For core 5807-45, the 15 m deviation can be explained by the imprecise description in the core lithology which mentions a 30 m thick part of slates, graywacke and claystone. It is not clear if this sequence is bedrock or loose solifluction material. Therefore, the model depth was put in between. The 8 m deviation of core 5807-25 occurs because the highest anomaly of the total magnetic field intensity was used for the thalweg reconstruction. Therefore, the thalweg runs on the left side of this core location and the model is not deep enough at the core position. The bedrock in cores 5807-91 and 5807-B8 is 6 m deeper than in the model. Here, the interpolation of the thalweg might have caused the deviation.

For the lava flow reconstruction, the model deviates at three core locations. The "Top lava" from core 5807-P3 at 386 m a.s.l. does not fit to the rest of the cores in the area where the lava top is at 378 (P4), 377 (5807-27) and 379 m a.s.l. (5807-14). This deviation of 10 m might be a core description mistake (Fig. 5.4). The deviation of 7 m at core 5807-P2 is according to the magnetic anomaly which enters the tributary quite far up and the lava flow was reconstructed thicker than in the core lithology. At core location 5807-B5 - close to the lava outlet, the lava top is at 374 m a.s.l. which is lower than at the 300 m distant core 5807-56 where lava top is at 380 m. It is nearly impossible that the height of the lava top in core 5807-B5 is correct unless it was eroded right after the eruption.

Generally, this model is an approximation to the past situation combining different input parameters. Sometimes even the input parameters are not consistent like the discussed core lithologies. As the cores were drilled between 1940 and 2014, a first error source can be the incorrect core position as topographic or cadastral maps were utilized for core localization. In

addition, several geologists described the core lithologies using different terms, varying precision and therefore providing space for interpretation for the user.

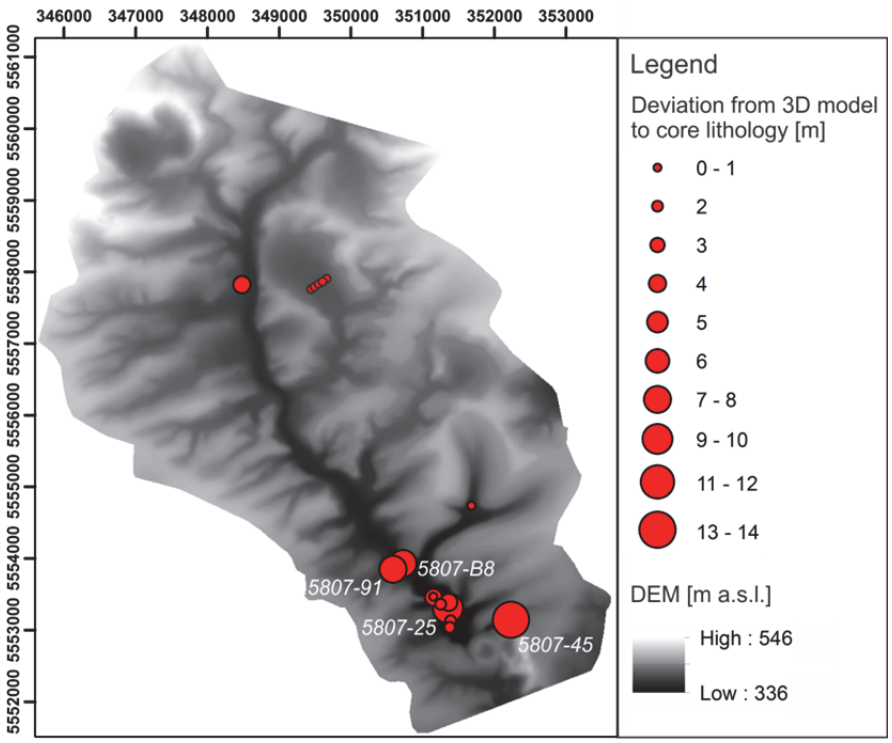

Fig. 5.3: Maps of the study area showing the deviation between the reconstructed 3D model and the bedrock surface depth taken from core lithologies.

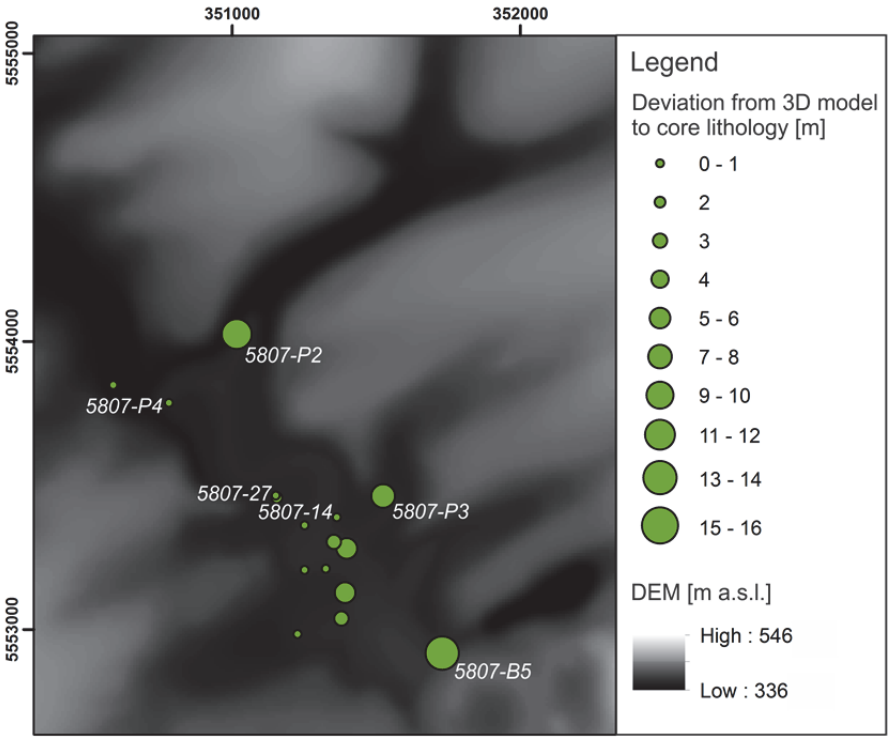

Fig. 5.4: Map of a part of the study area showing deviation between the reconstructed lava flow model and the “Top lava” depth taken from core lithologies.

Chapter 6

6. Synthesis

The aim of this study was to improve the understanding of the paleoenvironmental changes during the Middle to Late Pleniglacial in the West Eifel Volcanic Field (WEVF) by sedimentological investigations focusing on transport media, deposition structure, and GIS modelling to calculate volumes and denudation rates.

Therefore, the Paleolake Alf fluvio-lacustrine sediment archive was investigated applying a multiproxy approach containing field surveys; sedimentological, microscopic and geochemical analysis; geophysical surveys and GIS modelling.

The Paleolake basin architecture and the evolution of the sediment infill-process were reconstructed and compared to modern reservoirs regarding drawdowns and prograding deltas. Lamination structure was observed on thin sections and compared to modern monitoring studies from glacial or periglacial environments to clarify if it composes of clastic varves or not. Furthermore, the paleosurface of the Alf Valley after the end of the Wartgesberg eruptions was reconstructed to calculate the Strohn lava flow volume, and that of the lacustrine sediment to derive a Pleniglacial denudation rate. This thesis presents the first investigation on a volcanically-dammed lake in Central Europe and is a complementary study to maar lake records from the WEVF.

6.1 Main results

The main results of the thesis are summarized in the following:

- Paleolake Alf had a max. lake level of 410 m a.s.l., an elongated lake shape and a catchment area of 55 km² (Chapter 3).

- Paleolake Alf basin architecture resembles that of modern reservoirs with top-, fore- and bottomset sediments (Chapter 3).

- The most intensively-investigated sediment core was taken from the basin position with the highest sediment thickness as reconstructed from Paleolake Alf bathymetry (Chapters 3, 6).

- Lacustrine sediments predominantly originate from weathered Lower Devonian silt- and sandstones represented by, e.g., silt extraclasts; quartz, feldspar, transparent mica, chlorite minerals and kaolinite (Chapter 3).

- Lacustrine sediments can be separated into finely laminated *Unit I* formed during the Greenland Interstadial 3, and laminated *Unit II* formed during Greenland Stadial (GS) 3. Grainsize coarsening and calcium increase in *Unit II* are interpreted as resulting from enhanced loess input during GS 3 (Chapters 3, 4).

- Clastic lamination is probably seasonal and driven by fluvial processes from snowmelt and precipitation. Two microfacies types were differentiated: *Type I* - Laminae with normal grading and *Type II* - Lamination with graded sublayers (Chapter 4).

- A hiatus evident from a sudden grainsize change indicates a dam collapse at ~ 15 cal. ka BP which induced partly erosion of lacustrine sediments and subsequently fluvial sediment accumulation due to prograding Alf River delta (Chapter 3).

- Scoria-bearing “Lange Klopp” and Körperichberg are relicts of two eruption centers of the Wartgesberg Volcano Complex that were reconstructed whereas former scientists believed that they were single scoria cones (Chapter 5).

- Pleniglacial denudation rate derived from sediment volume and age model calculations amounts to 37.5 mm · ka^{-1} which fits to Pleniglacial erosion rates of the Allier River basin in France (Chapter 5).

6.2 Discussion

Unlike maar lakes, Paleolake Alf formed due to the Wartgesberg Volcano Complex eruptions at ~31±11 ka BP (Plateau age, Mertz et al. 2015). The Wartgesberg emitted two lava flows (Strohn and Sprink lava flow) and scoria which dammed the Alf Valley, impounded the Alf River and created an elongated lake. The archive covers 12,000 years in succession (33-21 cal. ka BP), in total from 33-13.8 cal. ka BP with a hiatus between 21 and 16 cal. ka BP. This time span is also documented in several investigated maar lake records, e.g., Auel Maar (Brunck et al. 2016), Dehner Maar (Sirocko et al. 2013) and Meerfelder Maar (Negendank 1989, Fig. 6.1).

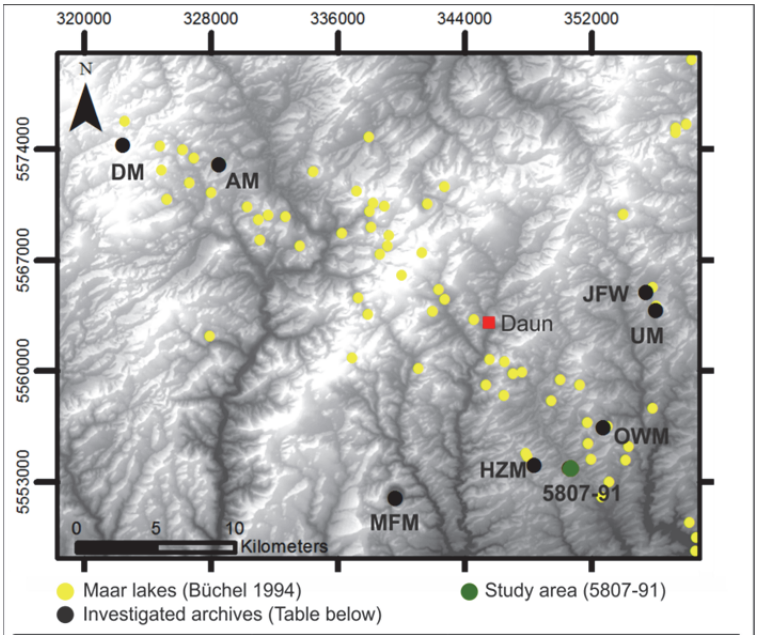

Archieve name	Investigated period	Literature
Auel Maar (AM)	64 - 10 ka BP	Brunck et al. (2016)
Oberwinkel Maar (OWM)	64 - 22 ka BP	Sirocko et al. (2013)
Jungfernweiher (JFW)	59 - 26 ka BP	Sirocko et al. (2013)
Dehner Maar (DM)	42 - 12 ka BP	Sirocko et al. (2013)
Meerfelder Maar (MFM)	35 ka BP - present	Negendank (1989)
Paleolake Alf (5807-91)	31 - 9.8 ka BP	Eichhorn (this study)
Holzmaar (HM)	23 ka BP - present	Brauer (1994), Negendank (1989)
Ulmener Maar (UM)	8 ka BP - present	Sirocko et al. (2013)

Fig. 6.1: Map showing the locations of maar lakes (Büchel 1994) in the West Eifel Volcanic Field and investigated archives with preserved documentation period compiled from literature cited in the table below.

6.2.1 Sediment structure and basin architecture

The sedimentary structures of the volcanically-dammed Paleolake Alf very much resemble that of the investigated maar lake records in the vicinity, e.g., Lake Holzmaar (Brauer 1994) and Lake Meerfelder Maar (Negendank 1989, Negendank et al. 1990).

The following sediment descriptions originate from a combination of the three cores 5807-91, 5807-B8 and 5807-70 (Pirrung et al. 2007) taken in the deepest part of the Paleolake Alf basin (Fig. 6.2).

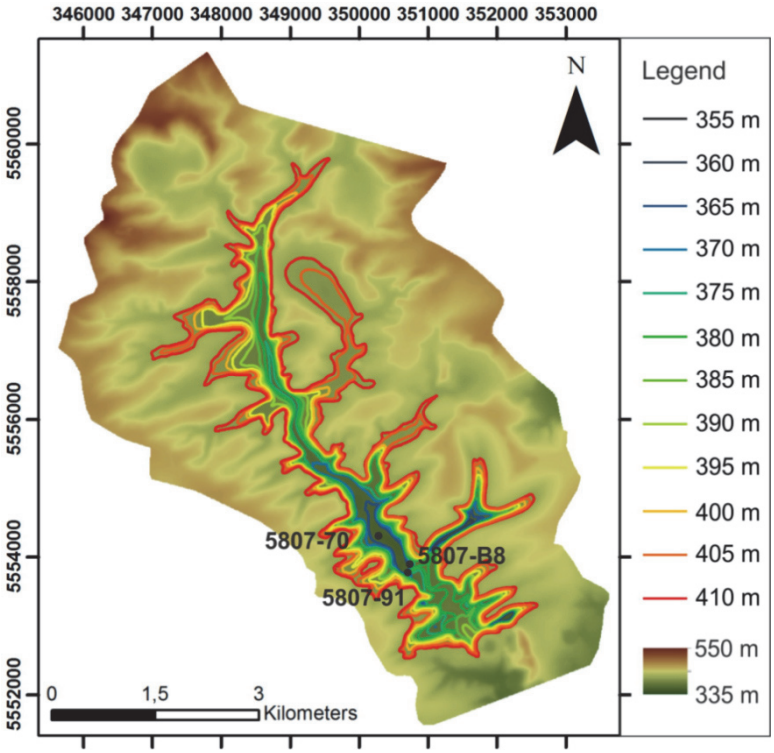

Fig. 6.2: Reconstructed Paleolake Alf bathymetry is shown with reconstructed DEM and Strohn lava flow. Dark blue colours indicate deepest parts of the lake basin, black dots symbolize core locations. Indicated meters mean m a.s.l..

Laminated lacustrine sediments of Paleolake Alf predominantly consist of weathered Lower Devonian silt- and sandstones eroded in the catchment, represented by, e.g., silt extraclasts; quartz, feldspar, transparent mica and chlorite minerals. Apart from that, clay mineralogy reveals illite, smectite and kaolinite - similar to Lake Holzmaar (Brauer 1994). Illite derives from Lower Devonian silt- and sandstone bedrocks and smectite most likely from weathered olivines and pyroxenes of volcanic ashes. Kaolinite derives from relicts of products from intense Tertiary subtropical weathering, i.e. paleosoils as documented from Lake Meerfelder Maar (Negendank 1989). The high amount of clayey silt might originate primarily from (a) physical weathering due to frequent frost-thaw changes of the active layer, (b) physical disintegration of bedrock due to phreatomagmatic maar eruptions in the catchment, (c) loess deposits and (d) Tertiary weathering relicts.

The lacustrine sediments were lithologically separated into *Units I* and *II*, Table 3. *Unit I* consists of four (5807-91) to ten (5807-70) meter thick finely laminated, silty clay-rich sediments which formed during the Greenland Interstadial 3 (Chapter 4 and this Chapter).

Sediments were eroded by precipitation and meltwater from the catchment and washed into the lake basin. The coarse fraction deposited at the inlet and the fine fraction reached the central, deep basin.

The hanging up to 16 m thick (core 5807-70) *Unit II* is characterized by dark (mean 10 μm) and light (mean 6 μm) silt-sized laminae with a couplet thickness averaging 8 mm. Particle coarsening is linked to an increase in the calcium content interpreted as redeposited loess input which is correlated to the Greenland Stadial 3 (this Chapter). The light laminae formed during winter when the lake was ice-covered, indicated by single up to gravel-sized rocks interpreted as dropstones or ice-rafted debris. Still-water conditions caused suspension fallout enabling especially phyllosilicates, e.g., mica to settle, forming light laminae. The dark laminae dominate in quartz and are enriched in calcite. The calcite originates predominantly from rounded grains and only a few calcites of rhombohedral shape are present. This implicates a mixture of two processes: (1) predominantly detrital origin of redeposited eolian input. The detrital calcite is transported into the lake basin by soil erosion of a carbonaceous loess cover from surrounding slopes during spring and summer. Eolian input is also documented from a high-resolution dust record from Eifel maar lake sediments – the Eifel Laminated Sediment Archive (ELSA) stack (Schaber and Sirocko 2005, Seelos et al. 2009) and the Holzmaar sediment record (Zolitschka et al. 2000). The product of the second process: (2) calcite precipitation in the water column during summer, triggered by algae blooms as it is evident from recent lakes (Koschel 1997) exists in low amount.

Similar formation processes of light and dark laminae are documented from recent periglacial lakes in the High Canadian Arctic (Chutko and Lamoureux 2008, Cook et al. 2009, Francus 2008, Menounos and Claque 2008) and can be transferred to the formation of the clastic lamination of Paleolake Alf.

The dark laminae can further be divided into two types: *Type I* - Laminae with normal grading, (19 % occurrence) and *Type II* - Laminae with graded sublayers, (81 % occurrence) which occurs randomly (Eichhorn et al. subm.). *Type I* - Grading of the dark laminae with a coarse base and a fining up implies suspension fall out of an over- or interflow reaching the basin center as described by Menounos and Clague (2008) from the Canadian Cheakamus Lake. Such conditions are promoted by an early-season discharge when the lake is still stratified due to temperature- and density-differences between the inflowing river and the epilimnion of the lake (Menounos and Clague 2008).

Type II suggests repeatedly occurring melting events during summer and/or enhanced precipitation events, as described by Chutko and Lamoureux (2008) for the Canadian Arctic,

forming stacked graded sublayers also described by Brauer (1994) from Holzmaar. However, in Lake Holzmaar these stacked graded sublayers occur only with 5 % in the upper part of the record between 15,200 and 13,900 a BP 95 % of the Holzmaar laminae contain graded laminae. This might be attributed to the differing sediment transport in different lake shapes. In Paleolake Alf predominantly repeatedly occurring melting events have been recorded due to the permanent water inflow whereas in Lake Holzmaar only after the LGM repeated discharge within one season was stimulated due to enhanced melting.

Table 3: Selected parameters of sedimentary units deposited in Paleolake Alf. Unit characterization refers to core 5807-91 (thickness variations include cores 5807-B8 and 5807-70), *[1] Types are described in the text, *[2] values derive from core 5807-70 (Pirrung et al. 2007). (Qtz-Quartz, Fsp-Feldspar, Ms-Muscovite, Cl-Chlorite, Ill-Illite, Sm-Smectite, Ka-Kaolinite, Ol-Olivine, Px-Pyroxene, Pl-Plagioclase) ·

Unit	Thickness [m]	Age [ka BP]	Structure	Mean Grainsize [µm]	Magn. Susc. [SI ·10^{-6}]	Mineralogy	TOC [%]	TIC [%]	Sedimentary features
Unit III 	5.8-7	9.8-<11.2 (13.8-<15.8 cal.)	mixture of gravel, sand and silt	630	3510		8.6*[2]	1.1*[2]	variable mixture of volcanic particles, peat and gravel to clay-sized Devonian material
Unit II 	13-16	17-<26.5 (21-<30.5 cal.)	8-mm lamination		850	Qtz, Fsp, Ms, Cl, Ill, Sm, Ka, Ol, Px, Pl	0.3	0.75	redeposited ash layers, graded beds
			Light lamina: Homogeneous clay cap	6		enriched in phyllosilicates (mica)			
			Dark lamina: Types I, II*[1]	10		enriched in quartz			
Unit I 	4-10	26.5-30 (30.5-34 cal.)	(sub)millimeter lamination	6	2514	Qtz, Fsp, Ms, Cl, Ill, Sm, Ka, Ol, Px, Pl	0.3	0.3	silt extraclasts, graded beds, ≤ 30 mm thick homogeneous sand layers, ≤ 30 cm thick slump structures, debris layers

Obviously, the periglacial laminae of Paleolake Alf have the same structure as clastic varves formed under present (peri)glacial conditions indicating annual deposits (De Geer 1912). However, it is difficult to determine if these laminae are of annual origin. As this clastic lamination is drainage-controlled it depends on whether seasonal discharge occurred or not, when and if it appeared once or several times a year, and if there is a lake-ice break-up or not. This information besides waterbody stratification influencing the sediment transport into the lake is important for interpretation. However, dropstones or ice-rafted debris implicates ice-cover – a seasonal signal which is supported by very regular and well-sorted laminae. Therefore, clastic lamination of Paleolake Alf is interpreted as seasonal similar to the clastic varves of Lake Holzmaar described by Brauer (1994).

The clastic lamination is interrupted by event-related deposits, e.g., turbidity layers varying between 70 mm (5807-91, basin center) and 130 mm (5807-B8, basin margin) thickness. These high energy hyperpycnal turbidity currents distribute as concentrated density flows or underflows during the late melt season due to the missing stratification as described by Menounos and Claque (2008) from Cheakamus Lake or if the inflowing river suspension is denser than the lake water. They are triggered by peak water discharge, slope failure or delta front collapse as described by Zolitschka (1996) from Lake C2 on northern Ellesmere Island, Canada. Turbidity layers are also described from Lake Holzmaar (max. 119 mm) and Lake Meerfelder Maar (max. 260 mm) (Brauer 1994). Brauer (1994) stated that the turbidity layer thickness is related to discharge. Catchment and therefore discharge is increased in Lake Meerfelder Maar. In comparison, in Paleolake Alf discharge should have been high but turbidity layer thickness is similar to Lake Holzmaar which might be explained by the steep crater walls of Lake Holzmaar shortly after its eruption.

In addition, debris layers of 80-150 mm thickness only occur at the margin of Paleolake Alf basin in core 5807-B8, also documented from Lake Holzmaar with 35-300 mm thickness (Brauer 1994) and 40-160 mm from Lake Meerfelder Maar (Drohmann and Negendank 1993).

Single olivine, pyroxene and a few plagioclase crystals intercalated in the sediment show the presence of volcanic deposits in the catchment area. The two identified ash layers in the Paleolake Alf sediments were neither described from Lake Holzmaar, Meerfelder Maar nor from the Auel Maar but flood events were recorded from that time from Auel Maar (Brunck et al. 2016) which supports the assumption that the ash layers are reworked. This is further supported by the fact that in core 5807-70 (Pirrung et al. 2007), a couple of layers were described that do not occur in the core analyzed in this study.

Only in *Unit II* (17 ≤ 26.5 ka BP), the two ostracod species *Cytherissa lacustris* and *Candona neglecta* were determined. The former is a glacial species that lives in the littoral and profundal zone of lakes and is not recently living in Central Europe but fossil occurrences in shallow glacial and interglacial lake sediments are known (Fuhrmann 2012, Meisch 2000). The latter is oligothermophil and recently occurs in northwest Saxony in permanent or slow-flowing water (Fuhrmann 2012). Both species were also found in the Dehner Maar in a depth between 7 and 34 m (Adams 2010), which is attributed to a time span between 15,000 and 34,000 b2k (Sirocko et al 2013).

The TOC averaging to 0.3 % is similar to periglacial deposits of Lake Holzmaar (0.5 %, Brauer 1994) and in the range of (peri)glacial environments, e.g., the Laptev Sea coast

(Schirrmeister et al. 2008) with low organic productivity and little microbial activity due to permafrost conditions.

The overlaying *Unit III* is characterized by an abrupt grainsize change to gravelly sand-sized sediments of ~ 7 m thickness composed of bedrock siltstones, quartz and volcanic material indicating higher transport energy. The rounding of many pebbles suggests rolling transport in a river. The formation of the units is presented in the following.

6.2.2 Evolution of the lake basin

Using sedimentological data from five further cores distributed northwards in the basin (5807-88, 5807-89, 5807-90, 5807-2, 5807-70) which were correlated by lithological descriptions, magnetic susceptibility and grainsize analysis, sediments of *Units I* and *II* gradually become coarser upstream (~ 5 km north of the dam). Coarse gravel-sized river sediments were deposited at the prodelta (5807-88), sand-sized material in the foreset region (5807-89 and 5807-90) and fine-grained clay and silt particles represent the bottomset area (5807-2, 5807-70, 5807-91, Fig. 3.1) similar to recent reservoir basins, e.g., Englebright Lake in northern California (Snyder et al. 2006). During the existence of Paleolake Alf, the lake might have leaked by water penetrating through porous scoria and along the contraction-joints of the lava flow at the dam. At the surface, frost-thaw changes continuously disintegrated the volcanic dam and meltwater runoff incised due to the steep slope of 6 % (between dam height of 410 m and reconstructed Alf thalweg height after the dam) illustrating a high erosion potential as described by e.g., Claque and Evans (1994) from natural dams in the Canadian Cordillera.

The abrupt grainsize change from silt (*Units I, II*) to gravelly sand (*Unit III*) is interpreted as a hiatus and a sudden change from a lacustrine to a fluvial deposition regime. By extrapolating the sedimentation rate from the lacustrine and fluvial regime, the hiatus would cover 5000 years (21-16 cal. ka BP). It is assumed that either due to enhanced discharge, backward erosion or a combination of both aspects, the dam became increasingly unstable, failed and parts of the lacustrine sequence (~ 6 m, equals sediment thickness when extrapolating the sedimentation rate of the fluvial deposits and lacustrine to the hiatus) were eroded corresponding to the new dam overflow at ~ 385 m a.s.l.. This process is perhaps comparable to what happened at the IVEX dam in northeast Ohio. Here, an intense rainfall event triggered a catastrophic dam failure including erosion (also of fine-grained sediment of the reservoir), flooding and sedimentation downstream (Evans et al. 2000). In total ~ 9-13 % of the reservoir fill were mobilized (Evans et al. 2000). As primary desposits of the Pulvermaar tephra were

not found in the lacustrine sequence of *Units I* and *II*, it is assumed that the eruption occurred during the time of the hiatus between ca. 21 and 16 cal. ka BP which fits to the assumed time period of 15 to 20 ka BP by Büchel (1984). The primary tephra was most likely removed together with other sedimentary material during the dam failure. Due to the lack of Holzmaar tephra in the Paleolake Alf record, it is possible that the maar is older than the Wartgesberg Volcano Complex which contradicts to the ^{14}C data of Brauer (1994) and Negendank (1989), Table 1.

Then, the fluvial sequence of *Unit III* was deposited between 11.2 and 9.8 ka BP due to both compaction of the lacustrine sequence after drainage and the low gradient in front of the dam preventing erosion. Here redeposited ashes and lapilli, i.e. sands and gravel, most likely from Pulvermaar and redeposited Laacher See Tephra (Löhr and Neyses 1997, Pirrung et al. 2007) which was emitted ~ 12.9 ka BP (Van den Bogaard 1995) were accumulated. During this time, sedimetation started in the Mürmes Maar (Straka 1975), older fluvio-lacustrine sediments do not exist and must have been eroded during the dam failure. Presently, River Alf is continuously incising into the Strohn lava and the fluvial deposits of *Unit III* with the future perspective to reach its ideal river profile someday (Fig. 6.3).

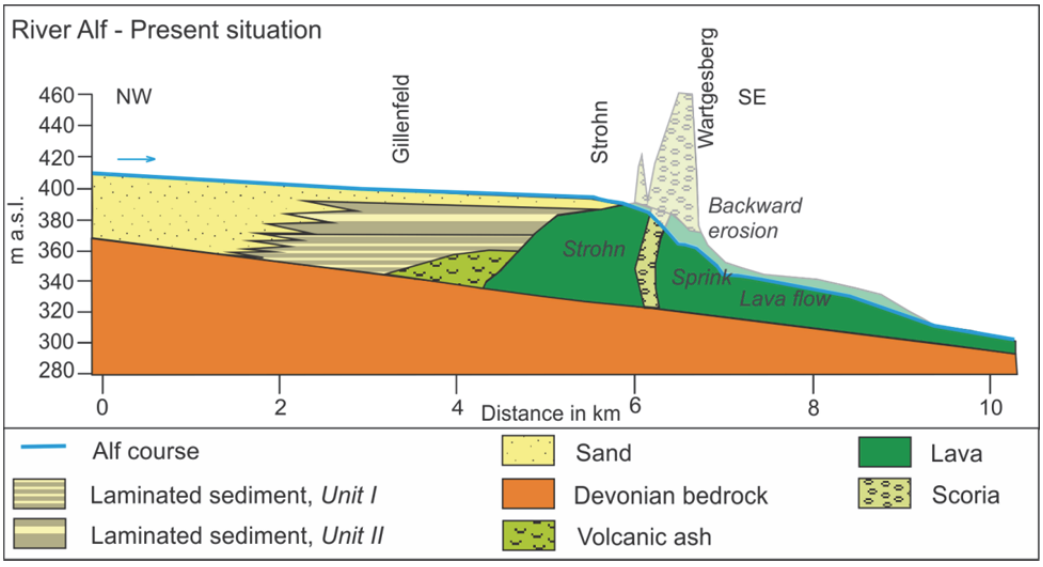

Fig. 6.3: Present situation of the Alf Valley showing the sediment architecture along a longitudinal profile in NW to SE direction. River Alf is regressively eroding the Strohn lava and parts of *Unit III,* modified from Eichhorn et al. (in prep.-a).

Before the Wartgesberg eruptions, the Alf thalweg was at ~ 332 m a.s.l. in front of the "Körperichberg" (Fig. 6.3). The reconstructed max. thickness of the emitted Strohn lava flow amounts to ~ 58 m and the deepest part in the Paleolake Alf basin was at 336 m a.s.l. (Eichhorn et al. in prep.-b). Concerning the amount of lacustrine deposits in the Paleolake Alf (*Units I* and *II)* basin, 25 Mio. m³ sediment were accumulated between 33 and 21 cal. ka BP

(Eichhorn et al. in prep.-b). By distributing this volume to an equal thickness on the catchment area, 0.45 m of land surface coverage would have been removed (37.5 mm · ka^{-1}). This value includes an uncertain amount of loess which accumulated during the Pleniglacial in the WEVF as documented by Sirocko et al. (2016) or Löhr and Neyses (1997). Frechen et al. (2003) describe loess deposits of ~ 1.5 m from the East Eifel at Schweinskopf (E: 387616, N: 5579852) and Tönchesberg (E: 282613, N: 5578848), 40 km NE of the Alf Valley. Comparing the Alf catchment denudation rate with, e.g., the Allier River basin in French Massif Central (Schaller et al. 2002) between 29 and 16 ka BP, it amounts to 40-56 mm · ka^{-1} which is in the same order of magnitude. The denudation rate in the Allier River basin might be increased due to a higher difference in relief of 700 m, compared to 160 m in the Paleolake Alf catchment. In contrast, the mean Holocene periglacial denudation rate for the high arctic Linnédalen Valley amounts to ~ 15 mm · ka^{-1}. This difference can be explained by a smaller catchment area of which 6 % is glaciated.

Generally, erosion depends on different parameters, e.g., type of the bedrock, relief, availability of water, average temperature, temperature range, isostatic rebound/ tectonic uplift, vegetation cover and dust input (Harrison 2000, Hinderer 2001, Schaller et al. 2002, Peizhen et al. 2001). For every comparison, these parameters have to be considered.

6.2.3 Comparison to other records

In order to correlate the Paleolake Alf record to other lacustrine sediment and ice-core records, volume-specific magnetic susceptibility data from Lake Holzmaar (Fig. 6.4), Lago Grande di Monticchio (Fig. 6.5) and calcium data from NGRIP (Fig. 6.6) were taken into consideration. Magnetic susceptibility from redeposited volcaniclastic material can be interpreted for all three lakes located in volcanic environments as a proxy for water discharge.

Lake Holzmaar is situated 2 km southeast of core 5807-91 from Paleolake Alf (Fig. 6.4), volcaniclastic material is available in both catchment areas. Generally, the pattern resembles well, only for the big spike at ~ 22 ka BP in Lake Holzmaar. This could be caused by a crater wall collapse resulting in a high amount of volcanic material deposited as turbidity or debris layers in the lake which is also documented in the Appendix data of Brauer (1994).

Deviations most likely relate to the different lake shapes - Lake Holzmaar is almost round and Paleolake Alf is elongated which influences sediment transport processes, e.g., by different transport lengths within the lake. Apart from that, the sediment inflow conditions differ from peripheral flow of the Sammet creek at the southwestern shore of Lake Holzmaar and

dendritically discharging tributaries together with the main inflow of River Alf into Paleolake Alf.

Regarding the record of Lago Grande di Monticchio, Wulf (2000) describes a high portion of volcaniclastic material in the Lago Grande di Monticchio composite record placed in the matrix of the lake sediment. Further, Wulf (2000) describes eight primary ash layers between 21 and 28 ka BP varying between 2 and 286 mm which originate from Phlegrean Fields, Mount Vesuvius and Monte Albani. Even if there are primary ash layers within the record, a general trend of magnetic mineral enrichment or depletion in the sediment matrix is observable which matches with the Paleolake Alf record. However, the applicability of magnetic susceptibility as a proxy for water discharge definitely depends on the availability of

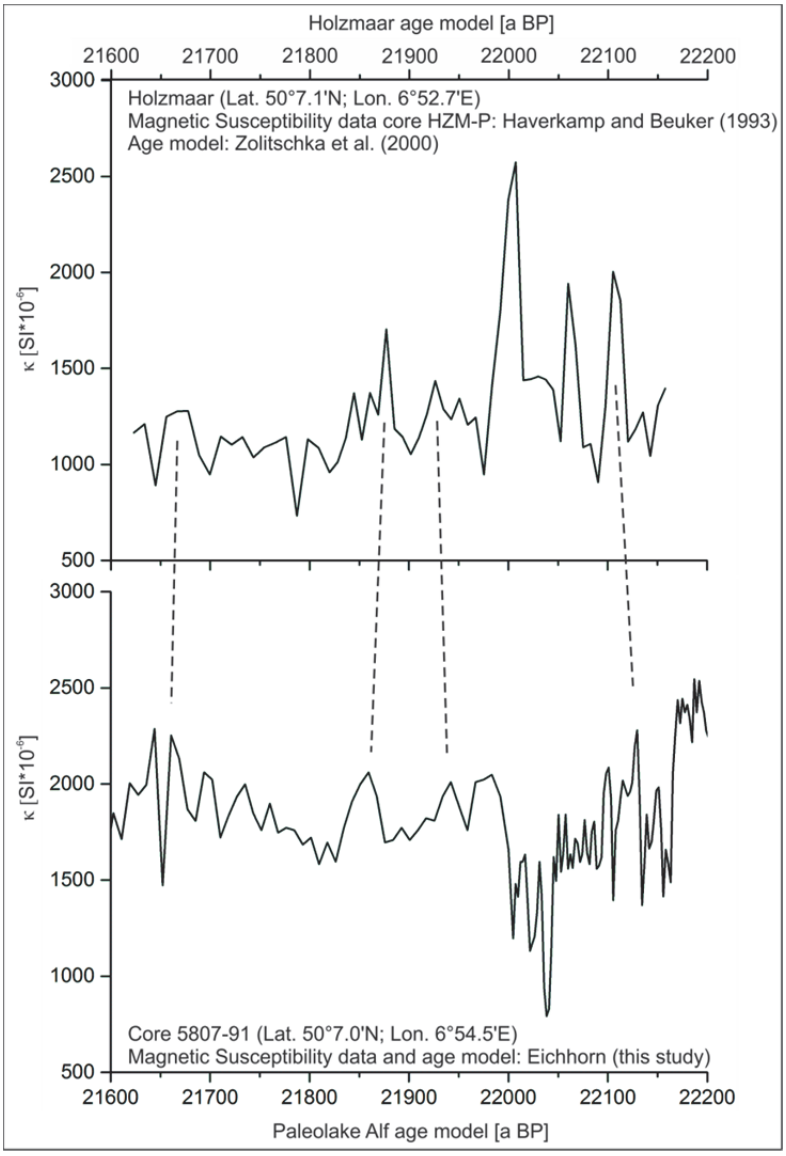

Fig. 6.4: Correlation of volume-specific magnetic susceptibility from Lake Holzmaar (Haverkamp and Beuker 1993, Zolitschka et al. 2000) and and Paleolake Alf (core 5807-91). Dashed lines indicate correlated sequences.

volcaniclastic material in the catchment area which itself results from the age, freshness and thickness of the tephra deposits around the lake. The applicability of the Lago Grande di Monticchio record for comparison with the Paleolake Alf archive is however difficult because Monticchio is situated south of the Alps which separate climatic connectivity (Fig. 6.5).

The NGRIP Ca^{2+} data is used because calcium is mainly transported with dust particles to Greenland (Fuhrer et al. 1993) during springtime (Rasmussen et al. 2006). Apart from seasonal fluctuations it can be used as a northern hemisphere dust proxy. Correlating the NGRIP Ca^{2+} with the Paleolake Alf Ca/coh curve, the Ca increase at Paleolake Alf at ~ 26.3 ka BP can be explained with the Greenland Stadial 3 (Fig. 6.6).

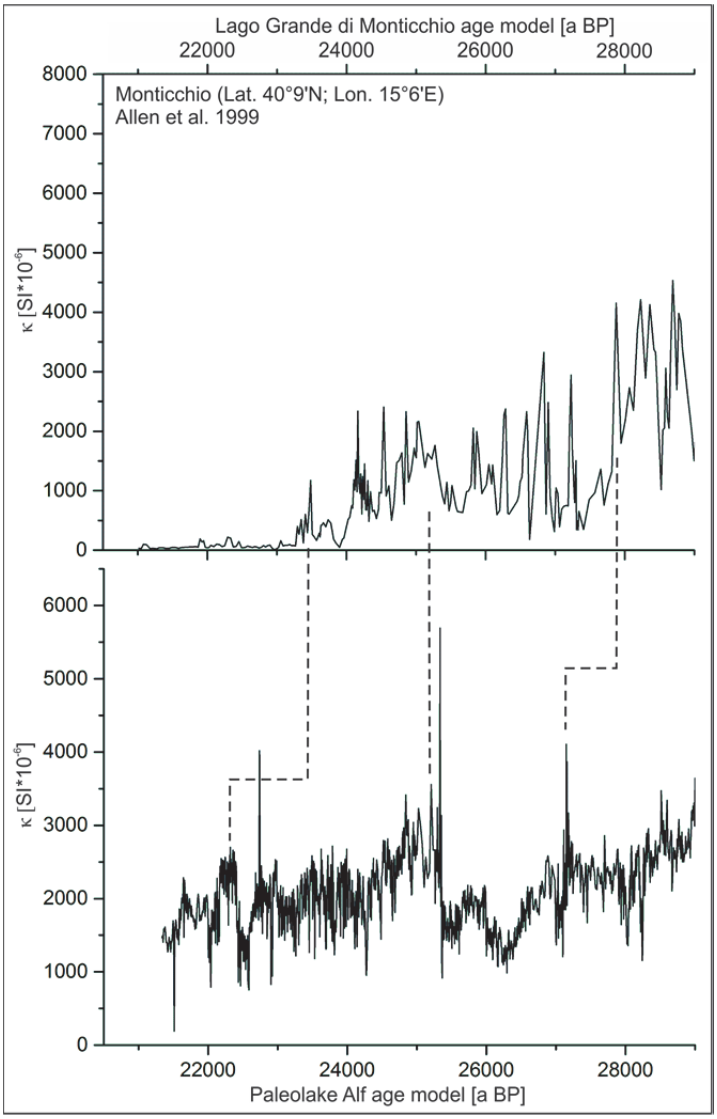

Fig. 6.5: Volume-specific magnetic susceptibility from Lago Grande di Monticchio (Allen et al. 1999) and Paleolake Alf (core 5807-91) were taken for correlation. Dashed lines indicate tentatively correlated sequences.

Generally, the correlation of the Paleolake Alf archive to other records is difficult due to data gaps, e.g., in the Ca curve, and the uncertainties in the age model based on ^{14}C dates of the humic acid fraction.

The humic acid fraction forms by microbial degradation of dead plant material and is stored in soils (Tan 2014). However, the retention time between the humic acid erosion, redeposition and final transport into the lake is unclear. In addition, at many locations in the Eifel even today, mantle CO_2 is outgassing (May 2002) that might have been incorporated into the plants leading to apparently too old ^{14}C ages. The uncertainty with ^{14}C ages could only be solved in the future choosing another suitable dating technique, e.g., Optical Stimulated Luminescence or paleomagnetic.

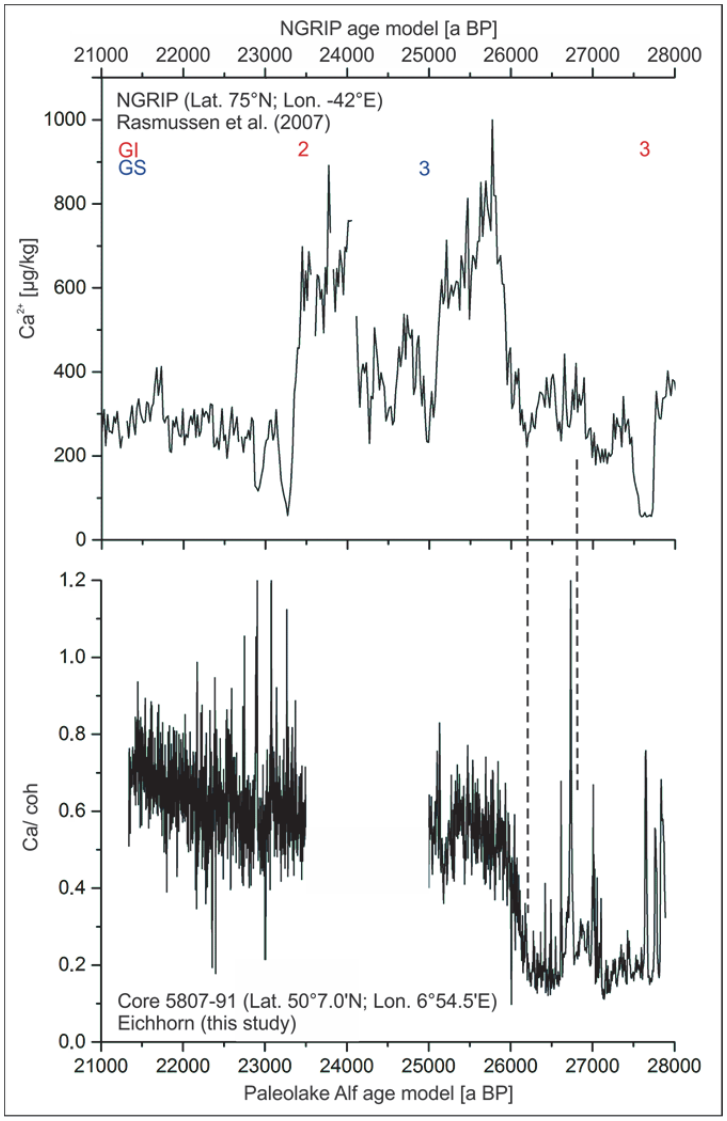

Fig. 6.6: Ca values were taken from NGRIP (Rasmussen et al. 2007) and Paleolake Alf (core 5807-91) for correlation due to the absence of carbonate rocks in the catchment and the low productivity in periglacial lakes. Calcium can be regarded as a predominantly dust derived proxy. GI (red) implicates

Greenland Interstadials (Svensson et al. 2006); GS (blue) reveals Greenland Stadials (Andersen et al. 2006). Dashed lines indicate correlated sequences.

6.3 Outlook

In order to improve the age model of Paleolake Alf, paleomagnetic investigations were already sampled within a 3 cm interval in July 2016 by Dr. B. Lougheed from the Uppsala University and will be measured in September 2016.

Another key point not yet fully understood is the absence of the meter-thick primary Pulvermaar deposits that should have been deposited in the Paleolake Alf basin due to its proximity. As mentioned before, only redeposited Pulvermaar tephra was detected. The current interpretation of the absence of primary Pulvermaar tephra is a dam collapse causing their erosion. Therefore, T. Lange is investigating the southern part of the Alf Valley in his PhD thesis in order to find evidences (1) for the sudden dam collapse with subsequent partial erosion of the sediment archive and (2) to find other archives where the primary Pulvermaar deposits are preserved.

The western part of the Sprinker maar crater wall might be a hint for the dam collapse as it is fully eroded and contains fluvial deposits next to lacustrine sediments from a temporal crater lake (Lange, pers. com. 2016). Regarding the primary Pulvermaar deposits, the Diefenbach will be investigated, filled by the Sprinker lava flow and was therefore dammed as well. Potentially, the primary Pulvermaar deposits will be found here. Another option is the Sprinker maar which will be investigated in 2017 in a coring campaign.

However, there are still open questions for numerous studies to come - so, future research will continue in this archive.

References

Adams, C. (2010). Häufigkeit und Isotopensignal von Ostrakoden in Sedimenten aus dem Dehner Trockenmaar (Eifel) für die Zeit 13.000-40.000 J.v.h.. Diplomarbeit. Johannes Gutenberg-Universität Mainz. (in German).

Allen, J. R. M., Brandt, U., Brauer, A., Hubberten, H.-W., Huntley, B., Keller, J., Kraml, M., Mackensen, A., Mingram, J., Negendank, J. F. W., Nowaczyk, N. R., Oberhänsli, H., Watts, W. A., Wulf, S., Zolitschka, B. (1999). Rapid environmental changes in Southern Europe during the last glacial period. Nature. 400. 740-743.

Amato, A., Aucelli, P. P. C., Cinque, A. (2003). The long-term denudation rate in the Southern Apennines chain (Italy): a GIS-aided estimation of the rock volumes eroded since Middle Pleistocene time. Quaternary International. 101-102. 3-11.

Andersen, K. K., Svensson, A., Johnsen, S. J., Rasmussen, S. O., Bigler, M., Röthlisberger, R., Ruth, U., Siggaard-Andersen, M.-L., Steffensen, J. P., Dahl-Jensen, D., Vinther, B. M., Clausen H. B. (2006). The Greenland ice core chronology 2005, 15-42 ka. Part 1: constructing the time scale. Quaternary Science Reviews. 25. 3246-3257.

Andersen, K. K., Bigler, M., Buchardt, S. L., Clausen, H. B., Dahl-Jensen, D., Davies, S. M., Fischer, H., Goto-Azuma, K., Hansson, M. E., Heinemeier, J., Johnsen, S. J., Larson, L. B., Muscheler, R., Olsen, G. J., Rasmussen, S. O., Röthlisberger, R., Ruth, U., Seierstad, I. K., Siggaard-Andersen, M.-L., Steffensen, J. P., Svensson, A. M., Vinther, B. M. (2007). Greenland ice core chronology 2005 (GICC05) and 20 year means of oxygen isotope data from ice core NGRIP. Data retrieved from www.pangaea.de.

Antoine, P., Rousseau, D.-D., Moine, O., Kunesch, S., Hatté, C., Lang, A., Tissoux, H., Zöller, L. (2009). Rapid and cyclic aeolian deposition during the Last Glacial in European loess: a high-resolution record from Nussloch, Germany. Quaternary Science Reviews. 28. 2955-2973.

Baranov, V., Naudy, H. (1964). Numerical calculation of the formula of reduction to the magnetic pole. Geophysics. 29. 67-79.

Bauer, A., Lanson, B., Ferrage, E., Emmerich, K., Taubald, H., Schild, D., Velde, B. (2006). The fate of smectite in KOH solutions. American Mineralogist. 91. 1313-1322.

Becker, H. J. (1977). Pyroxenites and hornblendites from the maar-type volcanoes of the Westeifel, Federal Republic of Germany. Contributions to Mineralalogy and Petrology. 65. 45-52.

Behre, K. E., van der Pflicht, J. (1992). Towards an absolute chronology for the last glacial period in Europe: Radiocarbon dates from Oerel, northern Germany. Vegetation History and Archaeobotany. 1. 111-117.

Blümel, W. D., Emmermann, R., Smykatz-Kloss, W. (1985). Vorkommen und Entstehung von tri-oktaedrischen Smektiten in den Basalten und Böden der König-Georg-Insel (S-Shetlands/West-Antarktis). Polarforschung. 55. 33-48. (in German).

Bos, J. A. A., Bohncke, S. J. P., Kasse, C., Vandenberghe, J. (2001). Vegetation and climate during the Weichselian Early Glacial and Pleniglacial in the Niederlausitz, Eastern Germany - macrofossil and pollen evidence. Journal of Quaternary Science. 16. 269-289.

Brauer, A. (1994). Weichselzeitliche Seesedimente des Holzmaars - Warvenchronologie des Hochglazials und Nachweis von Klimaschwankungen. Documenta naturae. 85. 1-210. (in German).

Brauer, A., Endres, C., Günter, C., Litt, T., Stebich, M., Negendank, J. F. W. (1999). High resolution sediment and vegetation responses to Younger Dryas climate change in varved lake sediments from Meerfelder Maar, Germany. Quaternary Science Reviews. 18. 321-329.

Brohan, P., Kennedy, J. J., Harris, I., Tett, S. F. B., Jones, P. D. (2006). Uncertainty estimates in regional and global observed temperature changes: a new data set from 1850. Journal of Geophysical Research. 111. 1-21.

Brunck, H., Sirocko, F., Albert, J. (2016). The ELSA-Flood-Stack: a reconstruction from the laminated sediments of Eifel maar structures during the last 60 000 years. Global and Planetary Change. 142. 136-146.

Büchel, G., Lorenz, V. (1982). Zum Alter des Maarvulkanismus der Westeifel. Neues Jahrbuch für Geologie und Paläontologie. 163. 1-22. (in German).

Büchel, G. (1984). Die Maare im Vulkanfeld der Westeifel, ihr geophysikalischer Nachweis, ihr Alter und ihre Beziehung zur Tektonik der Erdkruste. Dissertation. Johannes Gutenberg Universität Mainz. 1-385. (in German).

Büchel, G. (Hrsg.) (1994). Vulkanologische Karte der West- und Hocheifel (1:50.000). Institut für Geowissenschaften. Universität Mainz.

Capra, L. (2007). Volcanic natural dams: identification, stability, and secondary effects. Natural Hazards. 43. 45-61.

Chutko, K. J., Lamoureux, S. F. (2008). Identification of coherent links between interannual sedimentary structures and daily meteorological observations in arctic proglacial lacustrine varves: potentials and limitations. Canadian Journal of Earth Sciences. 45. 1-13.

Cipa, W. (1956). Der Vulkanismus in der Umgebung des Pulvermaares. Decheniana. 109. 53-75. (in German).

Cipa, W. (1958). Erdmagnetische Vermessung einiger Lavaströme und Tuffschlote in der Vorder-Eifel. Geologisches Jahrbuch. 75. 663-698. (in German).

Clague, J. J., Evans, S. G. (1994). Formation and failure of natural dams in the Canadian Cordillera. Geological Survey of Canada. Bulletin. 464. 1-40.

Cloetingh, S., Ziegler, P. A., Beekman, F., Andriessen, P. A. M., Matenco, L., Bada, G., Garcia-Castellanos, D., Hardebol, N., Dèzes, P., Sokoutis, D. (2005). Lithospheric memory, state of stress and rheology: neotectonic controls on Europe's intraplate continental topography. Quaternary Science Reviews. 24. 241-304.

Cook, T. L., Bradley, R. S., Stoner, J. S., Francus, P. (2009). Five thousand years of sediment transfer in a High Arctic watershed recorded in annually laminated sediments from Lower Murray Lake, Ellesmere Island, Nunavut, Canada. Journal of Paleolimnology. 41. 77-94.

Costa, J. E., Schuster, R. L. (1988). The formation and failure of natural dams. Geological Society of America Bulletin. 100. 1054-1068.

Croudace, I. W., Rindby, A., Rothwell, R. G. (2006). ITRAX: Description and evaluation of a new multi-function X-ray core scanner. - In: Rothwell, R. G. (Ed). New techniques in sediment core analysis. The Geological Society of London. Special Publications. 51-63.

Dearing, J. A. (1994). Environmental magnetic susceptibility: Using the Bartington MS2 System. Chi Publishing. Kenilworth. 1-104.

De Geer, G. (1912). A geochronology of the last 12,000 years. Compte rendus XI session du congres geologique international. Stockholm 1910. 241-257.

Demoulin, A., Hallot, E. (2009). Shape and amount of the Quaternary uplift of the Western Rhenish shield and the Ardennes (Western Europe). Tectonophysics. 474. 696-708.

Doran, P. T. (1993). Sedimentology of Colour Lake, a nonglacial High Arctic lake, Axel Heiberg Island, N.W.T., Canada. Arctic and Alpine Research. 25. 353-367.

Drohmann, D., Negendank, J. F. W. (1993). Turbidites in the sediments of Lake Meerfelder Maar (Germany) and the explanation of suspension sediments. – In: Negendank, J. F. W., Zolitschka, B. (Eds.). Paleolimnology of European Maar Lakes. Lecture Notes in Earth Sciences. 49. 195-208.

Druivenga, G., Grossmann, E., Grüneberg, S., Polom, U., Rode, W. (2005). Transportabler Scherwellenvibrator. Offenlegungsschrift DE10327757A1. Deutsches Patent und Markenamt.

Dunning, S. A., Rosser, N. J., Petley, D. N., Massey, C. R. (2006). Formation and failure of the Tsatichhu landslide dam, Bhutan. Landslides. 3. 107-113.

Eichhorn, L., Pirrung, M., Zolitschka, B., Büchel, G. (subm.). Pleniglacial sedimentation process reconstruction on laminated lacustrine sediments from lava-dammed Paleolake Alf, West Eifel Volcanic Field (Germany). Quaternary Science Reviews.

Eichhorn, L., Pirrung, M., Lange, T., Polom, U., Zolitschka, B., Köppen, K.-H., Büchel, G. (in prep.-a). Basin architecture of lava-dammed Paleolake Alf (Quaternary West Eifel Volcanic Field) compared to modern reservoirs.

Eichhorn, L., Engelhardt, J., Lange, T., Pirrung, M., Henschen, M., Büchel, G. (in prep.-b). Surface reconstruction for lava and sediment volume calculations using ArcGIS demonstrated on a case study of the Alf Valley, Quaternary West Eifel Volcanic Field.

Einsele, G., Hinderer, M. (1997). Terrestrial sediment yield and the lifetimes of reservoirs, lakes, and larger basins. Geologische Rundschau. 86. 288-310.

Evans, J. E., Mackey, S. D., Gottgens, J. F., Gill, W. M. (2000). Lessons from a dam failure. Ohio Journal of Science. 100. 121-131.

Felix-Henningsen, P. (1990). Die mesozoisch-tertiäre Verwitterungsdecke (MTV) im Rheinischen Schiefergebirge: Aufbau, Genese und quartäre Überprägung. Relief Boden Paläoklima. 6. Gebr. Borntraeger. Berlin. Stuttgart. 1-192. (in German).

Finck, N., Schlegel, M. L., Bauer, A. (2015). Structural iron in dioctahedral and trioctahedral smectites: A polarized XAS study. Physics and Chemistry of Minerals. 42. 847-859.

Finlay, C. C., Maus, S., Beggan, C. D., Bondar, T. N., Chambodut, A., Chernova, T. A., Chulliat, A., Golovkov, V. P., Hamilton, B., Hamoudi, M., Holme, R., Hulot, G., Kuang, W., Langlais, B., Lesur, V., Lowes, F. J., Lühr, H., Macmillan, S., Mandea, M., McLean, S., Manoj, C., Menvielle, M., Michaelis, I., Olsen, N., Rauberg, J., Rother, M., Sabaka, T. J., Tangborn, A., Tøffner-Clausen, L., Thébault, E., Thomson, A. W. P., Wardinski, I., Wei, Z., Zvereva, T. I. (2010). International geomagnetic

reference field: the eleventh generation. Geophysical Journal International. 183. 1216-1230.

Förster, M. W., Sirocko, F. (2016). The ELSA tephra stack: Volcanic activity in the Eifel during the last 500,000 years. Global and Planetary Change. 142. 100-107.

Francus, P., Bradley, R. S., Lewis, T., Abbott, M., Retelle, M., Stoner, J. S. (2008). Limnological and sedimentary processes at Sawtooth Lake, Canadian High Arctic, and their influence on varve formation. Journal of Paleolimnology. 40. 963-985.

Frechen, J. (1971). Siebengebirge am Rhein - Laacher Vulkangebiet - Maargebiet der Westeifel. Vulkanologisch-petrologische Exkursionen. 56. 2. Auflage. Gebr. Borntraeger. Stuttgart. 1-209. (in German).

Frechen, M., Oches, E. A., Kohfeld, K. E. (2003). Loess in Europe – mass accumulation rates during the last glacial period. Quaternary Science Reviews. 22. 1835-1857.

French, H. M. (2013). The periglacial environment. 3rd edition. John Wiley & Sons. 1-458.

Friedl, G., Wüest, A. (2002). Disrupting biogeochemical cycles – consequences of damming. Aquatic Scienes. 64. 55-65.

Friedrich, M., Remmele, S., Kromer, B., Hofmann, J., Spurk, M., Kaiser, K. F., Orcel, C., Küppers, M. (2004). The 12,460-year Hohenheim oak and pine tree-ring chronology from Central Europe – a unique annual record for radiocarbon calibration and paleoenvironment reconstructions. Radiocarbon. 46. 1111-1122.

Fritsch. Laser particle sizer analysette 22. Handbuch. 1-24. (in German). www.fritsch.de.

Fuchs, M., Kreutzer, S., Rousseau, D.-D., Antoine, P., Hatté, C., Lagroix, F., Moine, O., Gauthier, C., Svoboda, J., Lisá, L. (2013). The loess sequence of Dolní Věstonice, Czech Republic: a new OSL-based chronology of the last climatic cycle. Boreas. 42. 664-677.

Fuhrer, K., Neftel, A., Anklin, M., Maggi, V. (1993). Continuous measurements of hydrogen peroxide, formaldehyde, calcium and ammonium concentrations along the new GRIP ice core from Summit, Central Greenland. Atmospheric Environment. Part A. General Topics. 27. 1873-1880.

Fuhrmann, R. (2012). Atlas quartärer und rezenter Ostrakoden Mitteldeutschlands. Altenburger naturwissenschaftliche Forschungen. 15. 1-320. (in German).

Gabriel, G., Ellwanger, D., Hoselmann, C., Weidenfeller, M., Wielandt-Schuster, U., The Heidelberg basin project team (2013). The Heidelberg basin, upper Rhine Graben (Germany): a unique archive of Quaternary sediments in Central Europe. Quaternary International. 292. 43-58.

Gates, W. L. (1976). Modelling the ice-age climate. ACM SIGSIM simulation digest. 7. 66-72.

Gebhardt, I. (1963). Die Talbildung der Eifel im Ablauf der Klimate, des Vulkanismus und der periglazialen Bodenbildung im Quartär. Decheniana. 115. 143-214. (in German).

Geirsdóttir, Á., Miller, G. H., Thordarson, T., Ólafsdóttir, K. B. (2009). A 2000 year record of climate variations reconstructed from Haukadalsvatn, West Iceland. Journal of Paleolimnology. 41. 95-115.

Gemmell, A. M. D., Ralston, I. B. M. (1984). Some recent discoveries of ice-wedge cast networks in North-East Scotland. Scottish Journal of Geology. 20. 115-118.

GEM systems. Proton magnetometers reliable and robust for exploration. Environmental and engineering applications. 1-2. www.gemsys.ca.

Genty, D., Blamart, D., Ouahdi, R., Gilmour, M., Baker, A., Jouzel, J., Van-Exter, S. (2003). Precise dating of Dansgaard-Oeschger climate oscillations in Western Europe from stalagmite data. Nature. 421. 833-837.

©GeoBasis-DE/LVermGeoRP (2014). DGM. Landesamt für Vermessung und Geobasisinformationen Rheinland Pfalz.

Gleadow, A. J. W., Brown, R.W. (2000). Fission-track thermochronology and the long-term denudational response to tectonics. - In: Summerfield, M. A. (Ed.). Geomorphology and global tectonics. Wiley. 57-75.

Grawunder, A., Merten, D., Büchel, G. (2014). Origin of middle rare earth element enrichment in acid mine drainage-impacted areas. Environmental Science and Pollution Research. 21. 6812-6823.

Grönvold, K., Óskarsson, N., Johnsen, S. J., Clausen, H. B., Hammer, C., U., Bond, G., Bard, E. (1995). Ash layers from Iceland in the Greenland GRIP ice core correlated with oceanic and land sediments. Earth and Planetary Science Letters. 135. 149-155.

Guilizzoni, P., Marchetto, A., Lami, A., Brauer, A., Vigliotti, L., Musazzi, S., Langone, L., Manca, M., Lucchini, F., Calanchi, N., Dinelli, E., Mordenti, A. (2006). Records of environmental and climatic changes during the Late Holocene from Svalbard: palaeolimnology of Kongressvatnet. Journal of Paleolimnology. 36. 325-351.

Harrison, C. G. A. (2000). What factors control mechanical erosion rates? International Journal of Earth Sciences. 88. 752-763.

Haverkamp, B., Beuker, T. (1993). A paleomagnetic study of maar-lake sediments from the West Eifel. – In: Negendank, J. F. W., Zolitschka, B. (Eds.). Paleolimnology of European Maar Lakes. Lecture Notes in Earth Sciences. 49. Springer. 349-365.

Hemfler, M., Büchel G. (1991). Influente Verhältnisse als Folge der Trinkwassergewinnung im Alfbachtal bei Strohn (Westeifel). Pollichia. 78. 35-83. (in German).

Hewitt, G. (2000). The genetic legacy of the Quaternary ice ages. Nature. 405. 907-913.

Hinderer, M. (2001). Late Quaternary denudation of the Alps, valley and lake fillings and modern river loads. Geodinamica Acta. 14. 231-263.

Hopmann, M., Frechen, J., Knetsch, G. (1960). Die vulkanische Eifel. Geologische Reihe 2. Stollfuß Verlag. 1-143. (in German).

Houben, P. (2003). Spatio-temporally variable response of fluvial systems to Late Pleistocene climate change: a case study from Central Germany. Quaternary Science Reviews. 22. 2125-2140.

Huijzer, A., Isarin, R. (1997). The reconstruction of past climates using multi-proxy evidence: an example of the Weichselian Pleniglacial in Northwest and Central Europe. Quaternary Science Reviews. 16. 513-533.

Huijzer, B., Vandenberghe, J. (1998). Climatic reconstruction of the Weichselian Pleniglacial in Northwestern and Central Europe. Journal of Quaternary Science. 13. 391-417.

Juschus, O. (2012). Stauwassersedimente im brandenburgischen Abschnitt der Erdgasfernleitung OPAL südlich der Pommerschen Eisrandlage. Brandenburgische geowissenschaftliche Beiträge. 19. 19-27. (in German).

Kämpf, L., Brauer, A., Dulski, P., Feger, K.-H., Jacob, F., Klemt, E. (2012). Sediment imprint of the severe 2002 summer flood in the Lehnmühle reservoir, Eastern Erzgebirge (Germany). Eiszeitalter und Gegenwart – Quaternary Science Journal. 61. 3-15.

Kasse, C., Huijzer, A. S., Krzyszkowski, D., Bohncke, S. J. P., Coope, G. R. (1998). Weichselian Late Pleniglacial and late-glacial depositional environments, coleoptera and periglacial climatic records from Central Poland (Bełchatów). Journal of Quaternary Science. 13. 455-469.

Kolstrup, E., Mejdahl, V. (1986). Three frost wedge casts from Jutland (Denmark) and TL dating of their infill. Boreas. 15. 311-321.

Koschel, R. H. (1997). Structure and function of pelagic calcite precipitation in lake ecosystems. Verhandlungen des Internationalen Verein Limnologie. 26. 343-349.

Kottek, M., Grieser, J., Beck, C., Rudolf, B., Rubel, F. (2006). World map of the Köppen-Geiger climate classification updated. Meteorologische Zeitschrift. 15. 259-263.

Krause, U. (1984). Der Wartges-berg-Vulkankomplex bei Strohn. Zweimonatige Kartierung. Institut für Geowissenschaften. Johannes Gutenberg Universität Mainz. 1-57. (in German).

Krawczyk, C. M., Polom, U., Beilecke, T. (2013). Shear-wave reflection seismics as a valuable tool for near-surface urban applications. The Leading Edge. 32. 256-263.

Lamoureux, S. (2000). Five centuries of interannual sediment yield and rainfall-induced erosion in the Canadian High Arctic recorded in lacustrine varves. Water Resources Research. 36. 309-318.

Landesamt für Umwelt (2003). Deutsches gewässerkundliches Jahrbuch: Rheingebiet. Teil III. Mittel- und Niederrhein mit deutschem Issel- und Maasgebiet. 2003. Rheinland Pfalz. (in German).

Lange, T. (2014). Paläotalrekonstruktion des Alfbachtals im Zuge morphologischer Detailanalyse eines DGMs und geophysikalischer Geländeuntersuchung bei Gillenfeld und Strohn. Diplomarbeit. Institut für Geowissenschaften. Friedrich-Schiller-Universität Jena. 1-170. (in German).

Langenstrassen, F. (1983). Neritic sedimentation of the Lower and Middle Devonian in the Rheinische Schiefergebirge East of the river Rhine. – In: Martin, H., Eder, F. W. (Eds.). Intracontinental Fold Belts. Springer. 43-76.

Lauer, T., Von Suchodoletz, H., Vollmann, H., Meszner, S., Frechen, M., Tinapp, C., Goldmann, L., Müller, S., Zielhofer, C. (2014). Landscape aridification in Central Germany during the Late Weichselian Pleniglacial – results from the Zauschwitz loess site in Western Saxony. Zeitschrift für Geomorphologie. 58. 27-50.

Leonard, E. M. (1997). The relationship between glacial activity and sediment production: Evidence from a 4450-year varve record of neoglacial sedimentation in Hector Lake, Alberta, Canada. Journal of Paleolimnology. 17. 319-330.

Leyk, H.-J., Lippold, H. J. (1997). $^{40}Ar/^{39}Ar$-Untersuchungen an spätquartären Vulkaniten der Eifel – Neue Arbeitsansätze zur Datierung junger Lavaströme. Berichte der Deutschen Mineralogischen Gesellschaft. Beihefte zum Europäischen Jahrbuch für Mineralogie. 11/1. 1-145. (in German).

Liestøl, O. (1956). Glacier dammed lakes in Norway. Norwegian Journal of Geography. 15. 122-149.

Likens, G. E. (Ed.) (2010). Lake ecosystem ecology: a global perspective. 1st edition. Academic Press. 1-480.

Linnebacher, P. (1985). Geologische Untersuchung der Vulkane und ihrer Förderprodukte im Raum Gillenfeld/Westeifel. Zweimonatige Kartierung – Frühjahr 1985. Institut für Geowissenschaften. Johannes Gutenberg Universität Mainz. 1-78. (in German).

Linsbauer, A., Paul, F., Hoelzle, M., Frey, H., Haeberli, W. (2009). The Swiss Alps without glaciers – a GIS-based modelling approach for reconstruction of glacier beds. – In: Purves, R. S., Gruber, S., Straumann, R. K., Hengl, T. (Eds). Proceedings of Geomorphometry 2009. Zurich. University of Zurich. 243-247.

Litt, T., Behre, K.-E., Meyer, K.-D., Stephan, H.-J., Wansa, S. (2007). Stratigraphische Begriffe für das Quartär des norddeutschen Vereisungsgebietes. Eiszeitalter und Gegenwart – Quaternary Science Journal. 56. 7-65. (in German).

Löhnertz, W. (2003). Eocene paleovalleys in the Eifel: Mapping, geology, dating and implications for the reconstruction of the paleosurfaces and vertical movements of the lithosphere at the edges of the Rhenish shield. Géologie de la France. 1. 57-62.

Löhr, H., Neyses, M. (1997). Späteiszeitliche bis mittelalterliche Ablagerungen im Alfbachtal zwischen Udler und Saxler (Kreis Daun) und ihre dendrochronologische Datierung. – In: Funde und Ausgrabungen im Bezirk Trier. 29. 51-66.

Macaire, J.-J., Bossuet, G., Choquier, A., Cocirta, C., De Luca, P., Dupis, A., Gay, I., Mathey, E., Guenet, P. (1997). Sediment yield during Late Glacial and Holocene periods in the Lac Chambon watershed, Massif Central, France. Earth Surface Processes and Landforms. 22. 473-489.

Marks, L., Gałązka, D., Woronko, B. (2015). Climate, environment and stratigraphy of the last Pleistocene Glacial stage in Poland. Quaternary International. 1-13.

Mathews, W. H. (1956). Physical limnology and sedimentation in a glacial lake. Geological Society of America Bulletin. 67. 537-552.

May, F. (2002). Quantifizierung des CO_2-Flusses zur Abbildung magmatischer Prozesse im Untergrund der Westeifel. Shaker Verlag. 1-168. (in German).

McLennan, S. (1989). Rare earth elements in sedimentary rocks; influence of provenance and sedimentary processes. Reviews in Mineralogy and Geochemistry 21. 169-200.

McNulty, W. E., Cookson, J. N. (2013). Nordeuropa nach der Eiszeit. - In: Die Suche nach Doggerland. National Geographic. 95-105. (in German).

Meisch, C. (2000). Freshwater ostracoda of Western and Central Europe. – In: Schwoerbel, J., Zwick, P. (Eds.): Süßwasserfauna von Mitteleuropa. Spektrum Akademischer Verlag. 1-522.

Menounos, B., Clague, J. J. (2008). Reconstructing hydro-climatic events and glacier fluctuations over the past millennium from annually laminated sediments of Cheakamus Lake, Southern Coast Mountains, British Columbia, Canada. Quaternary Science Reviews. 27. 701-713.

Mertes, H. (1983). Aufbau und Genese des Westeifeler Vulkanfeldes. Bochumer geologische und geotechnische Arbeiten 9. 1-415. (in German).

Mertes, H., Schmincke, H.-U. (1985). Mafic potassic lavas of the Quaternary West Eifel Volcanic Field. Contributions to Mineralogy and Petrology. 89. 330-345.

Mertz, D. F., Löhnertz, W., Nomade, S., Pereira, A., Prelevic, D., Renne, P. R. (2015). Temporal-spatial evolution of low-SiO_2 volcanism in the Pleistocene West Eifel Volcanic Field (West Germany) and relationship to upwelling asthenosphere. Journal of Geodynamics. 88. 59-79.

Meyer, H., Hetzel, R., Strauss, H. (2010). Erosion rates on different timescales derived from cosmogenic ^{10}Be and river loads: implications for landscape evolution in the Rhenish Massif, Germany. International Journal of Earth Sciences. 99. 395-412.

Meyer, W., Stets, J. (1998). Junge Tektonik im Rheinischen Schiefergebirge und ihre Quantifizierung. Zeitschrift der Deutschen Geologischen Gesellschaft. 149. Heft 3. 359-379.

Meyer, W. (2013). Geologie der Eifel. Schweizerbart. 4. Auflage. 1-704. (in German).

Mol, J., Vandenberghe, J., Kasse, C. (2000). River response to variations of periglacial climate in mid-latitude Europe. Geomorphology. 33. 131-148.

Mulder, T., Alexander, J. (2001). The physical character of subaqueous sedimentary density flows and their deposits. Sedimentolology. 48. 269-299.

Müller, U. C., Pross, J., Bibus, E. (2003). Vegetation response to rapid climate change in Central Europe during the past 140,000 yr based on evidence from the Füramoos pollen record. Quaternary Research. 59. 235-245.

Nadeau, M.-J., Schleicher, M., Grootes, P. M., Erlenkeuser, H., Gottdang, A., Mous, D. J. W., Sarntheim, J. M., Willkomm, H. (1997). The Leibniz-Labor AMS facility at the Christian-Albrechts University, Kiel, Germany. – In: Breese, M, Rehn, L. E., Trautmann, C., Vickridge, I. C. (Eds.). Nuclear instruments and methods in physics research section B: Beam interactions with materials and atoms. Elsevier. 123. 22-30.

Nakoinz, O. (2001). Die Siedlungsgeschichte der südlichen Vulkaneifel. Trierer Zeitschrift. 64. 9-48.

Negendank, J. F. W. (1989). Pleistozäne und holozäne Maarsedimente der Eifel. Zeitschrift der Deutschen Geologischen Gesellschaft. 140. 13-24.

Negendank, J. F. W., Brauer, A., Zolitschka, B. (1990). Die Eifelmaare als erdgeschichtliche Fallen und Quellen zur Rekonstruktion des Paläoenvironments. Mainzer geowissenschaftliche Mitteilungen. 19. 235-262.

Negendank, J. F. W., Zolitschka, B. (1993). Maars and maar lakes of the Westeifel Volcanic Field. - In: Negendank, J. F. W., Zolitschka, B. (Eds.). Paleolimnology of European Maar Lakes. Lecture Notes in Earth Sciences. 49. Springer. 61-80.

Neugebauer, I., Brauer, A., Dräger, N., Dulski, P., Wulf, S., Plessen, Mingram, J., Herzschuh, U., Brande, A. (2012). A Younger Dryas varve chronology from the Rehwiese palaeolake record in NE-Germany. Quaternary Science Reviews. 36. 91-102.

Ojala, A. E. K., Francus, P., Zolitschka, B., Besonen, M., Lamoureux, S. F. (2012). Characteristics of sedimentary varve chronologies - a review. Quaternary Science Reviews. 43. 45-60.

Peizhen, Z., Molnar, P., Downs, W. R. (2001). Increased sedimentation rates and grain sizes 2-4 Myr ago due to the influence of climate change on erosion rates. Nature. 410. 891-897.

Pirrung, M., Büchel, G., Köppen, K.-H. (2007). Hochauflösende fluviolakustrine Sedimente des jüngeren Pleistozän aus dem Alfbachtal bei Gillenfeld (Westeifel) - erste Ergebnisse. Mainzer geowissenschaftliche Mitteilungen. 35. 51-80.

Prodehl, C., Mueller, S., Haak, V. (1995). The European Cenozoic rift system. - In: Olsen, K. H. (Ed.). Continental rifts: evolution, structure, tectonics. Developments in Geotectonics. 25. 133-212.

Rahm, G. (1958). Der quartäre Vulkanismus im südöstlichen Teile der Westeifel: Ein Beitrag zum Problem des Maarvulkanismus. Gewässer und Abwässer. 19. 7-39.

Rasmussen, S. O., Seierstad, I. K., Andersen, K. K., Bigler, M., Dahl-Jensen, D., Johnsen, S. J. (2007). Synchronization of the NGRIP, GRIP, and GISP2 ice cores across MIS 2 and palaeoclimatic implications. Quaternary Science Reviews. 27. 18-28. Data retrieved from www.pangaea.de.

Reichsamt für Landesaufnahme (1936). Topographische Karte 1: 25 000. Blatt 5807 Gillenfeld. Preußische Landesaufnahme 1886. Berlin.

Reille, M., Andrieu, V., de Beaulieu, J.-L., Guenet, P., Goeury, C. (1998). A long pollen record from Lac du Bouchet, Massif Central, France: for the period ca. 325 to 100 ka BP (OIS 9c to OIS 5e). Quaternary Science Reviews. 17. 1107-1123.

Reimer, P. J., Bard, E., Bayliss, A., Beck, J. W., Blackwell, P. G., Ramsey, C. B., Buck, C. E., Cheng, H., Edwards, R. L., Friedrich, M., Grootes, P. M., Guilderson, T. P., Haflidason, H., Hajdas, I., Hatté, C., Heaton, T. J., Hoffmann, D. L., Hogg, A. G., Hughen, K. A., Kaiser, K. F., Kromer, B., Manning, S. W., Niu, M., Reimer, R. W., Richards, D. A., Scott, E. M., Southon, J. R., Staff, R. A., Turney, C. S. M., van der Plicht, J. (2013). $IntCal_{13}$ and $marine_{13}$ radiocarbon age calibration curves 0–50,000 years cal BP. Radiocarbon. 55. 1869-1887.

Renssen, H., Kasse, C., Vandenberghe, J., Lorenz, S. J. (2007). Weichselian Late Pleniglacial surface winds over Northwest and Central Europe: a model-data comparison. Journal of Quaternary Science. 22. 281-293.

Retelle, M. J., Child, J. K. (1996). Suspended sediment transport and deposition in a High Arctic meromictic lake. Journal of Paleolimnology. 16. 151-167.

Ritter, J. R. R., Jordan, M., Christensen, U. R., Achauer, U. (2001). A mantle plume below the Eifel Volcanic Fields, Germany. Earth and Planetary Science Letters. 186. 7-14.

Rode, W., Cramm, S. (2007). Oscillation generator for seismic applications. DE102006055457A1.

Schaber, K., Sirocko, F. (2005). Lithologie und Stratigraphie der spätpleistozänen Trockenmaare der Eifel. Mainzer Geowissenschaftliche Mitteilungen. 33. 295-340. (in German).

Schaller, M., von Blanckenburg, F., Veldkamp, A., Tebbens, L. A., Hovius, N., Kubik, P. W. (2002). A 30 000 yr record of erosion rates from cosmogenic ^{10}Be in Middle European river terraces. Earth and Planetary Science Letters. 204. 307-320.

Schirmer, U. (1999). Pollenstratigraphische Gliederung des Spätglazials im Rheinland. Eiszeitalter und Gegenwart. 49. 132-143. (in German).

Schirrmeister, L., Grosse, G., Kunitsky, V., Magens, D., Meyer, H., Dereviagin, A., Kuznetsova, T., Andreev, A., Babiy, O., Kienast, F., Grigoriev, M., Overdiun, P. P., Preusser, F. (2008). Periglacial landscape evolution and environmental changes of

Arctic lowland areas for the last 60 000 years (Western Laptev Sea coast, Cape Mamontov Klyk). Polar Research. 27. 249-272.

Schmidt, C., Schaarschmidt, M., Kolb, T., Büchel, G., Richter, D., Zöller, L. (in prep.). Luminescence dating of Late Pleistocene eruptions in the Eifel Volcanic Field, Germany.

Schmincke, H.-U., Lorenz, V., Seck, H. A. (1983). The Quaternary Eifel Volcanic Fields. – In: Fuchs, K., von Gehlen, K., Mälzer, H., Murawski, H., Semmel, A. (Eds.). Plateau uplift. The Rhenish Shield – a case history. Springer. 139-151.

Schrott, L., Hufschmidt, G., Hankammer, M., Hoffmann, T., Dikau, R. (2003). Spatial distribution of sediment storage types and quantification of valley fill deposits in an alpine basin, Reintal, Bavarian Alps, Germany. Geomorphology. 55. 45-63.

Schwamborn, G., Schirrmeister, L., Frütsch, F., Diekmann, B. (2012). Quartz weathering in freeze-thaw cycles: experiment and application to the El'Gygytgyn crater lake record for tracing Siberian permafrost history. Geografiska Annaler: Series A. Physical Geography. 94. 481-499.

Seelos, K., Sirocko, F., Dietrich, S. (2009). A continuous high-resolution dust record for the reconstruction of wind systems in Central Europe (Eifel, Western Germany) over the past 133 ka. Geophysical Research Letters. 36. 1-6.

Shaw, C. S. J., Eyzaguirre, J. (2000). Origin of megacrysts in the mafic alkaline lavas of the West Eifel Volcanic Field, Germany. Lithos. 50. 75-95.

Sirocko, F., Seelos, K., Schaber, K., Rein, B., Dreher, F., Diehl, M., Lehne, R, Jäger, K., Krbetschek, M., Degering, D. (2005). A Late Eemian aridity pulse in Central Europe during the last glacial inception. Nature. 436. 833-836.

Sirocko, F., Dietrich, S., Veres, D., Grootes, P. M., Schaber-Mohr, K., Seelos, K., Nadeau, M.-J., Kromer, B., Rothacker, L., Röhner, M., Krbetschek, M., Appleby, P., Hambach, U., Rolf, C., Sudo, M., Grim, S. (2013). Multi-proxy dating of Holocene maar lakes and Pleistocene dry maar sediments in the Eifel, Germany. Quaternary Science Reviews. 62. 56-76.

Sirocko, F., Knapp, H., Dreher, F., Förster, M. W., Albert, J., Brunck, H., Veres, D., Dietrich, S., Zech, M., Hambach, U., Röhner, M., Rudert, S., Schwibus, K., Adams, C., Sigl, P. (2016). The ELSA-vegetation-stack: reconstruction of landscape evolution zones (LEZ) from laminated Eifel maar sediments of the last 60,000 years. Global and Planetary Change. 142. 108-135.

Snyder, N. P., Wright, S. A., Alpers, C. N., Flint, L. E., Holmes, C. W., Rubin, D. M. (2006). Reconstructing depositional processes and history from reservoir stratigraphy: Englebright Lake, Yuba River, northern California. Journal of Geophysical Research 111. 1-16.

Staiger, J., Gosse, J., Toracinta, R., Oglesby, B., Fastook, J., Johnson, J. V. (2007). Atmospheric scaling of cosmogenic nuclide production: climate effect. Journal of Geophysical Research. 112. 1-8.

Straka, H. (1975). Die spätquartäre Vegetationsgeschichte der Vulkaneifel. Pollenanalytische Untersuchungen an vermoorten Maaren. Beiträge zur Landespflege in Rheinland-Pfalz. Beiheft 3. 1-163. (in German).

Stuiver, M., Reimer, J. (1993). Extended ^{14}C data base and revised CALIB 3.0 ^{14}C age calibration program. Radiocarbon. 35. 215-230.

Svendsen, J. I., Mangerud, J., Miller, G. H. (1989). Denudation rates in the Arctic estimated from lake sediments on Spitsbergen, Svalbard. Palaeogeography, Palaeoclimatology, Palaeoecology. 76. 153-168.

Svensson, A., Andersen, K. K., Bigler, M., Clausen, H. B., Dahl-Jensen, D., Davies, S. M., Davies, S. M., Johnsen, S. J., Muscheler, R., Rasmunssen, S. O., Röthlisberger, R., Steffensen, J. P., Vinther, B. M. (2006). The Greenland ice core chronology 2005, 15-42 ka. Part 2: comparison to other records. Quaternary Science Reviews. 25. 3258-3267.

Tan, K. H. (2014). Humic matter in soil and the environment: principles and controversies. 2nd edition. CRC Press. 1-439.

Telford, W. M., Geldart, L. P., Sheriff, R. E. (1991). Applied geophysics. 2nd edition. Cambridge University Press. 1-792.

Thompson, R., Oldfield, F. (1986). Environmental magnetism. Allen & Unwin. 1-220.

Trauth, M. H., Strecker, M. R. (1999). Formation of landslide-dammed lakes during a wet period between 40,000 and 25,000 yr BP in Northwestern Argentina. Palaeogeography, Palaeoclimatology, Palaeoecology. 153. 277-287.

Van Balen, R. T., Houtgast, R. F., van der Wateren, F. M., Vandenberghe, J., Bogaart, P. W. (2000). Sediment budget and tectonic evolution of the Meuse catchment in the Ardennes and the Roer Valley rift system. Global and Planetary Change. 27. 113-129.

Vandenberghe, J. (1985). Paleoenvironment and stratigraphy during the Last Glacial in the Belgian-Dutch border region. Quaternary Research. 24. 23-38.

Vandenberghe, J., Pissart, A. (1993). Permafrost changes in Europe during the Last Glacial. Permafrost and Periglacial Processes. 4. 121-135.

Vandenberghe, J., Woo, M.-k. (2002). Modern and ancient periglacial river types. Progress in Physical Geography. 26. 479-506.

Vandenberghe, J. (2003). Climate forcing of fluvial system development: an evolution of ideas. Quaternary Science Reviews. 22. 2053-2060.

Van den Bogaard, P. (1995). $^{40}Ar/^{39}Ar$ ages of sanidine phenocrysts from Laacher See Tephra (12,900 yr BP): chronostratigraphic and petrological significance. Earth and Planetary Science Letters. 133. 163-174.

Velichko, A. A., Kononov, Y. M., Faustova, M. A. (1997). The last glaciation of Earth: size and volume of ice-sheets. Quaternary International. 41. 43-51.

Vos, H., Sanchez, A., Zolitschka, B., Brauer, A., Negendank, J. F. W. (1997). Solar activity variations recorded in varved sediments from the crater lake of Holzmaar – a maar lake in the Westeifel Volcanic Field, Germany. Surveys in Geophysics. 18. 163-182.

Vuichard, D., Zimmermann, M. (1987). The 1985 catastrophic drainage of a moraine-dammed lake, Khumbu Himal, Nepal: cause and consequences. Mountain Research and Development. 7. 91-110.

Wienecke, K. (1979). Geologische und geophysikalische Untersuchungen im Vulkangebiet SE Gillenfeld (Westeifel). Diplomarbeit. Friedrich-Wilhelms-Universität Bonn. 1-108. (in German).

Woda, C. (2000). Elektron-Spin-Resonanz-Datierung von Quartz. Dissertation. Universität Heidenberg. 1-156. (in German).

Woda, C., Mangini, A., Wagner, G. A. (2001). ESR dating of xenolithic quartz in volcanic rocks. Quaternary Science Reviews. 20. 993-998.

Wulf, S. (2000). Das tephrochronologische Referenzprofil des Lago Grande di Monticchio: Eine detaillierte Stratigraphie des süditalienischen explosiven Vulkanismus der letzten 100.000 Jahre. Dissertation. GeoForschungsZentrum Potsdam. Universität Potsdam. 1-185. (in German).

Zelt, C. A., Barton, P. J. (1998). Three-dimensional seismic refraction tomography: a comparison of two methods applied to data from the Faeroe Basin. Journal of Geophysical Research. 103. 7187–7210.

Zimanowski, B. (1986). Fragmentationsprozesse beim explosiven Vulkanismus in der Westeifel. Dissertation. Johannes Gutenberg-Universität Mainz. 1-252. (in German).

Zitzmann, A., Grünig, S., Meyer, W., Stets, J., Mittmeyer, H.-G., Konrad, H. J., Ribbert, K.-H., Fuchs, G, Hammerschmidt, M.. (1987). Geologische Übersichtskarte 1:200 000. Blatt CC 6302 Trier. Bundesanstalt für Geowissenschaften und Rohstoffe. Hannover.

Zöller, L. (1989). Das Alter des Mosenberg-Vulkans in der Vulkaneifel. – In: Die Eifel. 84. Heft 6. 415-418.

Zöller, L., Blanchard, H. (2009). The partial heat - longest plateau technique: testing TL dating of Middle and Upper Quaternary volcanic eruptions in the Eifel area, Germany. Eiszeitalter und Gegenwart – Quaternary Science Journal. 58. 86-106.

Zöller, L., Hambach, U., Blanchard, H., Fischer, S., Köhne, S., Stritzke, R. (2010). Der Rodderbergkrater bei Bonn. Ein komplexes Geoarchiv. Eiszeitalter und Gegenwart – Quaternary Science Journal. 59. 44-58. (in German).

Zolitschka, B. (1989). Jahreszeitlich geschichtete Seesedimente aus dem Holzmaar und dem Meerfelder Maar. Zeitschrift der Deutschen Geologischen Gesellschaft. 140. 25-33. (in German).

Zolitschka, B. (1996). Recent sedimentation in a High Arctic lake, northern Ellesmere Island, Canada. Journal of Paleolimnology. 16. 169-186.

Zolitschka, B., Brauer, A., Negendank, J. F., Stockhausen, H., Lang, A. (2000). Annually dated Late Weichselian continental paleoclimate record from the Eifel, Germany. Geology. 28. 783-786.

Zolitschka, B., Francus, P., Ojala, A. E. K., Schimmelmann, A. (2015). Varves in lake sediments – a review. Quaternary Science Reviews. 117. 1-41.

Appendixes

Appendix A:

Core photos

Appendix B:

^{14}C age dating

Core 5807-91

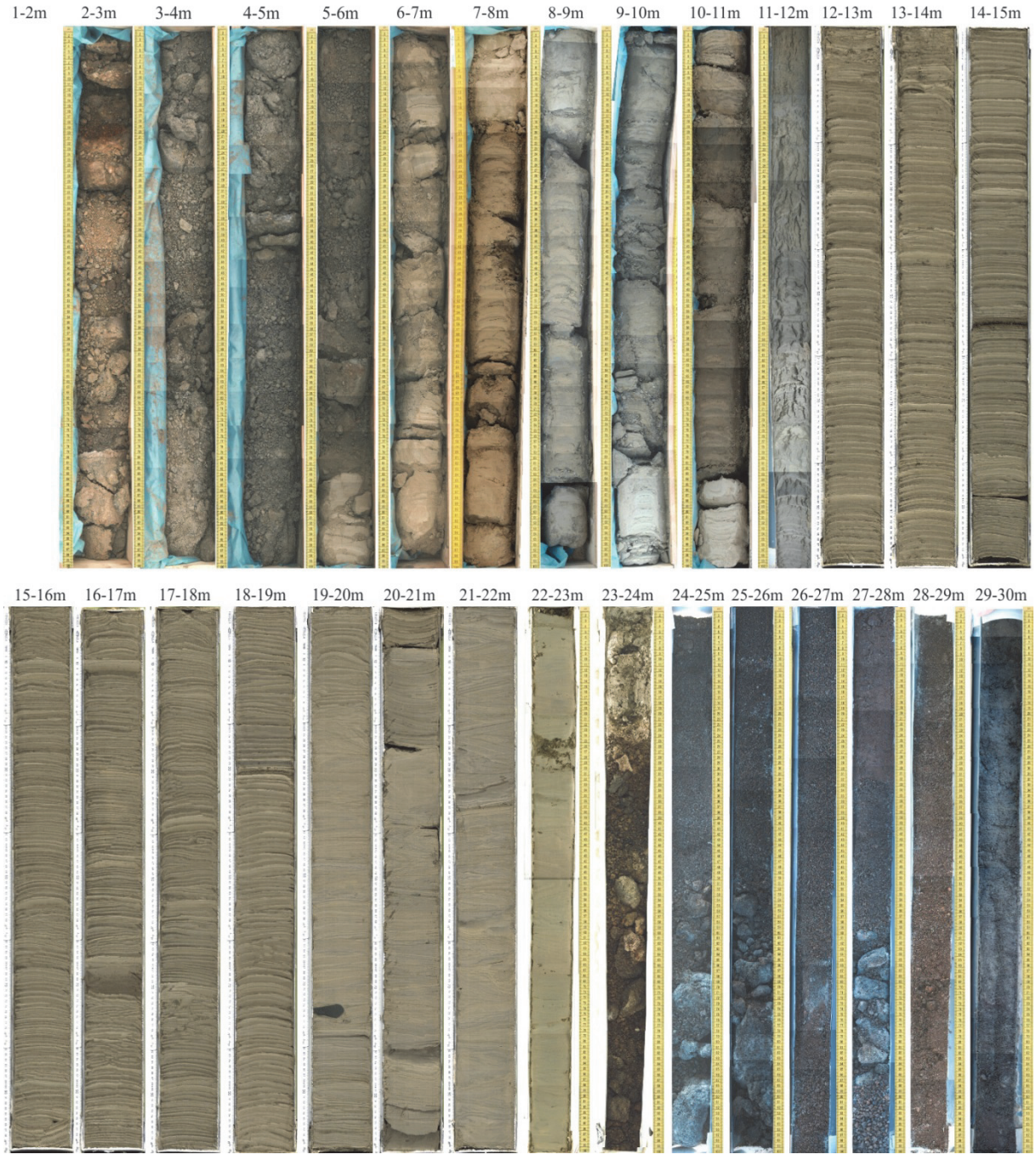

A.1: Photos of core 5807-91. Core meters 2-11 and 23-29 were manually photographed. Core meters 12-22 were photographed with a core scanner. All core meters were digitally lightened in CorelDRAW.

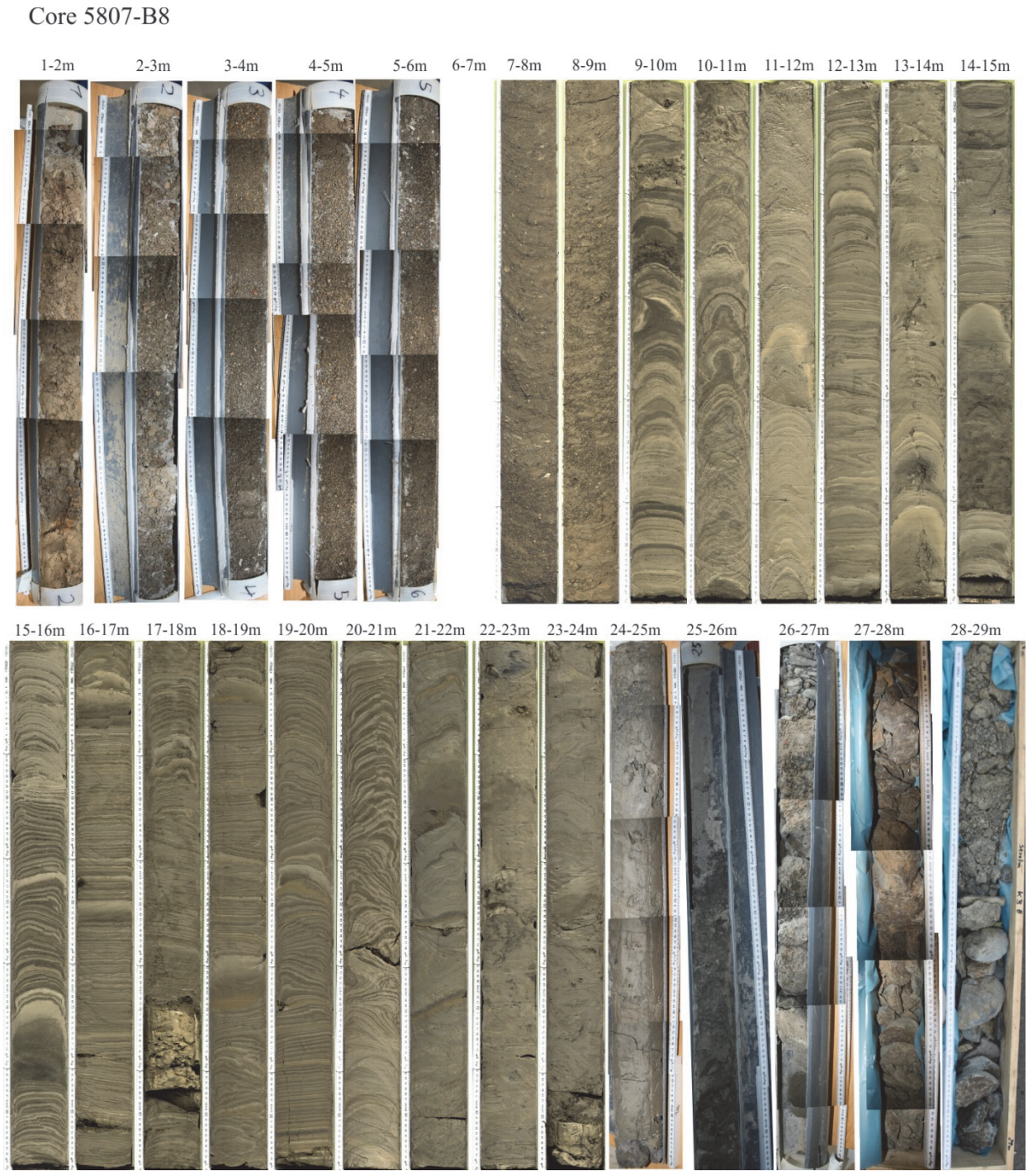

A.2: Photos of core 5807-B8. Core meters 1-5 and 24-28 were manually photographed. Core meters 7-23 were photographed with a core scanner. All core meters were digitally lightened in CorelDRAW.

B.1: Utilized ^{14}C ages of humic acid fraction of cores 5807-70 (Pirrung et al. 2007), 5807-B8 and 5807-91.

Core	Sample name	Original sample depth [m]	Humic acid [a BP]	Depth [m] projected on core 5807-91	Humic acid [cal. a BP]
5807-70	KIA30251	2.08	12260 ± 50	1.40	14224 ± 50
5807-70	KIA32746	3.01	12400 ± 50	2.30	14486 ± 50
5807-70	KIA32747	12.15	20760 ± 120	11.48	24968 ± 120
5807-B8	KIA 50678	15.35	23800 ± 245	13.75	27962 ± 245
5807-70	KIA30254	14.67	22410 ± 260	14.03	26690 ± 260
5807-70	KIA30253	17.27	23530 ± 220	16.65	27690 ± 220
5807-B8	KIA 50679	19.90	25260 ± 285	18.21	29422 ± 285
5807-B8	KIA 50680	20.90	26630 ± 400	19.82	30591 ± 400
5807-B8	KIA 50681	21.80	27230 ± 420	20.53	31318 ± 420
5807-B8	KIA 50682	23.80	28870 ± 510	21.71	32748 ± 510
5807-91	KIA50012	22.08	29160 ± 795	22.16	33004 ± 795

Acknowledgements

This thesis would not have been possible without the financial support of the International Max Planck Research School for Global Biogeochemical Cycles, Jena and the scientific, personal and technical assistance of many people during my research at the Friedrich Schiller University Jena.

First of all, I would like to thank **Georg Büchel** and **Michael Pirrung** for being my supervisors and providing continuous support, stimulation and encouragement.

Georg, I thank you very much for the opportunity to do research in your working group, your absolute optimism in my work, your open door for every scientific question, the countless valuable discussions and the financial support beyond my scholarship.

Michael, I thank you very much for your scientific support, the inspiring discussions, valuable advices, patience, constructive manuscript feedbacks and the good excursion collaboration.

Thanks a lot to all my colleagues of the Institute of Geosciences for creating a pleasant working environment, especially to:

my room mates Arno Märten, Jörn Engelhardt and Anika Kötschau for the nice room atmosphere, regard and help.

Daniela Sporleder and Katja Nebelung for the inspiring discussions during lunchtime.

Regina Piechnick, John Schmidt and Steffi Rothardt for managing all administrative, travelling and coordinative issues.

Thomas Lange, Marcel Henschen, Peter Frenzel, Thomas Voigt, Ralph Bolanz, Maria Wierzbicka-Wieczorek, Lothar Viereck, Dirk Merten, Franziska Mosebach and Anja Grawunder for the scientific support and valuable discussions.

Sigrid Bergmann, Frank Linde, Michael Ude, Mike Lippold, Michael Achtellik, Ines Kamp, Gerit Weinzierl, Ulrike Buhler, Frank Buchwald and Volker Schwarz for technical support.

Thanks to my external manuscript co-authors Bernd Zolitschka and Ulrich Polom for data supply, constructive comments and feedbacks. Thanks to S. Stahl for XRF and A. Bauer for clay mineralogy XRD measurements.

Thanks to Áslaug Geirsdóttir and Thor Thordarson for the instructive and impressive research stay at Iceland with valuable discussions.

Thanks to Karl-Heinz Köppen from the Engineering Company "Wasser und Boden GmbH" and the Water Supply Company Cochem-Zell for providing the sediment cores, the State Office for Geology and Mining in Rhineland-Palatinate (Mainz) for the core lithology data from the Alf Valley, and the State Office for Survey and Geobasis Information Rhineland-Palatinate for the digital elevation model data.
Thanks to the Integrierte Fluiddynamik in Sedimentbecken (INFLUINS) project and the GFZ Potsdam for the opportunity of taking high-resolution core-scan photos.

Many thanks to Thomas Kasper, Thorsten Haberzettl and Gerhard Daut for scientific and technical support as well as encouragements during hard times.
Sincere thanks to Irene Satoris for the warm welcome and support during my fieldwork in the Alf Valley.

Special thanks go to my friends **Luise**, **Clara**, **Kerstin**, **Anja**, **Johanna**, **Gunnar**, **Lionel, Nadja** and **Manuel** in Jena for the cheerful time spent together. I am so grateful to know you. Without you, my PhD time would not have been half that enjoyment.

Finally, very special thanks to **my parents** Petra and Thomas Eichhorn for encouraging and supporting me on my path. Spending much of my childhood outdoors and on trips abroad certainly inspired my curiosity for nature and the interest to understand connections which attracted me to science.

L U I S E E I C H H O R N

Dipl. Geographer

Born on 10th of October 1986

Schkeuditz, Germany

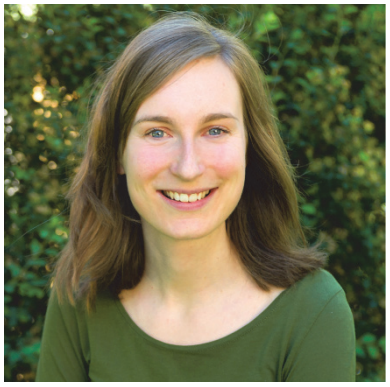

Education

2012 – 2016	**PhD student**, Friedrich-Schiller-University Jena, Institute for Geoscience (Germany) Scholarship of the International Max Planck Research School Thesis: "*Reconstruction of environmental change and sedimentation processes during the Pleniglacial using fluvio-lacustrine sediments from volcanically-dammed Paleolake Alf, West Eifel Volcanic Field, Germany*"
2014	Research Stay at the Department of Earth Sciences, Iceland
2006 – 2012	**Diploma in Geography**, Dresden University of Technology (Germany) (grade: 1.7) Thesis: "*Holocene paleoenvironmental reconstruction of the Buor Khaya Peninsula - A multiproxy approach*" at Alfred Wegener Institute Potsdam
1994 – 2005	**High School,** Friedrich-Schiller-Gymnasium, Leipzig (Germany) (grade: 2.0)

Professional Experience

2014, 2016	**Teaching assistant**, FSU Jena, Institute for Geoscience (Germany) Preparing and leading of excursions; teaching engineering geology
2014	GESEP School Erlangen "Initial Drill-Core Processing, Analyses and Archiving"
2010	**Internship** at Estación Científica San Francisco (**ECSF) Ecuador**
2010	**Internship** at **Centre National de la Recherche Scientifique** (CNRS), Bordeaux, with focus on multiproxy analysis of laminated marine sediment cores from the Pacific Ocean
2010	**Internship** at **German Research Centre for Geosciences** (GFZ), Potsdam, section Climate Dynamics and Landscape Evolution, with focus on the detection of the Alleröd/ Younger Dryas transition using varved lacustrine sediment cores
2008 – 2009	**Research Assistant** at the chair of landscape ecology/ soil science

2007 **Internship** at **Leibniz Centre for Agricultural Landscape Research** (ZALF) e.V. Müncheberg, Germany, with focus on the emission of trace gases CO_2, CH_4 and N_2O from fens using chambers

Languages

German: Mother tongue
English: Fluent
Spanish: Fluent
French: Fluent

Membership

Deutsche Gesellschaft für Polarforschung (DGP), since 2011
Permafrost Young Researchers Network (PYRN), since 2011

Conference contributions

Oral Presentation

Eichhorn L, Pirrung M, Zolitschka B, Büchel G (2016): Process interpretation of laminated lacustrine sediments from the valley of the river Alf, Quaternary West Eifel Volcanic Field, Germany. Geophysical Research Abstracts Vol. 18, EGU2016-8664-2.

Posters

Eichhorn L, Engelhardt J, Lange T, Pirrung M, Büchel G (accepted): Das Potenzial des fluviolakustrinen Sedimentarchives im Alfbachtal in der Westeifel, Deutschland. DEUQUA-Tagung "Übergänge im Quartär" to be held September 25 -30, 2016 in Dresden.

Eichhorn L, Lange T, Engelhardt J, Polom U, Pirrung M, Büchel G (2015): Sedimentation architecture of the volcanically-dammed Alf valley in the West Eifel Volcanic Field, Germany. EGU, April 12-17, 2015 in Vienna. Geophys. Res. Abs. 17, EGU2015-12133-4, 2015.

Eichhorn L, Lange T, Polom U, Pirrung M, Büchel G (2014): Volcanically-dammed lake archive from the Last Glacial Maximum in the West Eifel Volcanic Field - sedimentation history in the Alf valley. GeoFrankfurt, September 21-24, 2014 in Frankfurt.

Eichhorn L, Pirrung M, Heimann M, Büchel G (2014): Reconstruction of biogeochemical and endogenic processes in the Alf valley, Quaternary West Eifel Volcanic Field, Germany. Earth System Science, March 12-14, 2014 in Jena.

Publications in peer-reviewed journals

Eichhorn L, Pirrung M, Zolitschka B, Büchel G (submitted): Pleniglacial process reconstruction on laminated lacustrine sediments from lava-dammed Paleolake Alf, West Eifel Volcanic Field (Germany). Quaternary Science Reviews.

Strauss J, Schirrmeister L, Mangelsdorf K, **Eichhorn L**, Wetterich S, Herzschuh U (2015): Organic-matter quality of deep permafrost carbon – a study from Arctic Siberia. Biogeosciences. 12. 2227-2245.

Statement of authorship/ Selbstständigkeitserklärung

Ich erkläre, dass ich die vorliegende Arbeit selbstständig und unter Verwendung der angegebenen Hilfsmittel, persönlichen Mitteilungen und Quellen angefertigt habe.

I declare that I prepared this thesis independently and using the specified tools, personal messages and sources.

Jena, 12.09.2016 _____

Luise Eichhorn